AUGMENTED FRAMEWORK FOR ECONOMIC VIABILITY-BASED POWERTRAIN DESIGN AND EMISSIONS ANALYSIS OF MEDIUM/ HEAVY-DUTY PLUG-IN HYBRID ELECTRIC VEHICLES

A Dissertation

Submitted to the Faculty

of

Purdue University

by

Vaidehi Y. Hoshing

In Partial Fulfillment of the

Requirements for the Degree

of

Doctor of Philosophy

December 2018

Purdue University

West Lafayette, Indiana

THE PURDUE UNIVERSITY GRADUATE SCHOOL
STATEMENT OF DISSERTATION APPROVAL

Dr. Gregory Shaver, Chair

School of Mechanical Engineering

Dr. Oleg Wasynczuk

School of Electrical and Computer Engineering

Dr. Edwin García

School of Material Science Engineering

Dr. Scott Sudhoff

School of Electrical and Computer Engineering

Approved by:

Dr. Jay Gore

Head of the School Graduate Program

To my parents and my brother,

I am because you are.

ACKNOWLEDGMENTS

I am highly indebted to my advisor, Dr. Greg Shaver, who gave me the opportunity to learn and grow under his guidance. He introduced me to HEV research, and patiently guided me through the process of performing research and sharing my work. I am also thankful to him for allowing me to continue the research as a Ph.D. student. I have learned a lot from his hardworking nature, and protective, encouraging and productivity-building approach towards his students. I am also incredibly thankful to Dr. Oleg Wasynczuk and Dr. Edwin García, for their guidance and insights during all the team meetings. I am also thankful to Dr. Scott Sudhoff for his valuable comments and insights. Each one of them has significantly shaped my research.

The project would not have been as much fun without all my team mates: Dr. Ashish Vora, who has been a mentor par excellence, who has always been there to guide and help; Dr. Xing Jin, a friend I could share everything with, who would push me to be better; Tridib Saha, a very helpful friend and colleague, who keeps our presentations in check; and Aniruddha Jana, very hard working and thorough researcher. The memories of the days and nights spent in the lab running simulations and getting models to work, crashing hard-drives, with them, are priceless. The vastness of knowledge and experience that they all kindly shared with me is indescribable. I am also extremely thankful to Dr. Subbarao Varigonda, who has always been more than a sponsor, who guided the project and was always available for answering our questions.

Special thanks are also due to Orkan Kurtulus and Vatsal Shah, who patiently dealt with my never ending questions on cooling systems. I have also thoroughly enjoyed working with Miles, Sharon, Harsha, Dr. Aswin, Kalen, and Nachiket, on the other Shaver group projects. I am also thankful to Dr. Steven Son for his guidance

and help, and Anushree for being the energetic, enthusiastic co-TA, during my ME440 TA phase. I have thoroughly enjoyed working with, and troubling, them all.

I sincerely thank all my friends at Purdue who have been with me through my thick and thin. I am lucky to have met such great friends and research companions along the way as Cody, Aswin, Mrunal, Miles, Neeraj and Amar, Vasu, Yeshaswi and Akash, and Chaitu, with whom I have enjoyed some "deep" discussions on research and life. I am also incredibly thankful to Kalen, Ife, Alex, Mukta, Soumy, Ishita, Amit, Kanak, Shambhavi, Mayura, Bhise, Pramod, Leon, Parveen, and Yingying, each of whom has contributed to my growth personally or professionally. I am thankful to all the present and previous members of the Herrick Student Committee for the fun experiences planning Herrick picnics, parties and guest talks alike. I am extremely thankful to Dr. Patricia Davies, Donna Cackley, Cindy Sue Cory and the staff at Herrick Labs for making our working environment warm and comfortable.

I will be forever grateful to all the teachers and staff at Cummins College, Pune, and especially to the Purdue-Cummins Fellowship Program; Dr. Supriya Kelkar, Dr. Jay Gore and Cummins Inc. for starting and continuing this program. My journey at Purdue started because of it. I am grateful to Dr. Gayatri Adi, who was my first mentor after my Cummins fellowship application was accepted. My decision to stay for a PhD was made easier through her guidance and experience.

I am deeply thankful to DBG, now Dr. Dheeraj Gosala, a Shaver groupite, hard working, intelligent and unselfish person, whom I met on my first day at Herrick, my dearest friend, support, and help since then, who convinced me to continue for a Ph.D. I am thankful to Amma and Nanna for their support. Finally, I am profoundly grateful to my family, Aai, Baba, Omkar and my grandparents for being my cushion, although continents apart, who saw this dream with me, who are my roots of strength, whose support and blessings drive my growth.

TABLE OF CONTENTS

Page

LIST OF TABLES

LIST OF FIGURES

Figure Page

SYMBOLS

K_{AccP}	Low pass filter transfer function gain
T_1	Time constant of low pass filter transfer function
$AccPedal$	Acceleration pedal command
P_{whl}	Low pass filtered wheel power
t	Time
I	Battery current
$AhCap$	Ampere hour capacity of the cell
SOC_{init}	Battery initial SOC
SOC	Instantaneous SOC of the battery
V_{OC}	Cell open circuit voltage
R_{int}	Cell internal resistance
V_{term}	Cell terminal voltage
V_0	Voltage across R_0 in a first order ECM
I_0	Current through R_0 in a first order ECM
R_0	Series resistance in a first order ECM
V_1	Voltage across the R_1C_1 branch in a first order ECM
I_1	Current through R_1 in a first order ECM
I_{C}	Current through C_1 in a first order ECM
R_1	Resistance in the RC branch in a first order ECM
C_1	Capacitance in the RC branch in a first order ECM
V_{min}	Minimum voltage limit for the cell
V_{max}	Maximum voltage limit for the cell
$P_{\text{V\_dis\_max}}$	Voltage limit-based maximum discharge power
$P_{\text{V\_chg\_max}}$	Voltage limit-based maximum charge power
$C\text{-}rate_{\text{max}}$	Maximum C-rate

$I_{\text{C-rate\_max}}$	Cell current corresponding to the maximum C-rate
$P_{\text{C-rate\_dis\_max}}$	C-rate limit-based maximum discharge power
$P_{\text{C-rate\_chg\_max}}$	C-rate limit-based maximum charge power
$P_{\text{batt\_dis\_max}}$	Maximum discharge power for the battery
$P_{\text{batt\_chg\_max}}$	Maximum charge power for the battery
$P_{\text{batt\_max}}$	Maximum battery power demand during CD/CS mode
$P_{\text{batt\_min}}$	Minimum battery power demand during CD/CS mode
θ_{SOC_reg}	Parameter for SOC regulation in CS mode
SOC_{target}	Target SOC
F_{EngON}	Parameter for engine ON in CD mode
$P_{\text{eng\_hi}}$	Battery SOC based higher engine power limit
$P_{\text{eng\_lo}}$	Battery SOC based lower engine power limit
$P_{\text{eng\_opt}}$	Optimal engine power
$P_{\text{eng\_max}}$	Physical limit on engine power
ω_{eng}	Engine speed
P_{eng}	Engine power demand
$P_{\text{eng\_f}}$	Final engine power demand
P_{mot}	Motor power demand
$P_{\text{mot\_f}}$	Final motor power demand
NPV	Net present value
ISC	Initial System Cost
CF_i	Cash flow in i^{th} year
r	Social discount rate
$IntPrem$	Manufacturer's integration premium
A_0	Constant associated with the motor cost
A_1	Peak power based motor cost
A_2	Maximum capacity based battery cost
MPP	Motor peak power
$ESSCap$	Battery pack capacity

PBP	Payback Period
$AnnCS/mile$	Annual cost savings per mile
$CF_{\text{conv\_fuel}}$	Cash flow for fuel for the conventional vehicle
$CF_{\text{PHEV\_fuel}}$	Cash flow for fuel for the PHEV
$CF_{\text{PHEV\_elec}}$	Cash flow for electricity for the PHEV
$AVMT$	Annual vehicle miles traveled
$Q_{\text{loss,\%}}$	Capacity loss percentage
Q_{loss}	Capacity loss
T_{batt}	Battery temperature
E_{a}	Activation energy
R	Gas constant
UF	Utility Factor
CD_Range	CD mode range
$Daily\_VMT$	Daily vehicle miles traveled
Q_{SEI}	SEI growth related capacity loss
Q_{AM}	Active material loss related capacity loss
$k_{\text{SEI}}, E_{\text{SEI}}$	Parameters for capacity loss from SEI layer growth
$k_{\text{AM}}, E_{\text{AM}}$	Parameters for capacity loss from AM loss
λ, θ	Fitting parameters
$\dot{q_{\text{gen}}}$	Rate of heat generation of the battery
$\dot{q_{\text{abs}}}$	Rate of heat absorption by the heating/cooling system
m_{batt}	Mass of the battery
c_{batt}	Heat capacity of the battery
$\dot{W}$	Work required by the heating/cooling system
$\dot{m_{\text{fuel}}}$	Mass flow rate of fuel
LHV_{diesel}	Lower heating value of diesel
η_{eng}	Engine efficiency
η_{gen}	Generator efficiency
FC	Fuel consumption

ρ_{diesel}	Density of diesel
T_{amb}	Ambient temperature
h	Convective heat transfer coefficient
A	Surface area of the cell
$WTW_{\text{emissions}}$	Well to wheel emissions
WTP	Well to pump emissions
PTW	Pump to wheel emissions
E_{diesel}	Total diesel energy used
$E_{\text{diesel\_CD}}$	Diesel energy used in CD mode
$E_{\text{diesel\_CS}}$	Diesel energy used in CS mode
$WTW_{\text{daily\_diesel}}$	Daily well to wheel emissions due to diesel usage
WTW_{diesel}	Well to wheel emissions per mile due to diesel usage
η_{charging}	Charging efficiency
$E_{\text{daily\_electricity}}$	Electrical energy used daily for charging the PHEV battery
$WTW_{\text{daily\_total}}$	Daily total well to wheel emissions from a PHEV
$WTW_{\text{daily\_electricity}}$	Daily well to wheel emissions from electricity usage

ABBREVIATIONS

AC	Air-conditioning
Ah	Ampere-hour
AM	Active Material
AVMT	Annual Vehicle Miles Traveled
BEB	Battery Electric Bus
BEV	Battery Electric Vehicle
CA3EM	China Automotive Energy, Environment and Economy Model
CC-CV	Constant current - constant voltage
CD	Charge Depleting Mode
CIDI	Compression Ignition Direct Injection
CNG	Compressed Natural Gas
CO	Carbon monoxide
CO_2	Carbon dioxide
COP	Coefficient of Performance
CS	Charge Sustaining Mode
DIRECT	Dividing Rectangles
DOD	Depth of Discharge
DOE	Design of Experiments
DP	Dynamic Programming
EC/DMC	Ethylene carbonate and Dimethyl carbonate
ECM	Equivalent Circuit Model
ECMS	Equivalent Consumption Minimization Strategy
EPA	Environmental Protection Agency
ESS	Energy Storage System
EV	Electric Vehicle

FCV	Fuel Cell Vehicle
GHG	Greenhouse Gases
GREET	Greenhouse Gases, Regulated Emissions and Energy Use in Transportation
HD	Heavy-Duty
HEV	Hybrid Electric Vehicle
ICE	Internal Combustion Engine
ICEV	Internal Combustion Engine Vehicle
IEA	International Energy Agency
INDC	Intended Nationally Determined Contributions
IPCC	Intergovernmental Panel on Climate Change
IRR	Internal Rate of Return
ISC	Initial System Cost
LFP	Lithium Ferrous Phosphate
LiPF6	Lithium hexafluorophosphate
LPG	Liquefied Petroleum Gas
MCMC	Markov Chain Monte Carlo
MD	Medium-Duty
M/G	Motor and Generator
NBIR	Net Benefit Investment Ratio
NHTSA	National Highway Traffic Safety Administration
NMC	Nickel Manganese Cobalt Oxide
NMC+LMO	Nickel Manganese Cobalt Oxide and Lithium Manganese Oxide
NPV	Net Present Value
NO_x	Nitrogen oxides
OECD	The Organization for Economic Co-operation and Development
OEM	Original Equipment Manufacturer
PBP	Payback Period
PCOA	Parallel Chaos Optimization Algorithm

PDF	Probability Distribution Function
PHEV	Plug-in Hybrid Electric Vehicle
$PM_{2.5}$	Particulate Matter with diameter less than 2.5 microns
PM_{10}	Particulate Matter with diameter less than 10 microns
PNGV	Partnership for a New Generation of Vehicles
PTW	Pump to Wheel
PV	Present Value
RC	Resistance Capacitance branch
R134a	Refrigerant 134a (Tetrafluoroethane)
SEI	Solid Electrolyte Interface
SOC	State of Charge
SO_x	Sulfur oxides
SUV	Sport Utility Vehicle
VMT	Vehicle Miles Traveled
VOC	Volatile Organic Compounds
WTP	Well to Pump
WTW	Well to Wheel

ABSTRACT

Hoshing, Vaidehi Y. Ph.D., Purdue University, December 2018. Augmented Framework for Economic Viability-Based Powertrain Design and Emissions Analysis of Medium/ Heavy-Duty Plug-in Hybrid Electric Vehicles. Major Professor: Dr. Gregory M. Shaver, School of Mechanical Engineering.

Plug-in hybrid electric vehicles (PHEVs) are being considered as an alternative to conventional medium-duty (MD) and heavy-duty (HD) commercial vehicles to reduce fuel consumption and tailpipe emissions. Lithium ion batteries, which are used in PHEVs due to their high energy density, are expensive. The battery contributes significantly towards the life-cycle cost of MD/HD PHEVs, as these vehicles, due to high mass and aggressive battery usage, require multiple battery replacements over their lifetime. Smaller batteries increase the fuel consumption and need more replacements, while bigger batteries increase the initial system cost. Powertrain design from a life-cycle cost perspective is required to explore this trade-off and maximize the economic gains obtained from PHEVs.

Powertrain design entails component sizing, control strategy selection as well as architecture selection. Different powertrain designs yield different lifetime economic gains. A variety of applications exist for MD/HD vehicles, which differ in their ways of powertrain usage, due to variations in required acceleration, available braking, and average and maximum speeds. Therefore, different powertrain designs are needed depending on the application and usage scenario. The powertrain design space needs to be explored, and solutions that maximize the economic gains within the specified constraints need to be chosen.

This dissertation compares the economic viability of two PHEV applications (MD Truck and HD Transit Bus), with options of series and parallel hybrid architectures, over multiple drivecycles, for four economic scenarios (years 2015, 2020, 2025 and

2030). It is shown that hybridizing the transit bus achieves payback sooner than hybridizing the truck. Further, the results for the transit bus application, over the Manhattan drivecycle, show that implementation of the parallel architecture is economically viable in the 2015(present) scenario, while the series architecture becomes viable in 2020, due to significantly lower initial costs involved in the parallel architecture.

A methodology to select a solution out of the explored design space that maximizes the economic gains is demonstrated. Variations in the economic and vehicle usage conditions for which this solution is designed, can be expected. It is therefore necessary to check the robustness of this solution to change in external factors such as vehicle mass, annual vehicle miles travelled (AVMT), component and fuel costs. It is shown that the economic gains are affected by the battery cost, fuel cost, AVMT and vehicle mass, while the number of battery replacements are affected by AVMT and vehicle mass.

A probability-based approach is demonstrated to obtain confidence in the economic and battery life predictions. Specifically, probability-based variations are provided to variables such as miles traveled between recharge, recharge C-rate and battery temperature. It is shown that battery life is affected the most by battery temperature.

A battery heating/cooling system is required to maintain constant battery temperature of operation during all seasons, but these systems incur additional fuel costs. A framework that utilizes just the Coefficient of Performance (COP) of the heating/cooling system to calculate the excess fuel cost is proposed and demonstrated. An increase of 0.9-1.8% in fuel consumption is shown, depending on the drivecycle and ambient temperature.

Further, the well-to-wheel (WTW) fuel-cycle emissions from conventional and PHEV transit buses operating in Indiana and California are assessed using the "Greenhouse Gases, Regulated Emissions, and Energy Use in Transportation" (GREET) Model 2017, developed by Argonne National Labs. It is shown that 59% and 63%

greenhouse gas (GHG) reductions can be achieved in Indiana and California respectively, along with reduction in carbon monoxide (CO), nitrogen oxides (NO_x), particulate matter with diameter less than 2.5 microns ($PM_{2.5}$) and volatile organic compounds (VOC) emissions for both the states. However, an increase in sulfur oxides (SO_x) emissions for both the states, and particulate matter with diameter less than 10 microns (PM_{10}) increase for Indiana, are observed.

1. INTRODUCTION

1.1 Motivation

Earth surface temperatures have been rising at a very high rate, and have risen by approximately 1.5°F since the late 1970s (Figure 1.1 [1]). This report [1] also lists the significant risks that this rate of increase in temperature poses to the weather changes, ecosystems and human health. The transportation sector is a significant contributor to green house gas emissions (27%), with the medium and heavy duty vehicles contributing significantly(Figure 1.2 [2]). With the energy consumption by buses and trucks set to increase by close to 20% by 2050 (Figure 1.3 [3]), it is necessary to devise and implement technologies that can minimize the overall carbon footprint.

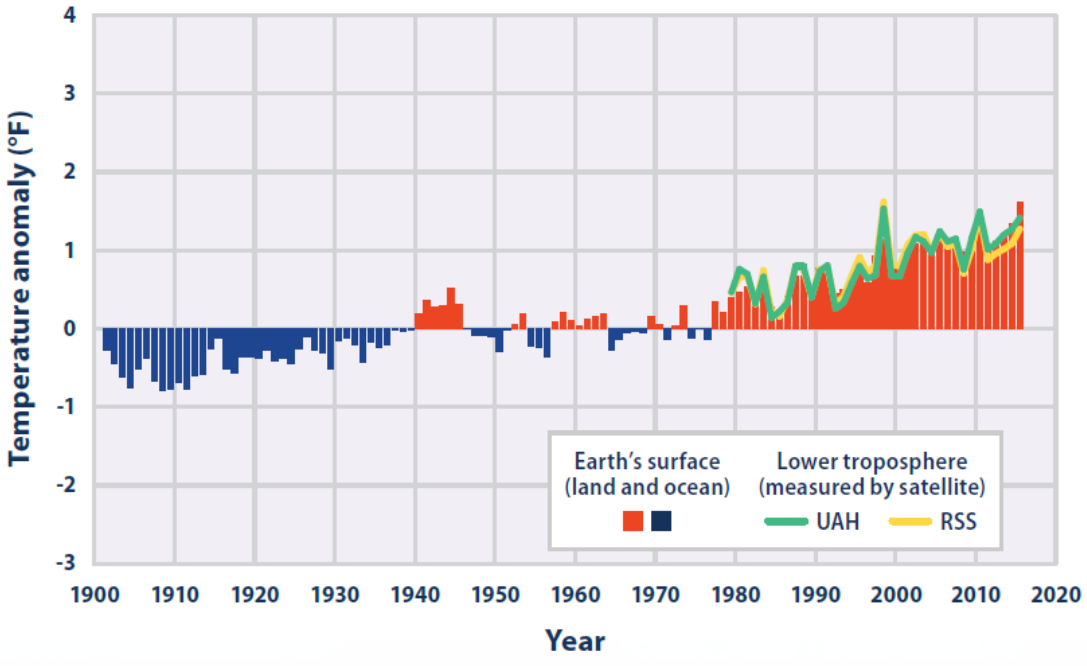

Figure 1.1. Global annual average surface temperatures [1].

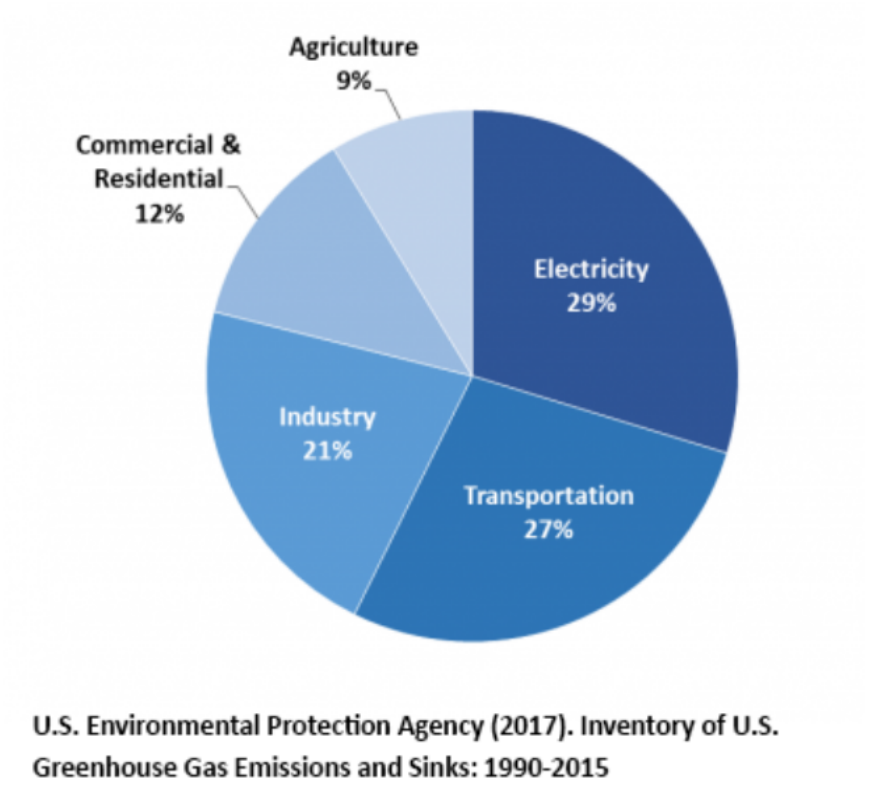

Figure 1.2. Total U.S. greenhouse gas contributions by economic sector in 2015 [2].

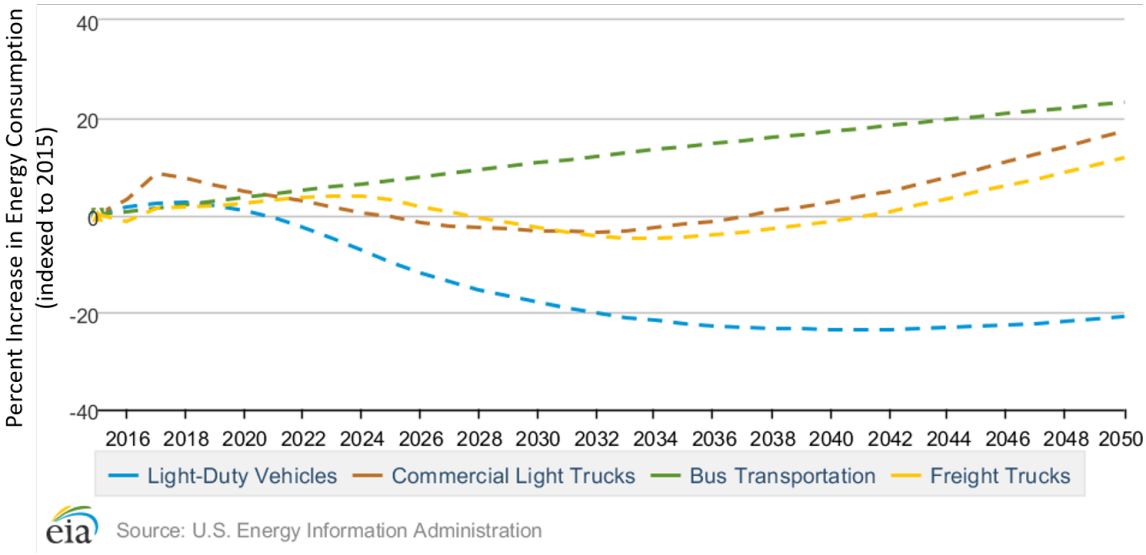

Figure 1.3. Projections of percent increase (indexed to 2015) in energy consumption by mode in the reference case [3].

The EPA and the NHTSA have proposed a national program to reduce the carbon dioxide emissions by about 1.1 billion metric tonnes and reduce oil consumption by about 2 billion barrels over the lifetime of the vehicle, helping the vehicle owners save $170 billion in fuel costs [4]. This calls for the usage of alternate fuel sources that have high energy densities and energy conversion that is more efficient. Hybrid electrification is one such promising opportunity.

Hybrid electric vehicles and plug-in hybrid electric vehicles use a battery as an Energy Storage System (ESS) along with an Internal Combustion Engine (ICE) to provide tractive power to the wheels. The ESS allows energy recovery during braking (called regenerative braking), because the ESS allows opportunity charging, and also downsizing of the engine and flexibility in it's region of operation, because the ESS is now able to assist the engine when required. Therefore, significant reduction in fuel consumption and tailpipe-out emissions can be achieved. The goal of the efforts outlined in this report is to use a previously developed framework [5] to understand the economic gains vs system cost trade-off to enable optimal component sizing, control and architecture selection for medium- and heavy-duty applications. Additionally, for a selected architecture and powertrain configuration, the goal is to develop methods to understand the uncertainty in battery life prediction due to variations in vehicle and battery usage.

1.2 Background

Powertrain optimization and component sizing for a hybrid electric vehicle have been studied previously by many. Reference [6] proposes a simulation design environment for alternative powertrains and demonstrates it for design of a hybrid diesel-electric powertrain by optimizing for fuel economy and further provides a robustness analysis for this design. Reference [7] proposed a design optimization algorithm using DIRECT (DIviding RECTangles) to minimize fuel consumption over a composite drivecycle, and also compared the results with optimization using Simulated Anneal-

ing and Genetic Algorithm. Reference [8] performs a multi-objective optimization for the performance requirements specified by PNGV, using genetic algorithms to find the Pareto-optimal solution set for sizing and control parameters. Certain other studies also perform concurrent optimization of sizing and controls of series or parallel HEVs to minimize fuel consumption, emissions, and/or drivability and gradability [9] [10] [11] [12]. [13] optimize battery size, charging and power management of PHEV to reduce carbon dioxide emissions from the ICE and grid generation plants. Reference [14] propose a novel approach for engine and motor sizing using Degree of Hybridization as a metric and further also explains and implements a fuzzy logic controller to maximize the fuel economy on a full-sized parallel HEV.

Many others focus on optimizing control strategies to minimize fuel economy and/or emissions for hybrid electric vehicles, typically using variations of genetic algorithms, ECMS, DP or supervisory control [15] [16] [17] [18] [19]. Battery degradation and cost minimization are not considered in these studies.

Minimization of fuel and electricity cost for uncertain driving conditions also has been considered [20] [21] [22]. A total cost of ownership analysis for light-duty gasoline series PHEV for Germany is also performed [23]. These studies do not consider battery degradation or replacement.

Battery degradation, or loss of battery energy and/or power capacity over use, is a major concern for powertrain design considering life-cycle costs. Since battery life is often times lesser than the vehicle life, especially for medium- and heavy-duty applications, where the battery can be used more aggressively due to higher vehicle mass, leading to atleast one battery replacement over the life of the vehicle. This can significantly impact the gains obtained due to fuel consumption consumption reduction, and can decide the fate of a powertrain design. Therefore, battery degradation should be considered in order to design robust hybrid electric powertrains. The authors of [24], studied the component sizing optimization for a PHEV using parallel chaos optimization algorithm (PCOA), to minimize component and battery replacement costs with drivability as a constraint, for 2 types of batteries. This is

performed for a mid-size sedan and battery replacement is assumed to occur every 100,000 miles. Causes for battery degradation and it's dependence on usage are not considered.

A method is proposed in [25] to optimize the energy management in a light duty PHEV by minimizing the daily costs associated with gasoline consumption, in-route charging and reduction in state of health of the battery. There are other studies that optimize the trade-off between energy consumption and battery health [26] [27]. The authors of [28] and [29] studied the effect of charging patterns to minimize the energy costs and daily battery health degradation. These studies did not consider optimization from a vehicle life-cycle cost perspective. A methodology to design for cost optimization, for minimization of powertrain costs of the vehicle life, has been proposed in [30], but for a light-duty non-plug in parallel hybrid diesel-electric vehicle with a planetary gear set and a single speed gear box, using a DP based energy management strategy.

There have been articles that review the hybrid electric architectures and their energy management strategies [31] [32] [33] [24]. Few also compare the architectures from a fuel economy, component efficiency and/or emissions standpoint ([34], [35], and [36] light-duty HEV, [37], and [38] light-duty PHEV). A control method to minimize fuel and energy consumption for light-duty PHEVs has been presented in [39] and has been compared on series and parallel PHEVs with EV and blended modes on standard and customized driving cycles. The series architecture is shown to achieve better fuel economy but with higher battery utilization, concluding that battery life, energy cost etc need to be considered to completely analyze PHEV performance. A comparison of the fuel economy and component efficiency of series, parallel (with and without integrated starter-alternator) architectures for a transit bus application on multiple drivecycles has been presented in [40], the fuel cost savings of the parallel architectures with respect to the series architecture for year 2006 and 2008 have been estimated. These studies either do not optimize the powertrain design and/or consider life-cycle costs and/or battery replacement.

It is necessary to understand, from a life-cycle perspective, the economic gains that a powertrain design and control strategy can achieve, considering battery degradation, for different hybrid electric architectures, for different application. This will help us understand if, when and under what usage conditions, an application should be electric hybridized.

Furthermore, as will be shown later, the battery temperature of operation contributes significantly to battery degradation and battery life. Hence, it is necessary to maintain the battery at a desired temperature, thus motivating the need for efficient battery thermal management systems. Although there have been detailed studies reviewing the types of cooling systems for HEV/EV batteries [41] [42] [43] [44], their numerical models and simulations [45], proposing new heating/cooling system for batteries [46] [47] [48] [49], there are very few that look at the fuel penalty of this system. The authors of [50] presented a numerical model and sizing of a vehicle cooling system for a HD Series HEV tracked vehicle, simulated it over a combined urban and cross-country drivecycle and estimated 8-12% cooling system power consumption relative to the power supplied by the engine with heat generated by all the powertrain components as the cooling system load. Modeling, experimental validation and simulation of a cabin, battery and motor integrated AC/heating system for a light-duty electric vehicle was performed in [51]. The effect of the heating/cooling system on the driving range was also investigated. With the availability of various types of heating and cooling systems, it becomes imperative to be able to evaluate the energy cost of operating these systems to maintain the battery at a desired temperature.

Furthermore, two biggest motivators for exploring alternative vehicle technologies as well as for improving the existing technology are limited availability of crude oil and rising of the Earth's surface temperature. While the fuel efficiency improvement achievable using variable degrees of hybridization has been established, there is significant curiosity and skepticism pertaining to the reduction of greenhouse gas (GHG) emissions for higher degrees of electric hybridization, which require charging from the electricity grid, due to the sources and processes used to generate electricity and

the resulting emissions. A number of studies have been conducted to understand the well-to-wheel emissions resulting from the usage of PHEVs that require charging from the grid, which include the emissions resulting from the production, distribution and usage of these vehicles. These emissions have been contrasted with those resulting from the production, distribution and usage of conventional diesel or gasoline vehicles of the same type. The authors in [52] analyzed the total and urban share of WTP emission contributions from different fuel pathways, PTW and WTW emissions from 9 vehicle types using fuel from these pathways. They concluded that the WTW emissions of criteria pollutants vary significantly in amounts as well as in locations for different vehicle and fuel systems.

Multiple studies have compared emissions from alternative fuel technologies, not just HEVs, [40] for mid-size SUVs, [53] for Class 8 trucks, concluding that HEVs are more efficient as compared to FCV or CNG vehicles from a WTW efficiency perspective. HEVs with varying degrees of hybridization have been found to produce less WTW GHG emissions across borders ([54] [55] [56] in China, [57] in UK and California, [58] in Switzerland, [59] [60] in the US, [61] for non-OECD Americas, US and Asia).

There have also been multiple studies that evaluate the emissions reduction potential of medium/heavy-duty trucks and buses, where all the studies have highlighted the potential benefits of hybridization for these vehicles in different driving and operation scenarios. The authors of [55] used the Tsinghua CA3EM and GREET to estimate the GHG emissions of AF buses currently in use/demonstrated in China to conclude that only the electric, LPG, and CNG buses are better in fuel economy and emissions as compared to the conventional buses and then provide technological and policy suggestions to improve the present GHG emissions scenario in China. Life-cycle assessment of CO_2 emissions was performed in [56] for three battery electric buses (BEBs) that were tested on-road in China, considering the fuel-cycle, they discuss the energy consumption with the AC on and off under multiple passenger load conditions to conclude that the fuel saving potential increased in heavy traffic, AC

operations and full passenger load, and that the AC contributes more to the EC than passenger load, and that the BEBs can reduce WTW petroleum consumption by over 85%, fossil fuel by 32% and CO_2 emissions by 19-35%. The authors of [62] analyzed CO_2 emissions from series and parallel MD truck PHEVs (on two drivecycles and with different control strategies) for four CO_2 intensities of electricity production it was shown that as compared to passenger cars MD trucks have a lower potential for CO_2 emissions reduction due to the higher engine efficiencies in general and that using a blended CD mode can lower the CO_2 emissions even further. A comprehensive holistic comparison of the life cycle costs was performed in [53], emissions and air pollution externalities costs of Class 8 trucks with different vehicle technologies to conclude that BE class 8 trucks outperform all other fuel techs including CNG.

Some studies have also performed powertrain optimization [63] and vehicle usage based technology allocation [64] to minimize GHG emissions and cost. Further, the authors of [65] analyzed the global historic road freight activity data and projected it to 2050 using IEAs Mobility Model, concluding that with the current INDCs the global GHG emissions would increase by 56% by 2050, but there is a potential to reduce them by 60%, and the policy improvements necessary to achieve it are also suggested.

Few studies have further assessed the uncertainties regarding the emissions reduction potential of PHEVs. Life-cycle assessment of air emissions and oil consumption from ICEVs, HEVs and PHEVs was performed in [66] to conclude that GHG emissions reduction/increase potentials of PHEVs are uncertain as compared to HEVs, due to the emissions from battery charging and manufacturing and that HEVs and PHEVs with smaller battery packs reduce the externality damages, offering more benefits per dollar and hence should be promoted. A vehicle life cycle assessment of GHG emissions from BEVs and gasoline vehicles in UK and California was performed in [57], to conclude that under urban driving schedules, mid-size BEVs in the UK reduced GHG emissions significantly but not for highway driving schedules, and the SUV class EVs in California reduced GHG emissions in both the cases thus

emphasizing that a general conclusion cannot be made about the relative GHG performance of BEVs rather life-cycle emissions including those from manufacturing as well as variations due to different grid intensities need to be considered. The authors of [61] performed a cost of ownership analysis and WTW GHG emissions analysis for various alternative technologies for light-duty vehicles, and also performed a sensitivity analysis with respect to changing component, fuel, electricity, natural gas and hydrogen costs for non-OECD Americas, US and Asia. They concluded that there are higher uncertainties for new technologies than ICEVs, although they reduce the GHG emissions as compared to ICEVs and that robust refueling infrastructure and policy initiatives required to achieve it are necessary for enabling the common customer to adapt these technologies.

Given the speculation around the potential of emissions reduction for hybrid electric vehicles, it becomes necessary to evaluate the well-to-wheel emissions along with the cost-of ownership assessment of these vehicles.

The efforts outlined in this thesis compare the economic gains of electric hybridizing two applications - medium-duty truck and transit bus for series and parallel hybrid electric architectures over a set of drivecycles. A methodology to select the optimal powertrain design and control strategy is demonstrated, and a sensitivity analysis of the economic gains and battery replacements is performed. Further, probabilistic variability in battery life depending on the variation of vehicle usage is assessed. A simple method is proposed and demonstrated to evaluate the excess fuel consumption due to the battery heating/cooling system. The WTW criteria pollutant emissions caused by operating a PHEV transit bus in Indiana and California are calculated and compared with those from a conventional diesel transit bus.

1.3 Contributions

In this thesis, a methodology to understand what economic and vehicle usage scenarios, as well as electricity generation scenarios that make medium/heavy-duty

PHEVs practicable, is presented. Contributions are made in: 1. Understanding the impact of variation in vehicle usage and economic scenarios on the economic gains and number of battery replacements. 2. Understanding the probabilistic variation in battery life depending on a probabilistic variation in vehicle usage. 3. Understanding the excess energy consumption required by the battery heating/cooling systems. 4. Understanding the well-to-wheel emissions from the operation of the heavy-duty PHEVs. These are described in detail in the following paragraphs.

1.3.1 Design-space Exploration of Series and Parallel PHEVs for Medium - duty Trucks and Heavy - duty Transit Buses

A framework for powertrain design including component sizing and control strategy optimization based on the total-cost-of-ownership of the PHEV was proposed and demonstrated. This framework forms the basis for the other analyses performed in this thesis and has been described in Chapter 3.
This effort was led by Ashish Vora, with help from Xing Jin, Tridib Saha and the author.

1.3.2 Selection of a Winning Solution and Sensitivity Analysis

A method to select a single customized powertrain configuration from the 800-1300 configurations explored, is presented. The sensitivity of the number of ESS replacements, fuel consumption reduction, Net Present Value and Payback Period to change in economic and vehicle parameters is analyzed. The framework, assumption and results have been outlined in Chapter 4.
This effort was led by the author with significant help from Ashish Vora, Xing Jin and Tridib Saha.

1.3.3 Uncertainty in Battery Life

Number of battery replacements significantly impact the life-cycle cost of the vehicle and depend upon the vehicle usage. Potential frameworks, with and without Markov Chain Monte Carlo, are discussed to understand the probabilistic variation in battery life depending on battery usage. Results are demonstrated using a framework to determine the probabilistic variation in battery life depending on the probabilistic variation of battery recharge C-rate, time between recharges, battery temperature of operation, without MCMC, for 2 drivecycles. The framework, assumptions and results have been outlined in Chapter 5 .

The development of the MCMC algorithm and code was led by Aniruddha Jana, while the validation of the algorithm was led by the author. The framework development and demonstration of results was led by the author with help from Xing Jin, Tridib Saha and Aniruddha Jana.

1.3.4 Effect of Heating/Cooling System on Fuel Consumption

Although multiple studies exist that propose different heating/cooling systems for batteries, a computationally efficient method to compare the fuel consumption impacts of these methods is required. A method to determine the excess fuel consumption caused by the battery heating/cooling system, when operated in different ambient temperatures is presented. The framework, assumptions, and results have been outlined in Chapter 6 .

This effort was led by the author.

1.3.5 WTW Emission Impacts of Series PHEV Transit Buses in Indiana and California

Apart from the life-cycle costs of the PHEVs, it is necessary to consider the well-to-wheel emissions caused by the PHEVs to get a more holistic understanding of

the advantages, disadvantages of these vehicles and an understanding of under what electricity generation scenarios do PHEV Transit Buses make sense. A framework utilizing GREET 2017 is discussed and demonstrated to calculate the WTW emissions of criteria pollutants from PHEV Transit Buses to be operated in Indiana and California and compared to those from conventional Transit Buses. This is discussed in Chapter 7.

This effort was led by the author with assistance from Nachiket Vatkar.

1.4 Outline

- CHAPTER 2: Simulation Models - In this chapter, the vehicle, battery performance, battery degradation and the economic models considered, are summarized.
- CHAPTER 3: Evaluating Economic Validity of MD Truck and Transit Bus - In this chapter, the economic validity of the medium-duty truck and transit bus over different drivecycles is compared, and architecture selection from the life-cycle cost perspective is explored.
- CHAPTER 4: Selection of Winning Solution and Robustness Analysis- In this chapter, a methodology to select an optimal powertrain design and control strategy, is proposed. A sensitivity analysis of battery replacements and economic gains to economic scenarios and vehicle parameters, is performed.
- CHAPTER 5: Determining Variability in Battery Life - In this chapter, a framework to understand the impact of variability of battery usage conditions on battery life and hence on the economic validity, is proposed and demonstrated.
- CHAPTER 6: Impact of battery heating/cooling system on fuel consumption and economic validity: In this chapter, a method to calculate the excess fuel consumption required to maintain the battery at desired temperatures for different ambient temperatures, is proposed.

- CHAPTER 7: Understanding WTW emission impacts of PHEV Transit Buses: In this chapter, the WTW emissions of criteria pollutants resulting from the operation of a PHEV transit bus in Indiana and California, are calculated and compared with the WTW emissions resulting from the operation of conventional diesel buses.

- CHAPTER 8: Conclusions: In this chapter, the findings from all the chapters are summarized.

- CHAPTER 9: Recommendations: In this chapter, possible directions for future work are recommended.

2. METHODS AND MODELS

2.1 Vehicle Simulation Model

A commercially available vehicle simulation tool, Autonomie, developed by Argonne National Labs, is used here. This is a MATLAB/Simulink based simulation tool that has component-level models of all components in the powertrain, driver, environment and vehicle controller. The models are flexible enough to allow modifications in each component. Two hybrid powertrain architectures have been considered in this study, as shown in Figure 2.1 and Figure 2.2. In the parallel architecture, the battery and motor are connected in parallel with the engine such that the motor and engine can independently provide torque to the wheels. In the series architecture, the engine is mechanically disconnected from the wheels. The tractive power required at the wheels comes from the motor only, thus requiring the motor to be large enough to source all the tractive power.

The driver is modeled with look-ahead, hence knows the drivecycle in advance as well as the current speed of the vehicle, from which it generates acceleration and brake

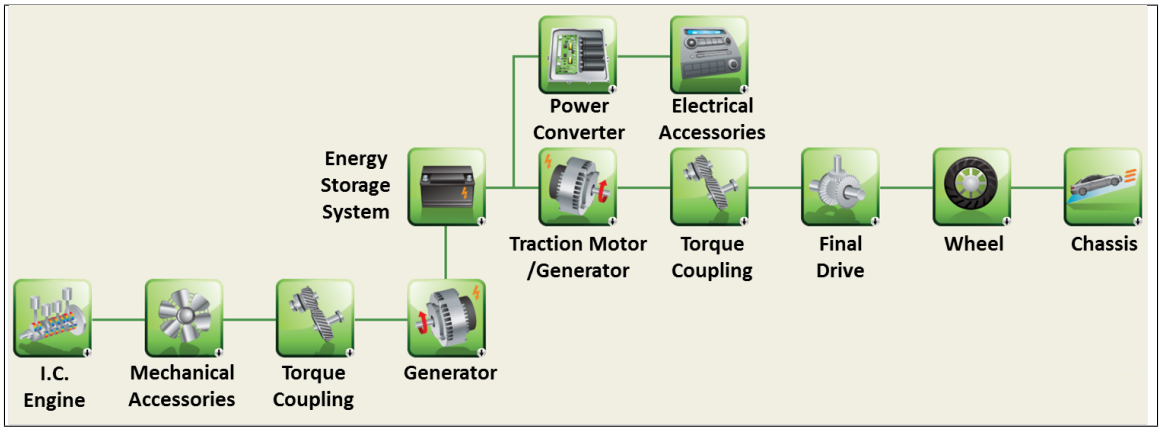

Figure 2.1. Series architecture.

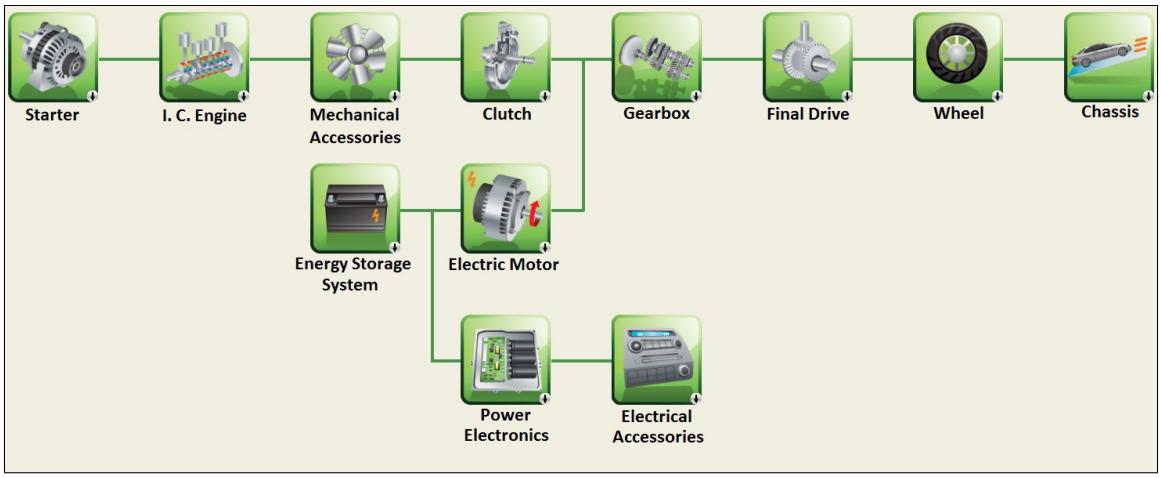

Figure 2.2. Parallel pre-transmission architecture.

pedal demands for the vehicle controller. The vehicle controller, while knowing the driver demands, also knows the instantaneous propulsion power limits of the engine, and motor (and generator for the series architecture) as well as the discharge and charging power limits for the battery. The vehicle controller implements a rule based power management strategy to determine the power split between the engine and the battery.

The acceleration pedal demand from the driver contains harsh transients, which can propagate to the engine or battery, affecting their life. Hence, it is first smoothed using a low pass filter (as described in (2.1), by K_{AccP} and T_1). This gives the power required at the wheels, P_{whl}. The combined engine and battery power needs to meet P_{whl}.

$$\textit{Low Pass Filter Transfer Function: } F(s) = \frac{K_{\text{AccP}}}{T_1 s + 1} \tag{2.1}$$

$$P_{\text{whl}} = \frac{K_{\text{AccP}}}{T_1} * \exp\left(-t/T_1\right) * \text{AccPedal} \tag{2.2}$$

The engine is modeled as torque and speed based efficiency, fuel rate and maximum torque maps for a CI engine, which can be scaled to meet the maximum power required from the engine, in any simulation. The motor is also modeled as a torque and speed based efficiency, continuous and peak torque maps for a permanent magnet motor, which are scaled as per the peak power required. This scaling for the motor can be further improved using FEA or other computationally efficient strategies such as the one suggested in [67].

2.1.1 Battery Performance Model

The battery performance model predicts the instantaneous values of battery terminal voltage and state of charge, depending on the current supplied by the battery. Classified in a broad sense, there are two types of battery performance models: electrochemical models [68] [69] [70] [71] and equivalent-circuit models [72] [73] [74]. Electrochemical models use differential equations to model the mass balance, charge

balance in the solid and and solution phases, and charge transport across the cell, which need to be solved simultaneously to determine the battery voltage. These are more physics based and require a knowledge of specific parameters related to the chemistry of the battery. Also, they typically require more computational time but can be applied during varying operating scenarios with minimal loss of accuracy. Equivalent-circuit models, on the other hand, represent the battery using a voltage source, a resistance and zero or more resistance-capacitance (RC) branches connected in series. The resistance-capacitance and voltage source values are typically a function of the state of charge (SOC) of the cell and temperature, and are obtained by fitting the voltage across the loop to the experimental charge-discharge characterization cycles of the cell. These models, although fitted to limited data, are computationally fast and accurate for the operating conditions over which the data was obtained. The equivalent-circuit models have been used for all sections of this study. Furthermore, depending on the number of RC branches used to model the cell, these models can be classified as 0^{th} order, 1^{st} order, etc. In either case, the ESS pack is considered to consist of 2 modules in parallel where each module consists of multiple cells in series. The voltage equations for each of these are discussed next. For both the cases the SOC is determined using Coulomb counting, as shown in (2.3), where SOC_{init} is the initial SOC of the cell, I is the current sourced/sunk by the cell and $AhCap$ is the ampere-hour capacity of the cell. The cells are assumed to be balanced, i.e. all cells in the battery pack are assumed to have the same SOC.

$$SOC = SOC_{\text{init}} - \frac{\int I dt}{AhCap} \tag{2.3}$$

0^{th} *Order Equivalent-Circuit Model*

The cell is modeled using a 0th order equivalent-circuit model, as shown in Figure 2.3, using an open-circuit voltage ($V_{\text{OC}}(SOC)$) that battery exhibits at it's terminals when there is no load attached to it, an internal resistance ($R_{\text{int}}(SOC)$) that emulates the resistance of the current collectors, the SEI layer etc. and the terminal voltage (V_{term})

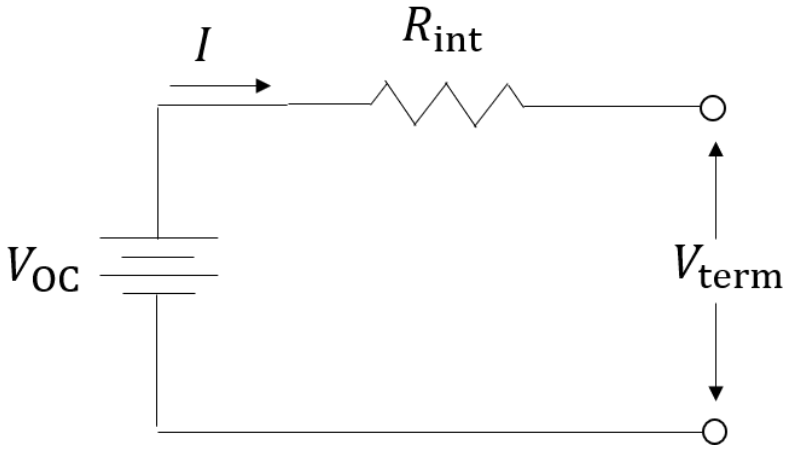

Figure 2.3. 0^{th} order equivalent-circuit model.

that emulates the voltage at the terminal of the battery when a load is attached to it and is calculated as shown in (2.4).

$$V_{\text{term}} = V_{\text{OC}} - I * R_0 \tag{2.4}$$

1^{st} *Order Equivalent-Circuit Model*

The cell is represented using the 1^{st} order equivalent-circuit model shown in Figure 2.4, where V_{OC} is the open-circuit voltage, V_{term} is the terminal voltage, V_0 and V_1 are voltages across the resistance and resistance-capacitance pair respectively. The cell is represented using R_0, which emulates the ohmic resistance of the current collectors and the separator and the R_1C_1 pair emulates the diffusion of Li ions from the anode to the cathode.

$$V_{\text{term}} = V_{\text{OC}} - V_0 - V_1 \tag{2.5}$$

$$V_0 = I_0 * R_0 \tag{2.6}$$

$$I_C = C * \frac{dV_1}{dt}; V_1 = (I_0 - I_C) * R_1 = I_1 * R_1 \tag{2.7}$$

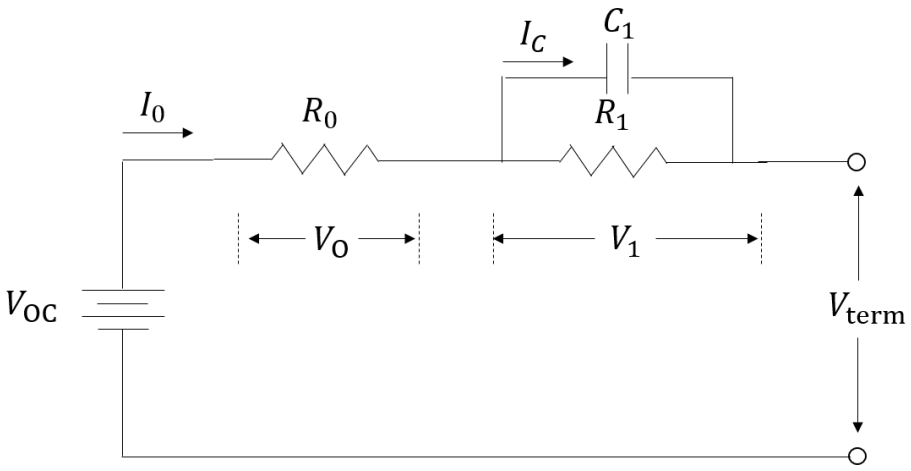

Figure 2.4. 1^{st} order equivalent-circuit model.

The terminal voltage of the battery is maintained within the manufacturer specified voltage limits ($V_{\max}$ and $V_{\min}$) by the battery management strategy to prevent failures and fires. (2.8) and (2.9) define the maximum discharge and charge powers for the entire SOC range, which ensure that the maximum terminal voltage does not increase beyond $V_{\max}$ during charge, and that it does in reduce lower than $V_{\min}$ during discharge.

$$P_{\text{V\_dis\_max}} = (V_{\text{OC}} - V_{\min}) * \frac{V_{\min}}{R_{\text{int}}} \tag{2.8}$$

$$P_{\text{V\_chg\_max}} = -(V_{\max} - V_{\text{OC}}) * \frac{V_{\max}}{R_{\text{int}}} \tag{2.9}$$

In addition to the voltage limits, current limits have been imposed to ensure no exposure to high C-rates that can aggravate battery degradation, as given by (2.10) where $C\text{-}rate_{\max}$ is the maximum allowed C-rate and $AhCap$ is the Ah capacity of the battery.

$$I_{\text{C-rate\_max}} = C\text{-}rate_{\max} * AhCap \tag{2.10}$$

The current limits are implemented as maximum charge and discharge powers using (2.11) and (2.12).

$$P_{\text{C-rate\_dis\_max}} = (V_{\text{OC}} - I_{\text{C-rate\_max}} * R_{\text{int}}) * I_{\text{C-rate\_max}} \tag{2.11}$$

$$P_{\text{C-rate\_chg\_max}} = -(V_{\text{OC}} + I_{\text{C-rate\_max}} * R_{\text{int}}) * I_{\text{C-rate\_max}} \tag{2.12}$$

Figure 2.5 is a representation of the variation of voltage based and C-rate based power limits with SOC. The final "physical" limit of the battery is the stricter of the voltage and C-rate based power limits during charge and discharge, as given in (2.13) and (2.14).

$$P_{\text{batt\_dis\_max}} = \min(P_{\text{V\_dis\_max}}, P_{\text{C-rate\_dis\_max}}) \tag{2.13}$$

$$P_{\text{batt\_chg\_max}} = \min(P_{\text{V\_chg\_max}}, P_{\text{C-rate\_chg\_max}}) \tag{2.14}$$

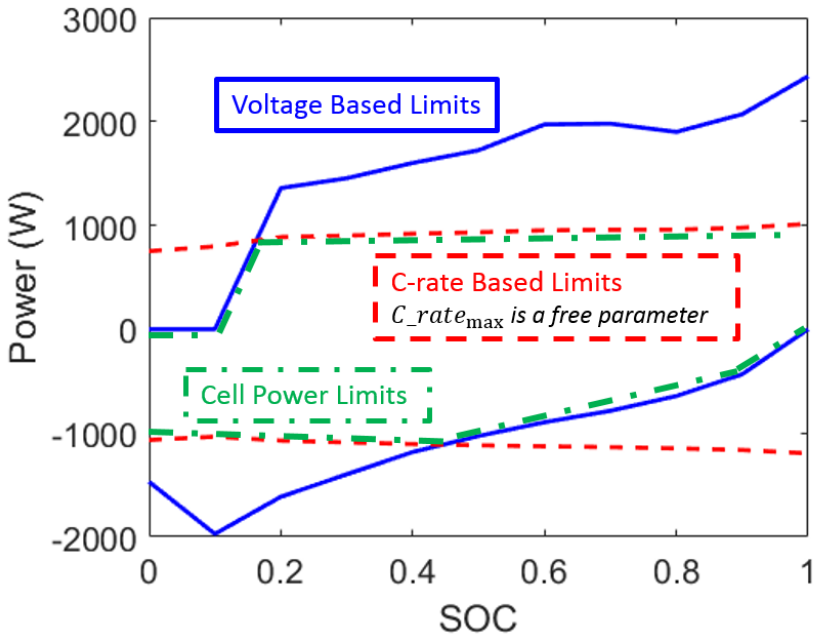

Figure 2.5. Voltage and C-rate based cell power limits.

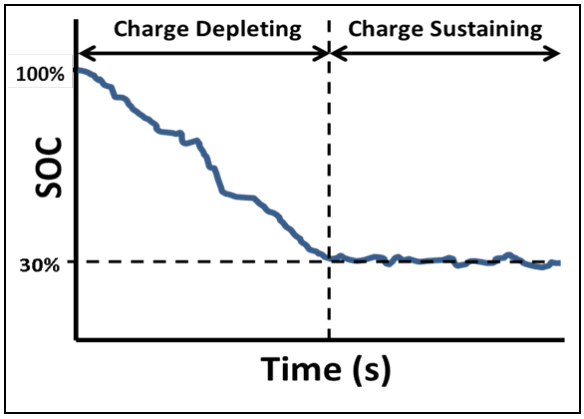

Figure 2.6. Vehicle modes of operation.

2.1.2 Modes of Operation

The vehicle operation is divided into two modes viz. charge depleting (CD) and charge sustaining (CS), as shown in Figure 2.6. Assuming that the battery is fully charged overnight, the first mode of operation for the day is the charge depleting mode in which the battery is used as the dominant source of power and is allowed to absorb the regenerative energy. The engine helps provide any excess power, if required, during this mode. Assuming that the SOC of the battery is 100 % at the beginning of this mode, it is allowed to deplete to 30 %, hence *'charge depleting'*. Once the battery reaches 30 % SOC it is not allowed to deplete any further. The engine becomes the dominant source of tractive power. The battery is allowed to absorb energy due to regenerative braking and release this energy to assist the engine such that an average SOC of 30 % is maintained, hence *'charge sustaining'*.

2.1.3 Control Strategy

Battery Power Demand

The battery power limits defined in the battery management strategy define the "physical" limits of the battery that shouldn't be exceeded to prevent aggravating battery degradation as well as failures. The battery region of operation, which dictates

the power provided by the battery in the CD and CS modes, is governed by the "control" power demand, which is different in both the modes. The area on the Power vs SOC plot allowed by the physical limits is sectioned to define the battery region of operation for both the modes. In the charge depleting mode, since the battery is required to be the dominant source of power, the maximum power demand is the same as maximum "physical" limit while the minimum power demand is zero, until the battery reaches the target SOC, as shown in (2.15) and Figure 2.7a.

$$P_{\text{batt\_min}} = 0; P_{\text{batt\_max}} = P_{\text{batt\_dis\_max}} \tag{2.15}$$

In the charge sustaining mode, the battery needs to maintain the target SOC. If the SOC shifts away from the target SOC, due to the battery assisting the engine or due to absorption of regenerative braking energy, the battery is made to discharge/recharge the excess energy. Therefore for $SOC > SOC_{\text{target}}$, the minimum power demand linearly increases as the SOC is further away from the target SOC, and the maximum power demand is equal to the maximum physical limits, as given in (2.16), and shown in Figure 2.7b. When $SOC < SOC_{\text{target}}$, the minimum power demand is equal to the charging power limit and the maximum power demand linearly becomes more negative further away from the target SOC, as shown in (2.17) and Figure 2.7b. The linear increase/decrease of the power demand is defined using $\tan(\theta_{\text{SOC\_reg}})$. With higher $\theta_{\text{SOC\_reg}}$, the target SOC will be maintained more aggressively.

$$P_{\text{batt\_min}} = \tan(\theta_{\text{SOC\_reg}}) * (SOC - SOC_{\text{target}}); P_{\text{batt\_max}} = P_{\text{batt\_dis\_max}} \tag{2.16}$$

$$P_{\text{batt\_min}} = P_{\text{batt\_chg\_max}}; P_{\text{batt\_max}} = \tan(\theta_{\text{SOC\_reg}}) * (SOC - SOC_{\text{target}}) \tag{2.17}$$

The determination of battery physical limits and control limits to maintain the region of operation is the same for both the series and parallel architectures. But since the engine and motor are connected differently to the wheels in both the architectures,

their respective power shares are determined differently.

Engine and Motor Power Demand

The strategy for calculating the power demands for the engine and motor, given the battery power demand, is the same for the CS mode and CD mode after the engine has turned ON. In the CD mode, the engine is allowed to turn ON to assist the battery only when the wheel power demand exceeds a fraction (F_{EngON}) of the instantaneous maximum discharge power limit of the battery, as shown in (2.18).

$$\textit{In the CD mode the engine turns ON if } P_{\text{whl}} > F_{\text{EngON}} * P_{\text{batt\_max}} \tag{2.18}$$

In the series architecture, since the engine is mechanically disconnected from the wheels, the engine has the flexibility to operate at it's most efficient point ($P_{\text{eng\_opt}}$), irrespective of the speed. The power demanded from the engine is then adjusted around this point of operation so as to complement the power provided by the battery. It is shown in Figure 2.8 and (2.19) how the battery SOC and mode dependant engine power limits are determined. These limits are then applied to the optimal point of engine operation, as shown in Figure 2.9 and (2.20), to provide the battery power dependant adjustment of engine power demand, followed by the physical maximum engine power limit to give the power demanded from the engine. Since the motor is connected in series with the wheels, it needs to provide all the power required at the wheels as given in (2.21).

$$P_{\text{eng\_hi}} = P_{\text{whl}} - P_{\text{batt\_min}}; P_{\text{eng\_lo}} = P_{\text{whl}} - P_{\text{batt\_max}} \tag{2.19}$$

$$P_{\text{eng}} = \min(P_{\text{eng\_max}}, \min(P_{\text{eng\_hi}}, \max(P_{\text{eng\_lo}}, P_{\text{eng\_opt}}))) \tag{2.20}$$

$$P_{\text{mot}} = P_{\text{whl}} \tag{2.21}$$

For the parallel architecture, although the engine is not mechanically disconnected from the wheels, a maximum efficiency operating point can be obtained for each en-

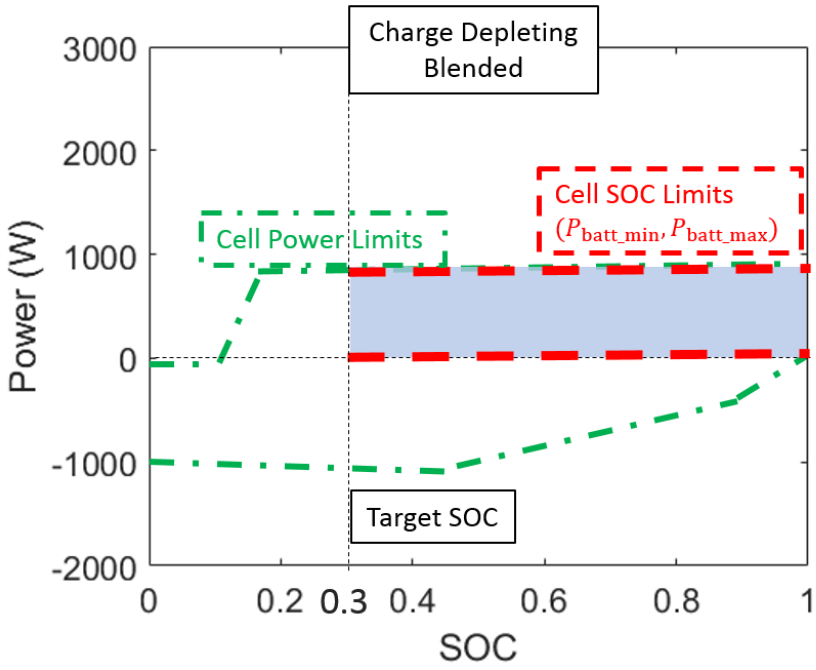

(a)

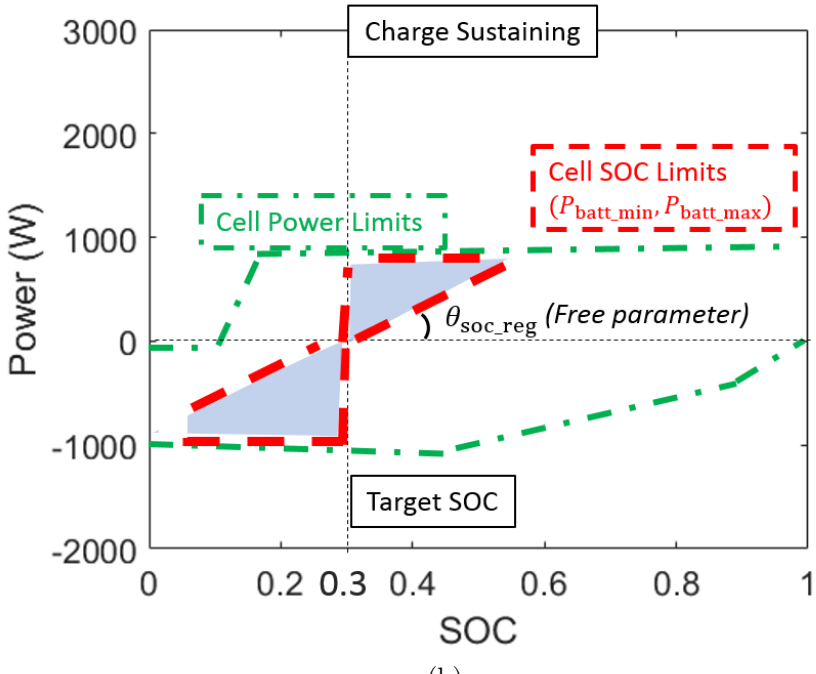

(b)

Figure 2.7. Cell limits in the (a) Charge Depleting mode and (b) Charge Sustaining mode.

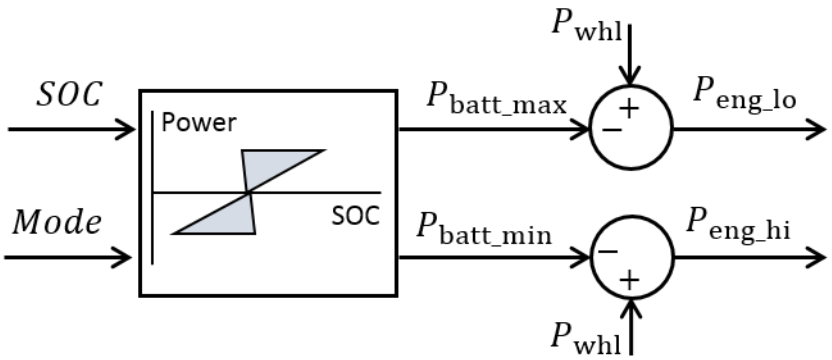

Figure 2.8. Battery SOC and vehicle mode based engine power limits.

gine speed. These points define the optimal curve for engine operation ($P_{\text{eng\_opt}}(w_{\text{eng}})$). Therefore, the determination of engine power demand is similar to the series architecture, except that $P_{\text{eng\_opt}}$ is now dependant on the engine speed, as shown in Figure 2.10a. $P_{\text{eng\_hi}}$ and $P_{\text{eng\_lo}}$ are defined in Figure 2.8. In the parallel architecture, the required power at the wheels is provided by a combination of the motor and engine powers. Therefore, the motor power demand is calculated from the engine and wheel power demands as given by (2.23). This motor power demand is further subjected to motor and battery power limits and the final engine power demand is recalculated as shown in Figure 2.10b to ensure that the required wheel power is met by the engine and the motor.

$$P_{\text{eng}} = \min P_{\text{eng\_max}}, \min[P_{\text{eng\_hi}}, \max(P_{\text{eng\_lo}}, P_{\text{eng\_opt}}(w_{\text{eng}})] \tag{2.22}$$

$$P_{\text{mot}} = P_{\text{whl}} - P_{\text{eng}} \tag{2.23}$$

2.2 Battery Degradation Models

While the battery performance models estimate the instantaneous battery terminal voltage and SOC, the battery degradation models are used to predict the change

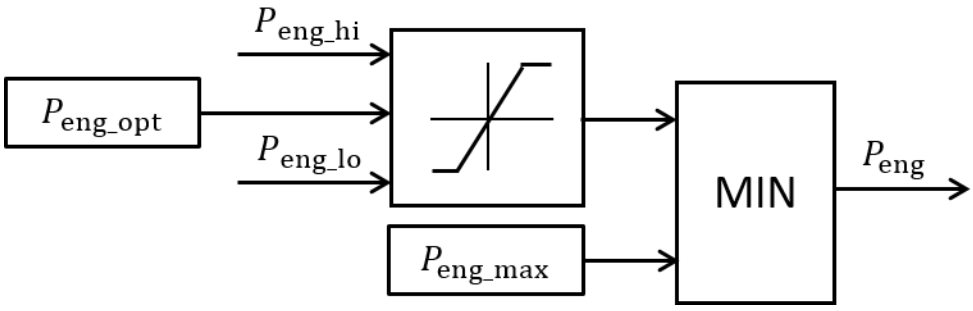

Figure 2.9. Engine power demand calculation based on a single optimal operating point for the series architecture.

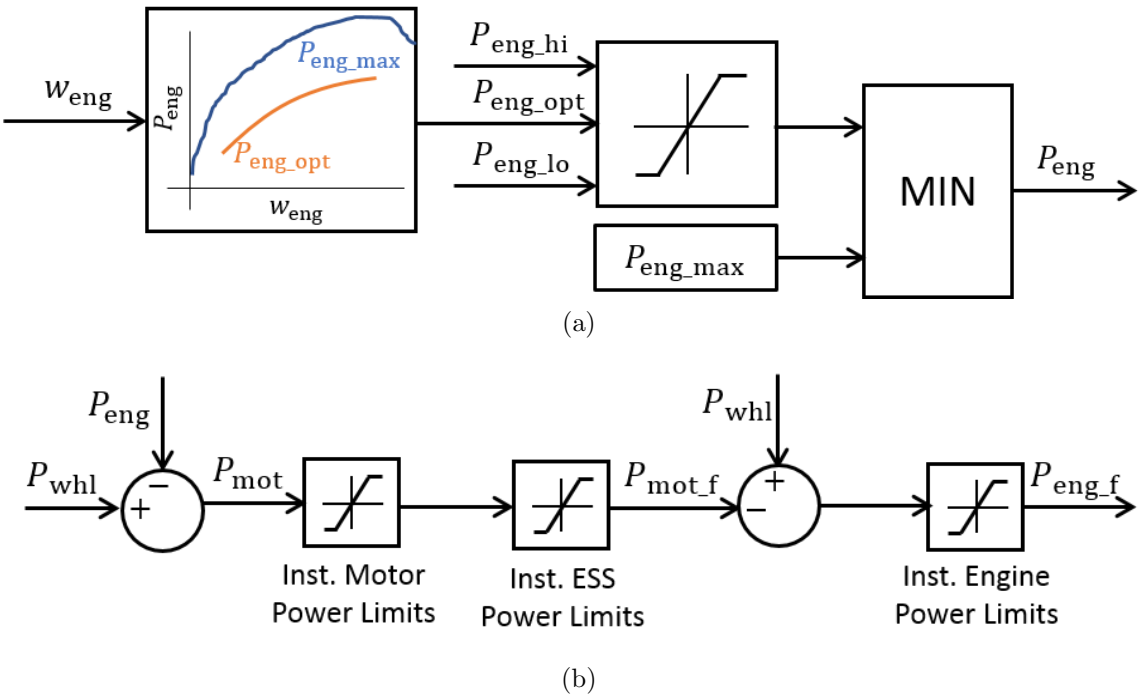

Figure 2.10. (a) Engine power demand and (b) motor power demand calculation for the parallel architecture.

in the energy capacity, power sourcing and sinking capability, losses associated with the battery over time and use. A battery consists of two electrodes - the anode and the cathode separated by a separator that is non-permeable to electrons, and electrolyte. The electrodes are made up of a matrix like structure that can be thought of as garages that house the Li-ions and electrons. During discharge, the Li-ion and electron pair separates at the anode, the electrons travel to the cathode from the external circuit while the LI-ions travel to the cathode from within the battery by crossing the separator, and both unite at the cathode. Reverse process happens during charging. Over usage, following dominant phenomena occur with graphite anodes in Li-ion batteries:

- The loss of cyclable Li-ions in the battery due irreversible side reactions consuming those ions to form other products (such as the Solid Electrolyte Interface (SEI) layer), thus rendering those Li-ions incapable of carrying charge. These products deposit on the active particle, making it difficult for the Li-ion to enter or exit and hence can also increase the internal resistance of the battery.

- The loss of the electrode active material ("garages") that house the Li-ion, which happens due to the continuous stresses due to insertion and de-insertion of Li-ions from the particle, which fracture the particle thereby losing the Li-ions already contained in it as well as not providing that space for the successive Li-ions. These fractured particles can also isolate other "good" active particles thereby further reducing the Li-ion holding capability of the electrode.

Other degradation mechanisms like dendrite growth, manganese poisoning, cathode active material loss also occur in batteries in varying proportions according to the cathode used along with the graphite anode and according to the operating conditions of the battery. But the mechanisms mentioned above are considered to be dominant for the purpose of this thesis.

Loss of energy capacity occurs due to the loss of cyclable Li-ions, or electrode active material in the battery, and is manifested as reduction in the CD mode range

for the PHEV. Loss of power capacity occurs due to an increase in the internal resistance of the battery, which results in the battery physical limits becoming stricter, thereby reducing the regenerative absorbing potential as well as power assist capability of the battery. Both of these reduce the contribution of the battery to tractive power, thereby increasing the fuel consumption of the vehicle. The impact of battery degradation on the fuel consumption of a parallel HEV transit bus was demonstrated by in [5] where about the fuel consumption was shown to increase by about 10% over the battery life. It is therefore necessary to capture battery degradation as accurately as possible.

The battery degradation models available in the literature can be broadly classified as empirical and phenomenological models. The empirical models rely on experimental battery degradation data to fit the capacity and/or power loss curves as functions of operating parameters such as temperature, DOD, Ah-throughput etc. These models are fast but reliably accurate only in the operating condition range they were tuned in [75] [76]. As long as their usage is limited to the operating conditions they were defined on, they can be used for large parametric simulations studies because of the minimal time penalty.

Phenomenological models, on the other hand, are based upon physics based complex mathematical expressions of the degradation phenomena that occur in the battery. While these expressions can be used across all operating conditions, these models are not very computationally efficient [68]. Also, to be able to mathematically model every new individual degradation phenomenon requires enough experimental data explaining the occurrence of the phenomenon, which is expensive. Realizing this gap in the literature, as further explained in [77], a reduced order physics based capacity loss model for graphite anodes was proposed that captures the phenomena explained previously and validates the model with experimental data for the Lithium ferrous phosphate/graphite (LFP/Graphite) cell [78].

Two of these models have been used for two different battery chemistries in this thesis. The empirical model for Nickel cobalt manganese + lithium manganese oxide

cathodes and graphite anodes (NCM+LMO/Graphite) as proposed in [75] has been used in Chapter 3 for the large parametric simulation study conducted for powertrain design of series and parallel PHEVs. The reduced order capacity loss model proposed in [78] is used in Chapter 5 for the LFP/Graphite batteries because of it's physics based nature that allows it to be used over a broader range of operating conditions.

2.3 Economic Calculations

The vehicle simulation model gives the energy (fuel and electricity) consumption of the vehicle. The battery degradation model provides the capacity loss of the battery. This capacity loss can then be used to determine the battery life and hence the number of battery replacements over vehicle life. The cost of battery replacements and the fuel and electricity charging costs define the operating cost of the PHEV. While the fuel and electricity costs occur each year, the battery replacement costs occur in the year the battery capacity reaches end-of-life. For the conventional vehicle, the fuel costs are considered as the operating costs. Also, since the PHEV powertrain consists of components like the battery and the motor that are not part of the conventional vehicle powertrain, the costs of these components is considered as the excess initial cost of the PHEV, considered to occur at day 0 of the vehicle life. The cost savings due to downsizing of the engine are not considered here. These three costs, viz. the operating cost of the PHEV, the operating cost of the conventional vehicle and the excess initial cost of the PHEV are used to compare the powertrain designs by calculating the following metrics:

- Net Present Value (NPV): This is the time-discounted value of the future costs of the powertrain design (battery replacement and energy costs) that gives it's worth in the present value, as shown in (2.24), where ISC is the initial system cost (\$) that occurs on day 0, CF_i is the total cash flow (\$) that occurs in year i, and r is the social discount rate. The ISC is defined as shown in (2.25), where IntPrem is the manufacturer integration premium or markup, $A_0(\$), A_1(\$/\text{kW})$

are the constant and per kW motor costs, and A_2 is the \$/kWh cost of the battery, MPP is the motor peak power and ESSCap is the kWh capacity of the battery. The Net Present Value considered in this thesis is the difference between the NPV of the PHEV and that of the conventional vehicle. Higher NPV is better.

$$\text{NPV}(\$) = \text{ISC} + \sum_{\text{i=1}}^{n} \frac{\text{CF}_i}{(1+r)^i} \tag{2.24}$$

$$\text{ISC}(\$) = \text{IntPrem} * (A_0 + \text{MPP} * A_1 + \text{ESSCap} * A_2) \tag{2.25}$$

- Payback Period (PBP): This is the time taken in years by a PHEV powertrain design to recover the initial system cost through the operating cost savings over the conventional vehicle, as shown in (2.26). The costs considered for the payback period calculation are not time discounted. Lower payback period is better.

$$\text{PBP} = n^* \text{such that} \text{NPV} = 0, \text{considering non-discounted cash flow} \tag{2.26}$$

- Annual Cost Savings per Mile (AnnCS/mile): This is difference in the annual operating costs of the PHEV and the conventional vehicle, not including the battery replacement costs, divided by the miles traveled annually to get a \$/mile number, as shown in (2.27), where $\text{CF}_{\text{conv\_fuel}}$ is the annual fuel cost for the conventional vehicle, $\text{CF}_{\text{PHEV\_fuel}}$ and $\text{CF}_{\text{PHEV\_elec}}$ are the annual fuel and electricity costs for the PHEV respectively. Note that this value is calculated using the non-discounted cash flows, the annualized cost savings per mile can be calculated by annualizing the NPV and then dividing it by the AVMT, thus taking the discounted value of the battery replacement costs and other future cost savings into account. For the purpose of this thesis, the simpler definition of

annual cost savings per mile as defined in (2.27) has been used. Higher annual cost savings per mile is better.

$$\text{AnnCS/mile} = \frac{\text{CF}_{\text{conv\_fuel}} - (\text{CF}_{\text{PHEV\_fuel}} + \text{CF}_{\text{PHEV\_elec}})}{\text{AVMT}} \tag{2.27}$$

2.4 Conclusions

In this chapter, an overview of the models and methods used in the thesis is presented. In particular, the vehicle simulation models for the series and parallel architectures are discussed. The battery performance models which estimate battery terminal voltage and SOC are shown. The battery needs to be maintained within the manufacturer specified voltage limits, the battery management strategy used to ensure this as well as limit the C-rate during charge and discharge is discussed. The control strategy that determines the power split between the battery, engine and motor is also discussed for both the architectures. Finally, the economic model used to calculate the Net Present Value, payback period, and annual cost savings/mile is discussed.

3. EVALUATING ECONOMIC VALIDITY OF MD TRUCK AND TRANSIT BUS

3.1 Simulation Setup

The simulation setup, as shown in Figure 3.1, consists of a vehicle simulation tool to predict the fuel consumption and battery duty cycle, battery degradation model to predict the capacity loss depending on the battery duty cycle, and economic post-processing to understand the number of battery replacements and total cost of ownership depending on the fuel consumption and battery capacity loss. The inputs to the vehicle simulation model is a deterministic drive cycle (e.g. Manhattan, Pickup and Delivery Class 6 etc.), vehicle parameters (e.g. coefficient of drag and rolling resistance, vehicle mass), control parameters for the power split, sizing parameters for the engine, motor and battery.

3.1.1 Vehicle Simulation Model

A commercially available vehicle simulation tool called Autonomie, developed by Argonne National Labs, is used here. This is a Simulink based forward simulation tool that has component level models of all components in the powertrain, driver, environment and vehicle controller that is flexible enough to allow modifications in

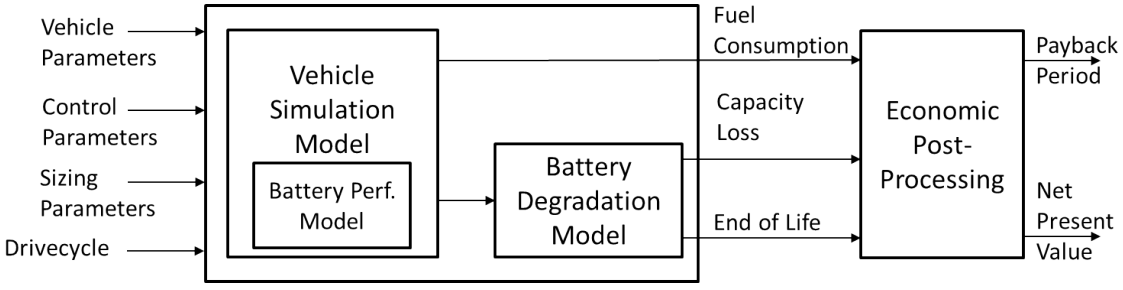

Figure 3.1. Simulation framework.

each component. Two hybrid powertrain architectures have been considered in this study, as shown in Figure 2.2 and Figure 2.1.

3.1.2 Modes of Operation

The vehicle operation is divided into two modes viz. charge depleting (CD) and charge sustaining (CS), as shown in Figure 3.2. Assuming that the battery is fully charged overnight, the first mode of operation for the day is the charge depleting mode where the battery is used as the dominant source of power. The engine helps provide any excess power if required during this mode. Assuming that the SOC of the battery is 100 % at the beginning of this mode, it is allowed to deplete to 30 %, hence *'charge depleting'*. The battery is allowed to absorb power from regenerative braking. Once the battery reaches 30 % SOC it is not allowed to deplete any further. The engine becomes the dominant source of tractive power. Additionally, the battery is allowed to absorb energy due to regenerative braking and release this energy to assist the engine such that an average SOC of 30 % is maintained, hence *'charge sustaining'*.

3.1.3 Powertrain Sizing and Control Strategy Parameters

The important parameters in powertrain sizing and control strategy considered in this study are:

- Sizing parameters: The energy sources and converters- engine, ESS, and motor -are considered for sizing in this study.
  - The engine and the motor are modeled as static maps which are scaled to match the peak power requested by the design of experiments.
  - The ESS performance model shown in Figure 3.1 is modeled by a cell-level 0^{th} order equivalent-circuit model, where the internal resistance of the battery is modeled by a single resistor. The cell-level voltage and current

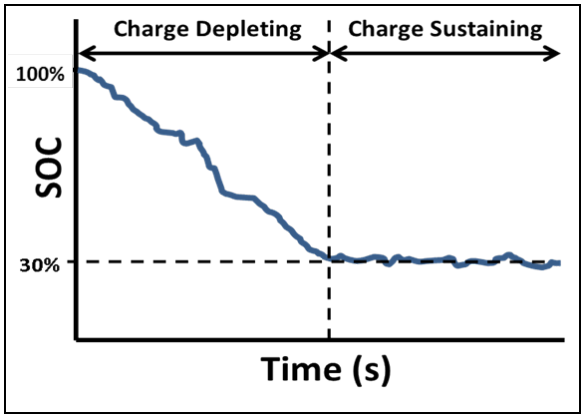

(a)

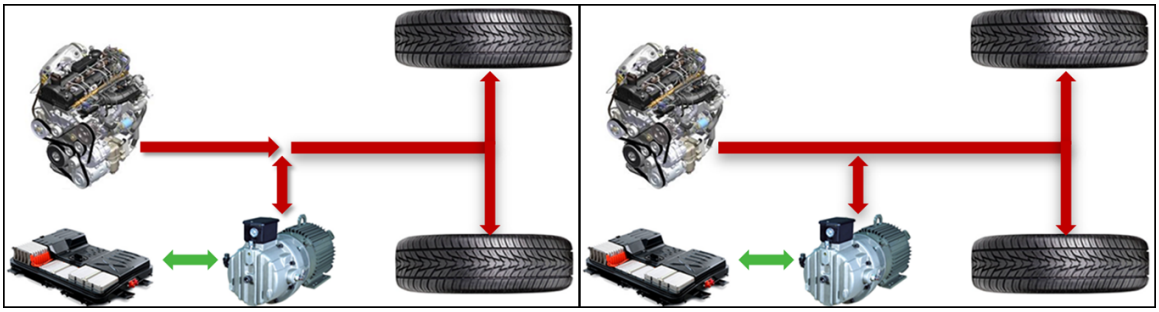

(b) (c)

Figure 3.2. (a) Vehicle modes of operation (b) Operation in charge depleting mode (c) Operation in charge sustaining mode.

are then scaled to the pack level voltage and current. The pack consists of two battery modules in parallel where each module consists of the same number of cells in series. This number of cells in series is varied in the design of experiments. The cell-to-cell variations have not been considered here.

- Vehicle Parameters: These are the parameters that the powertrain is designed for but vary over a day and also over the life of the vehicle.
  - Vehicle Mass: The mass of the truck or bus at any time is dependent on the mass of the chassis, which can be designed, and the mass of the cargo/passengers in the vehicle at any point of time. Though there are limits for the overall mass of cargo/passengers that can go into the vehicle, the actual vehicle mass varies throughout the day.
  - Coefficient of drag: This factor depends on the design and can change during manufacturing as well. It also changes due to wind directions, and the presence of other vehicles around our vehicle of interest.
  - Coefficient of rolling resistance: This factor depends on the conditions of the tires and can vary over the life of the tire.
- Control Parameters: These are knobs in the rule based control strategy that the energy management for the engine and the battery.
  - The maximum charge/discharge C-rate: This affects how fast the battery is allowed to charge/discharge, and hence maximum power that the battery can source or sink at any time.
  - Power filter time constant: This is the time constant of the first-order filter which is used to reduce the transients in the driver power demand.
  - ESS SOC regulation slope: This parameter is active only in the charge sustaining mode and regulates how aggressively the ESS SOC is maintained.

Table 3.1. Regression parameters for the battery degradation model [75].

a	8.61E-6, 1/Ah-K^2	I_{rate}	C_{rate}
b	-5.13E-3, 1/Ah-K	t	Days
c	7.63E-1, 1/Ah	E_{a}	24.5, kJ/mol
d	-6.7E-3, 1/K-C_{rate}	R	8.314, J/(mol-K)
e	2.35, 1/C_{rate}	T	K
f	14,876, 1/day$^{1/2}$		

– Fraction of power for the engine to turn ON: This parameter is active in charge depleting mode. When the wheel power demand exceeds this fraction of the maximum battery power, the engine is requested to turn ON.

3.1.4 Battery Degradation Model

The NMC+LMO/Graphite chemistry is considered here. An Ah throughput and temperature based capacity loss model proposed by [75], shown in (3.1), has been used. In this equation, *a,b,c,d,e,f* are regression coefficients. The model consists of two terms - calendar aging, which is proportional to the square root of time and has an Arrhenius relation with temperature, and cyclic aging, which is exponentially dependent on the C-rate and linearly dependent on Ah throughput. This model has been generated using experimental data up to a C-rate of 6.5C and 46°C, while the C-rate is limited to 4C in our simulation, hence the degradation predictions are assumed to be accurate enough for our use.

$$Q_{\text{loss},\%} = (aT_{\text{batt}}^2 + bT_{\text{batt}} + c)\exp[(dT_{\text{batt}} + e)C\_rate]Ah_{\text{throughput}} + ft^{0.5}\exp[\frac{-E_{\text{a}}}{RT_{\text{batt}}}] \tag{3.1}$$

3.1.5 Economic Calculations

The results obtained from each of the modes are weighted by the utility factor. This weighting is elaborated by (3.2) and (3.3).

$$\mathrm{UF} = \frac{\mathrm{CD\_Range}}{\mathrm{Daily\_VMT}} \tag{3.2}$$

$$\mathrm{Result_{UF}} = \mathrm{UF} * \mathrm{Result_{CD}} + (1 - \mathrm{UF}) * \mathrm{Result_{CS}} \tag{3.3}$$

The utility factor weighted results give the per day values for fuel consumption, energy consumption and capacity loss. These results are extrapolated to a year and used to estimate the number of battery replacements over the vehicle life (defined to be 12 years, here).

Additionally, four cost scenarios have been defined as shown in Table 3.2. The fuel prices are estimated from the predictions published by the U.S. Energy Information Administration in [79]. The battery and motor costs are estimated from the literature [80] and [81]. The battery and motor costs drop with time owing to better and cheaper technology and increase in demand. The fuel price increases due to depletion of resources. For a vehicle manufactured in 2015, for example, the fuel price over it's life is assumed to remain constant at \$2/gal to get a conservative estimate of costs. ESS replacement costs are treated similarly. A social discount rate of 10% on all cash flows and an OEM integration premium is assumed.

Furthermore, a constant electricity cost of \$0.1/kWh assuming negligible variation in electricity price from 2015 to 2030, and an AC charging efficiency of 90% is assumed [82] [83] [84]. The battery end-of-life is defined to be 70% of the original capacity i.e. a 30% loss of energy capacity.

The initial system cost of the plug-in HEV along with the operating costs which include the fuel cost, electrical energy costs and battery replacement cost are compared with those of the conventional vehicle to obtain comparison metrics like Payback Period, Net Present Value, Internal Rate of Return and Annualized cost savings/mile.

- Initial System Cost (ISC): This includes the cost of the motor, battery and an integration premium, as shown in (2.25).
- Net Present Value (NPV): This is the time discounted sum of cash flows, including the initial and operating costs, over the vehicle life. The NPV referred to in this document, is the difference between the NPV of the PHEV and the NPV of the conventional vehicle, as shown in (2.24).
- Payback Period (PBP): This is the time required to recover the additional initial cost of the PHEV with the fuel cost savings. The payback period calculations consider non-discounted cash flow, as shown in (2.26).
- Annualized cost savings per mile: This is the difference between the annual fuel and electricity costs for the PHEV and the conventional vehicle further divided by the AVMT, to get a $/mile number, as shown in (2.27).

Table 3.2. Economic assumptions - scenarios.

Parameter	Unit	2015	2020	2025	2030
Fuel Cost	$/gal	2	3.33	4.66	6
ESS Cost	$/kWh	500	300	200	150
Motor Cost - Slope	$/kW	33.3	27.4	21.5	15.6
Motor Cost - Intercept	$	503.5	455	406.5	358

Table 3.3. Vehicle usage assumptions.

Parameter	MD Truck	Transit Bus
Days used/year	300	300
Annual Vehicle Miles Traveled	25000	30000

3.1.6 Example Design of Experiments

An example of the variables considered and ranges used is shown in Table 3.4. The above framework is exercised for two vehicle applications, a Medium-duty truck and a Transit bus with series hybrid and parallel hybrid architectures. Three different drivecycles that cover the range of speeds and power demands that a medium-duty truck would be used on, and those that are available in literature, have been considered. They are Pickup and Delivery Class 6, Refuse Truck and New York Composite drivecycles. Similarly, the Manhattan, Orange County and two variations of the China drivecycle have been used for the transit bus. This is shown in Table 3.5.

Table 3.4. Example DOE.

Parameter	Unit	Min. Value	Max. Value
Vehicle Parameters			
Coefficient of drag	-	0.58	0.94
Coefficient of rolling resistance	-	0.006	0.008
Vehicle mass	kg	8850	15000
Powertrain Sizing Parameters			
M/G peak power	kW	150	300
Engine peak power	kW	75	200
ESS energy capacity	kWh	24.8	372.4
Control Strategy Parameters			
Maximum charge/discharge C-rate	-	1	4
Power filter time constant	-	0	0.5
ESS SOC regulation slope	W/SOC	200	20000
Fraction of power for the engine to turn on	-	0.3	0.9

Table 3.5. Scope of the present work.

Application		PD Class 6	Refuse Truck	NY Comp.	Man-hattan	Orange County	China Normal	China Aggres-sive
Truck	Series T=1300	✓	✓	✓				
	Parallel T=800	✓	✓	✓				
Bus	Series T=1000				✓	✓	✓	✓
	Parallel T=1300				✓	✓	✓	✓

3.2 Results and Discussion

800-1300 combinations of input parameters shown in Table 3.4 were simulated for each vehicle type, architecture and drivecycle combination shown in Table 3.5. Output of each simulation was evaluated for each of the four scenarios discussed above. Following were defined as the constraints for viability of any output and the outputs were filtered based on these constraints:

1. Drivecycle: The percentage of time for which the output speed of the simulation was more than 2 mph less than or greater than the desired speed (given by the drivecycle) should be less than 2%.

2. Gradability: The powertrain should be able to power the vehicle at a 7% grade and maintain 20mph.

3. Payback Period: The time required to recover the excess initial cost due to hybridization from the fuel savings as compared to the conventional vehicle should be less than 2 years.

4. ESS Replacements: The number of ESS replacements over the lifetime of the vehicle(12 years) are limited to 3.

The earliest scenario for which even one simulation passes all of the above criteria is the first scenario of economic viability, as shown in Table 3.6. This helps give an idea of when (under what fuel cost, motor cost and ESS cost) can an OEM hybridize a vehicle application, with which architecture, on what kinds of use cases (drivecycles). As the economic scenario becomes more favorable (higher fuel cost, lower motor and ESS costs), more solutions become viable as they pass the payback period constraint. Whether a solution passes the drivecycle, gradability and ESS replacement constraints for a given architecture, vehicle type and drivecycle combination depends only on the powertrain size, control strategy and vehicle parameters. It is shown in Table 3.6 that the Transit bus application becomes favorable for hybridization before the medium duty truck application. This can be primarily attributed to the vehicle mass differences between applications and the drivecycles of use. These

Table 3.6. First scenario of economic viability for MD truck and transit bus PHEV applications with series and parallel architectures.

Application		PD Class 6	Refuse Truck	NY Comp.	Man-hattan	Orange County	China Normal	China Aggres-sive
Truck	Series T=1300	2030	2030	2025				
	Parallel T=800	2025	2025	2025				
Bus	Series T=1000				2020	2025	2020	2020
	Parallel T=1300				2015	2020	2020	2015

two factors govern the tractive power requirement and hence the battery usage and hence battery replacements, and also the amount of regenerative energy that can be recovered. These effects can be more prominently observed in the cost savings that can be achieved by both the applications.

Annual cost savings/mile, which are savings with respect to the corresponding conventional vehicle on a drivecycle, vs. initial system cost for every application, architecture and drivecycle combination, are shown in Figure 3.3. All solutions having positive NPV, for the 2020 economic scenario, have been plotted in this figure. All points lying above the red dotted line have a payback period of less than two years, while those lying above the blue dotted line have a payback period of less than one year. As is shown in the figure, the transit bus application shows higher annual cost savings/mile than the MD truck. The transit bus has a greater mass as compared to the truck. The conventional bus thereby has a higher fuel consumption that the PHEV thereby leading to higher fuel savings.

Furthermore, the parallel architecture has lower initial system costs as compared to the series architecture. This is a result of the sizing requirement for the motor and the ESS. The series architecture requires all the tractive power to be sourced through the motor, thereby requiring bigger motors than the parallel architecture. This also results in earlier economic viability of the parallel architecture as compared to the series architectures, as shown in Table 3.6.

Similarly, the annual cost savings/mile vs initial system cost for the 2030 economic scenario are shown in Figure 3.4. The number of solutions having a positive NPV are greater, because of a favorable economic scenario. The annual cost savings/mile are also higher because the fuel cost is higher, causing the conventional vehicles to be more expensive to operate as compared to the PHEVs. The initial system costs are lower as well. More solutions have a payback period less than 2 years. Also, for a transit bus, highest savings are obtained for the Manhattan drivecycle, followed by the aggressive variant of the China drivecycle. For the MD truck on the other hand, the NY Composite drivecycle provides highest cost savings. This is due to the higher

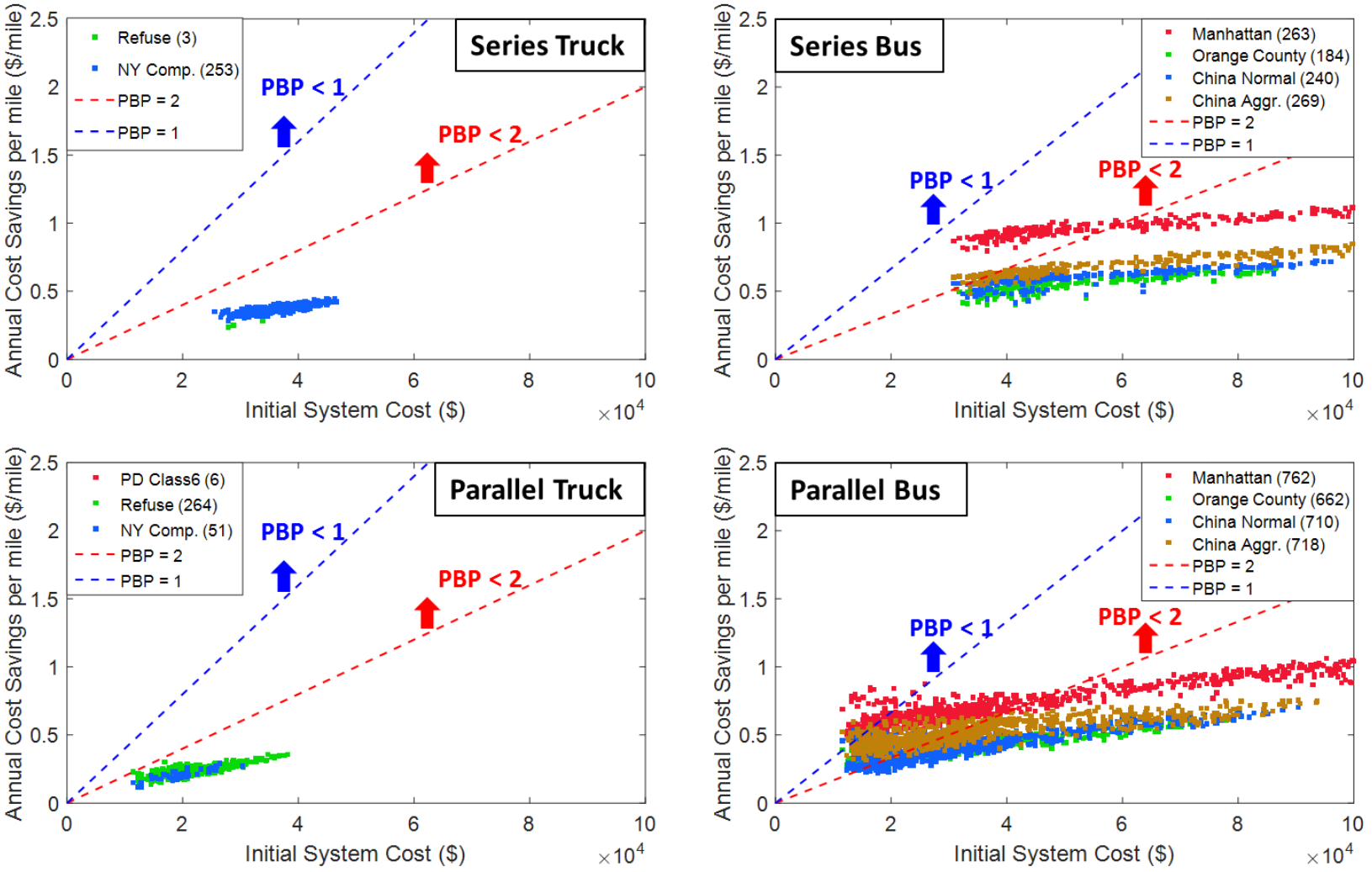

Figure 3.3. Comparison of annual cost savings/mile across architectures, applications and drivecycles (solutions with positive NPV for the **2020** economic scenario have been plotted).

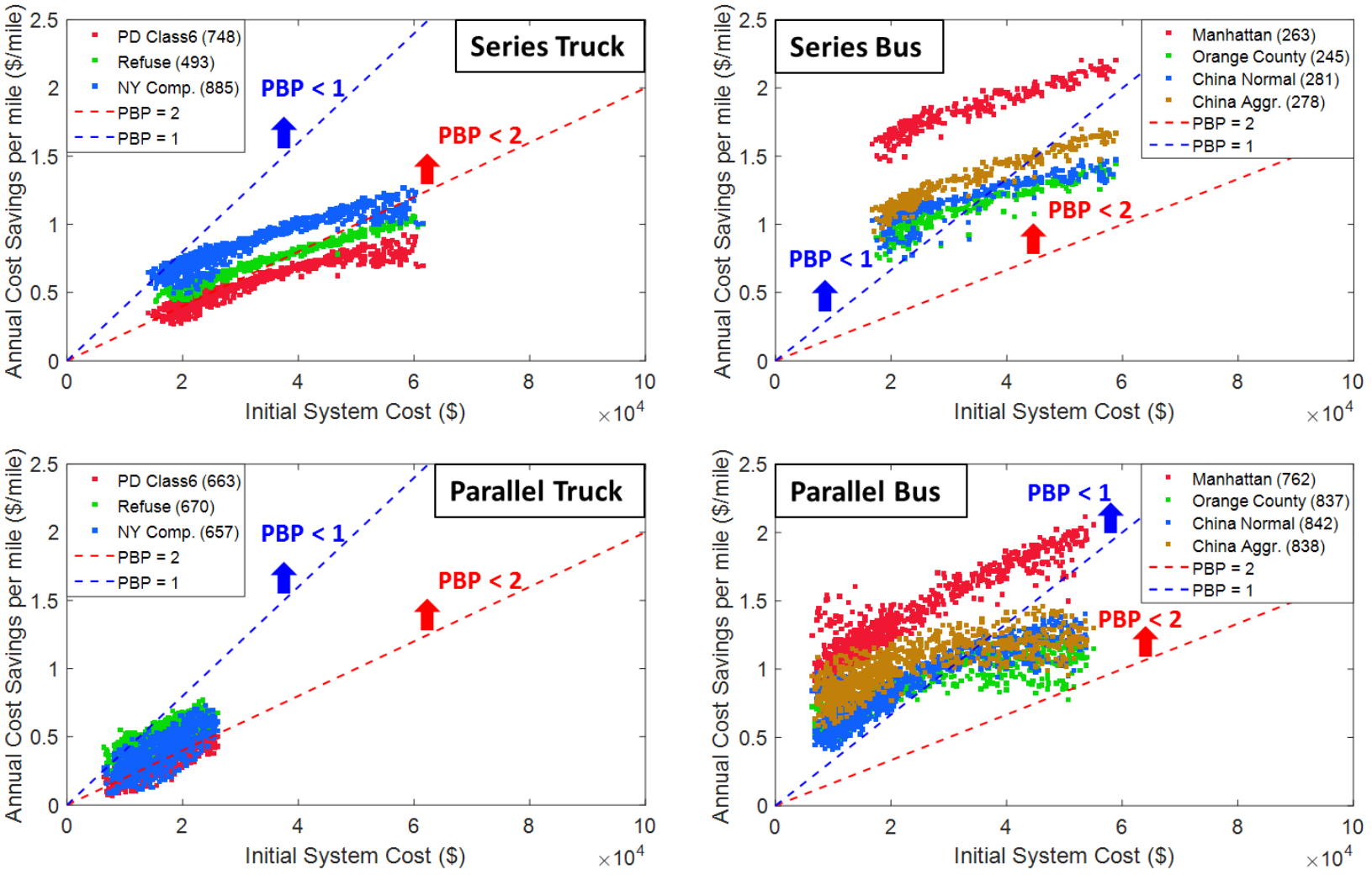

Figure 3.4. Comparison of annual cost savings/mile across architectures, applications and drivecycles (solutions with positive NPV for the **2030** economic scenario have been plotted).

braking energy available, leading to higher regenerative braking, for these drivecycles as compared to the others. This is reflected in the first scenario of economic viability in Table 3.6, where these drivecycles become favorable for hybridization earlier than the others in their group.

ESS replacements and the corresponding payback period obtained for the solutions having positive NPV for applications with a series architecture across the four scenarios are shown in Figures 3.5 and 3.6. Our region of interest is payback period less than two and ESS replacements less than three. As the economic scenario becomes more favorable, the payback period of the solutions drops, the points come closer together and more solutions lie in the desired space. Minimum one ESS replacement is obtained in all cases which implies maximum ESS life is approximately six years. Even with no ESS usage, considering it as a limiting case, ESS still undergoes capacity fade (referred to as calendar aging), which limits the ESS life. Furthermore, solutions with minimum ESS replacements have a higher payback period, implying that those solutions had a bigger battery, leading to lesser degradation but higher cost.

Furthermore, the higher favorability of more urban drivecycles for hybridization is seen in these figures as well. The NY Composite drivecycle for MD truck and the Manhattan drivecycle for the transit bus application show lower payback periods than the others.

3.3 Conclusions

In this chapter, a comparison of economic viability for two architectures - Series and Pre-transmission Parallel, over two applications - a MD Truck and a Transit Bus, was presented. The simulation framework proposed previously by the team was used. The underlying control strategies for both the architectures were discussed and the architectures and applications were compared from a life-cycle cost perspective. Both the architectures are compared from an annual cost savings perspective. The transit

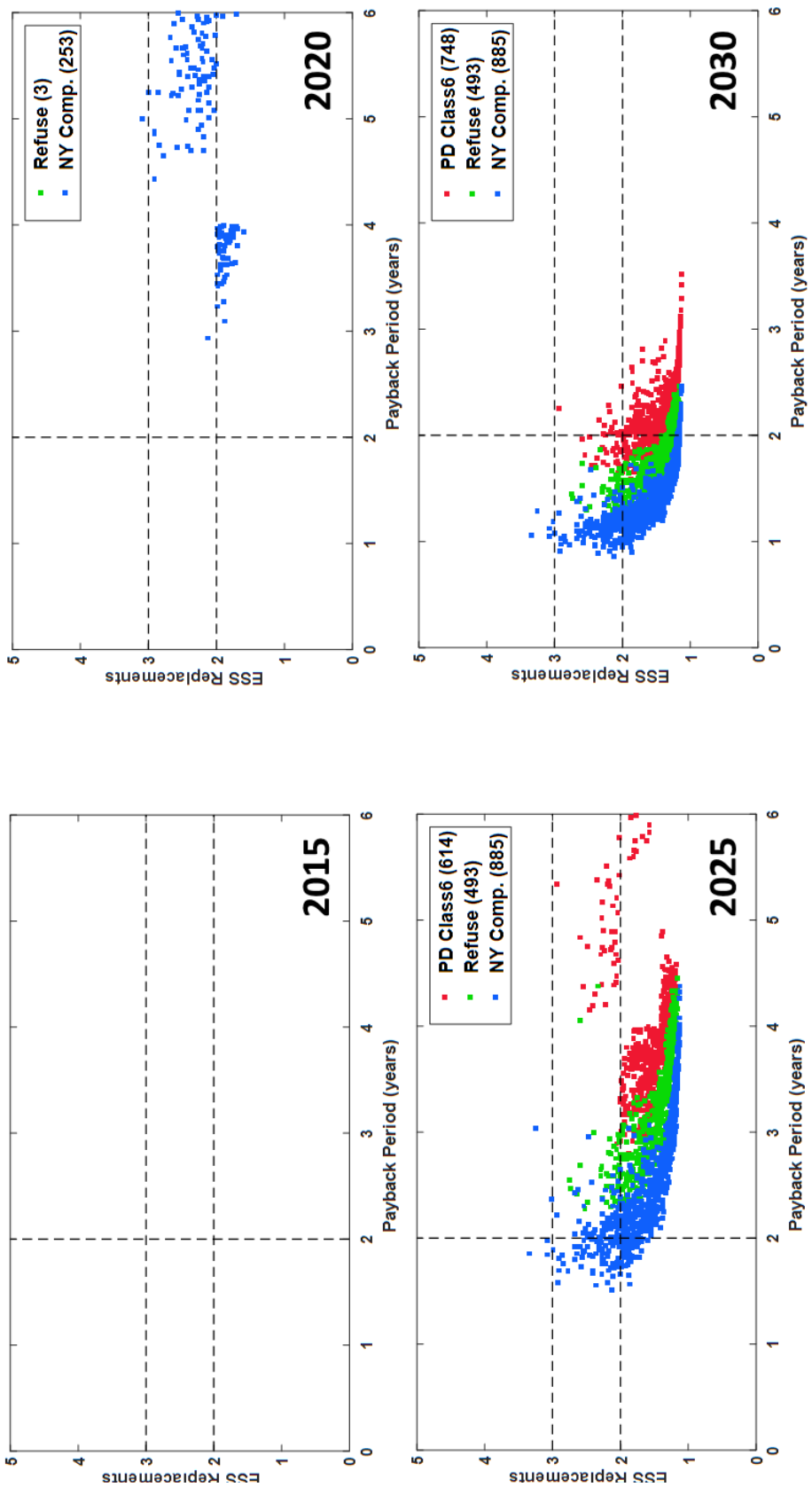

Figure 3.5. Effect of change in economic scenario on the ESS replacements versus payback period trade-off for a series truck (solutions with positive NPV have been plotted).

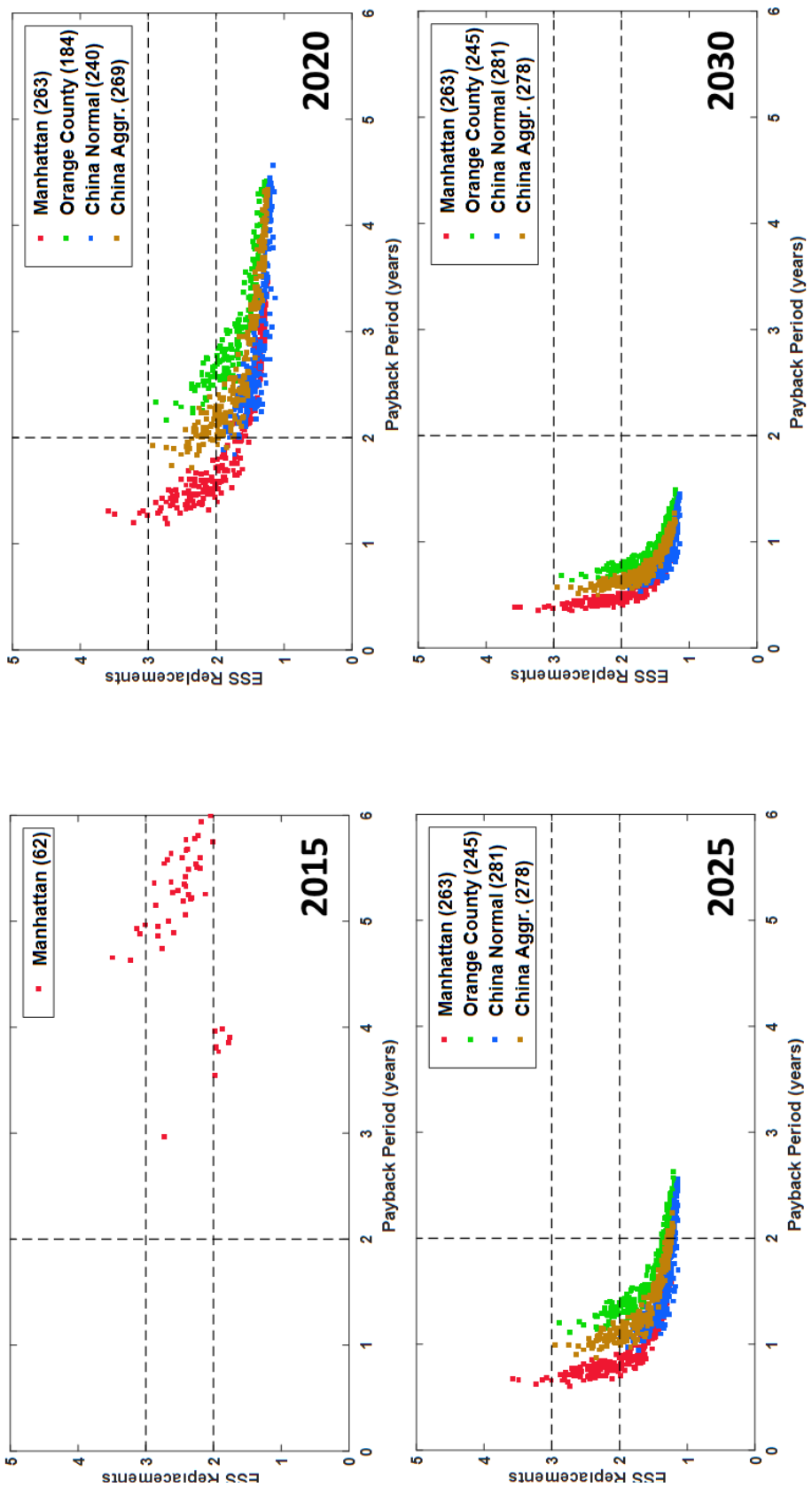

Figure 3.6. Effect of change in economic scenario on the ESS replacements versus payback period trade-off for a series bus (solutions with positive NPV have been plotted).

bus with the parallel architecture was shown to become economically viable earlier for hybridization.

Although fuel economy or cost savings is usually the point of comparison for the hybrid architectures, leading to selection of an architecture with the best fuel economy, it only partly paints the picture especially for the early economic scenarios when the component prices are high and the fuel prices are low. In this chapter, the parallel architecture was shown to have lesser initial system cost and hence had early payback although the series architecture showed slightly higher annual cost savings. This lays further stress on the need for a life-cycle cost based analysis of hybrid vehicles. Additionally, between the MD Truck and the Transit bus, the transit bus was shown to provide higher cost savings leading to quicker payback with similar initial system costs, making it viable for hybridization earlier. The urban-use cases were shown to be more favorable for hybridization where the Series Transit Bus achieves earliest payback the Manhattan drivecycle and the MD Truck achieves earliest payback on the NY Composite drivecycle. The actual cost-based metrics obtained here are dependant on the battery degradation as well as economic assumptions made, and hence should be considered representative.

The impact of opportunity charging on the electricity and fuel consumption, battery utilization, and hence on the economic metrics and number of battery replacements can be considered as part of the future work.

4. SELECTION OF WINNING SOLUTION AND ROBUSTNESS ANALYSIS

4.1 Introduction

As shown in Figures 3.5 and 3.6, there can be more than one powertrain and control strategy solution that satisfies the drivability, gradability, payback period and ESS replacement constraint. Which of these solutions is the best and the most robust? The effort outlined in this chapter aims to answer this question. The focus is on the series architecture for a transit bus application, and the solutions obtained for the Manhattan drivecycle have been considered.

4.2 Choosing a Winning Solution

To select one solution from amongst all the feasible solutions, ones that pass the viability constraints, the *Net Benefit Investment Ratio (NBIR)*, as defined in (4.1), has been used.

$$\text{NBIR} = \frac{\text{PV(Benefits)} - \text{PV(Operating Costs)}}{\text{PV(Investment Cost)}} \tag{4.1}$$

where, PV denotes the present value of the benefit or cost, benefits are the fuel consumption savings, operating costs include the ESS replacement and electrical energy costs and investment cost is the initial system cost. Higher the NBIR for a solution, more are the benefits per dollar of investment. This metric helps select a solution with optimum ESS replacement and energy consumption costs, without having to buy a big battery, which leads to higher initial system cost and larger payback period. This is one approach to select the optimal solution on the 'Pareto optimal curve' shown in Figures 3.5 and 3.6. The solution with the highest NBIR, for a series architecture transit bus operating on the Manhattan drivecycle is shown in Table 4.1.

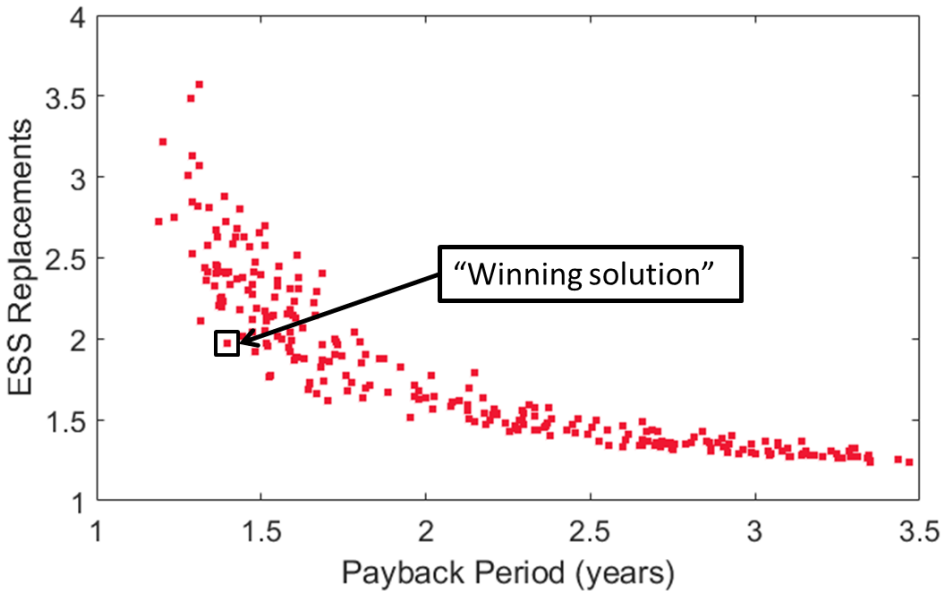

Figure 4.1. Winning solution.

Table 4.1. Example winning solution.

Parameter	Unit	Value
Powertrain Sizing Parameters		
M/G peak power	kW	174
Engine peak power	kW	104
ESS energy capacity	kWh	44.4
Control Strategy Parameters		
Maximum charge/discharge C-rate	-	2.6
Power filter time constant	-	0.31
ESS SOC regulation slope	W/SOC	19966
Fraction of power for the engine to turn on	-	0.34

4.3 Sensitivity Analysis DOE

After obtaining the winning solution, it needs to be tested for its robustness. The winning solution fixes the powertrain and control strategy, which guarantees that the drivability and gradability criteria for feasibility are met. The feasibility criteria that are dependent on other parameters that may be uncertain are the number of ESS replacements and the payback period. The parameters that are uncertain and those that would affect the number of ESS replacements and payback period include the vehicle parameters (C_{d}, C_{rr}, Vehicle Mass), the economic assumptions (Fuel cost, component costs) and vehicle usage (e.g. vehicle miles traveled).

In order to understand the robustness of the selected solution, a (5x5x5)x(5x5x5x5) DoE over the parameters shown in Table 4.2 was performed, with 5 equally spaced sample points taken for each parameter. Additionally, the selected winning solution was simulated over the other drivecycles to understand their effects.

Table 4.2. Example sensitivity analysis design of experiments.

Parameter	Unit	Min. Value	Nom. Value	Max. Value
Vehicle Parameters				
Coefficient of drag * Frontal Area	-	4.12	5.18	6.25
Coefficient of rolling resistance	-	0.005	0.006	0.007
Vehicle Mass	kg	12000	15000	18000
Vehicle Usage Parameter				
Annual vehicle miles traveled	miles	25000	35000	45000
Economic Assumptions				
Fuel cost	$/gal	2	4	6
ESS cost	$/kWh	150	300	700
M/G and PE cost (slope,intercept)	($/kWh,$)	(15.6,358)	(27.4,455)	(39.2,552)

4.4 Results and Discussion

The tornado plots for the metrics of interest are shown in Figures 4.2 to 4.5. The tables on the left define the minimum, maximum and nominal values of the parameters considered. One parameter is varied at a time while the other parameters assume their nominal values. The blue bars indicate the effect of reducing the value of the parameter below its nominal value. The red bars indicate the effect of increasing the value of the parameter above its nominal value. The parameters have been sorted in the descending order of magnitude of their impact. In order to foresee the impact of the worst case scenario on the metrics of interest, the parameters are made to assume the extreme values in a direction that is undesirable for the metric of interest, to obtain the worst case value of the metric. These values have been marked in red. For example, it is desirable to minimize the number of ESS replacements, but increasing AVMT increases this number, hence the worst case value of AVMT is its maximum value (45000 miles), when the number of ESS replacements is concerned. Additionally, the impact of changing the drivecycle is shown here as well. Manhattan is the nominal drivecycle, it is also the drivecycle for the worst case scenario.

The tornado plot for the number of ESS replacements is shown in Figure 4.2. Operation over the non-urban drivecycles leads to lesser number of ESS replacements, possibly because of lesser aggressive usage of the battery. AVMT and vehicle mass have a significant impact on the number of ESS replacements as well. The absolute difference in the number of ESS replacements obtained when the AVMT increases from 35000 miles to 45000 miles is approximately the same as the difference obtained when it is reduced from 35000 miles to 25000 miles. This suggests a linear relationship between AVMT and ESS replacements over this range. The worst case number of ESS replacements is lesser than the maximum number of ESS replacements for feasibility (i.e. 3).

The tornado plot for Net Present Value is shown in Figure 4.3. Higher NPV is desirable. Fuel price has the highest impact on the NPV. Higher the fuel price, more

Min	Nom	Max	Variables
-	Man	-	Drivecycle
25K	35K	45K	AVMT (miles)
12K	15K	18K	Vehicle Mass (kg)
5	6	7	Crr(*10³)
4.12	5.18	6.25	Cd*A
150	300	700	ESS Price ($/kWh)
15.6	27.4	39.2	Motor Price (slope)
2	4	6	Fuel Price ($/gal)

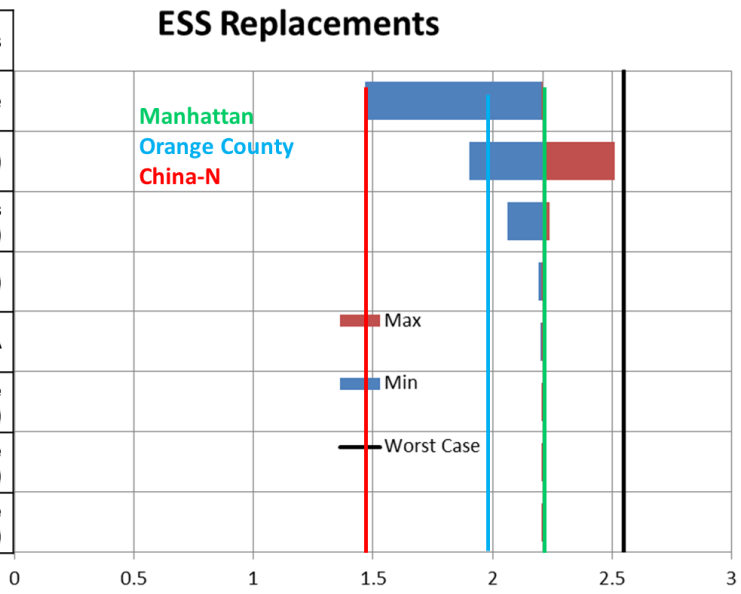

Figure 4.2. Tornado plot for number of ESS replacements.

Min	Nom	Max	Variables
2	4	6	Fuel Price ($/gal)
25K	35K	45K	AVMT (miles)
-	Man	-	Drivecycle
150	300	700	ESS Price ($/kWh)
15.6	27.4	39.2	Motor Price (slope)
5	6	7	Crr(*10³)
12K	15K	18K	Vehicle Mass (kg)
4.12	5.18	6.25	Cd*A

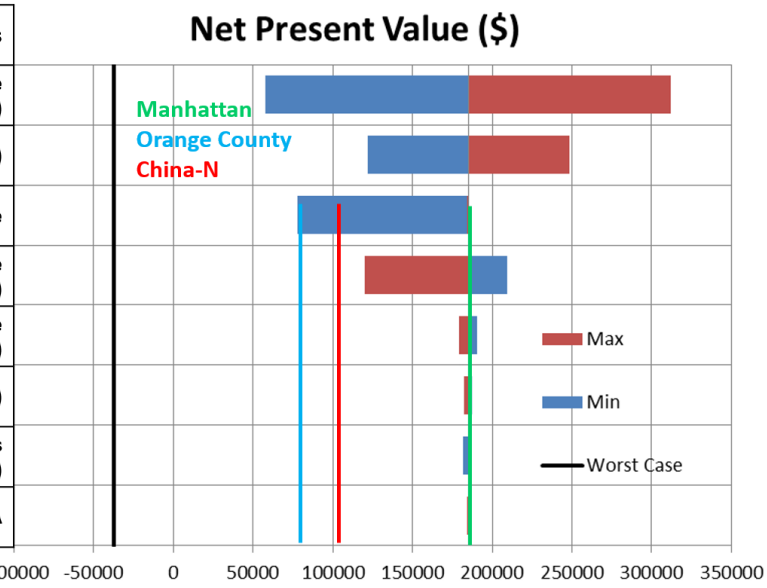

Figure 4.3. Tornado plot for net present value.

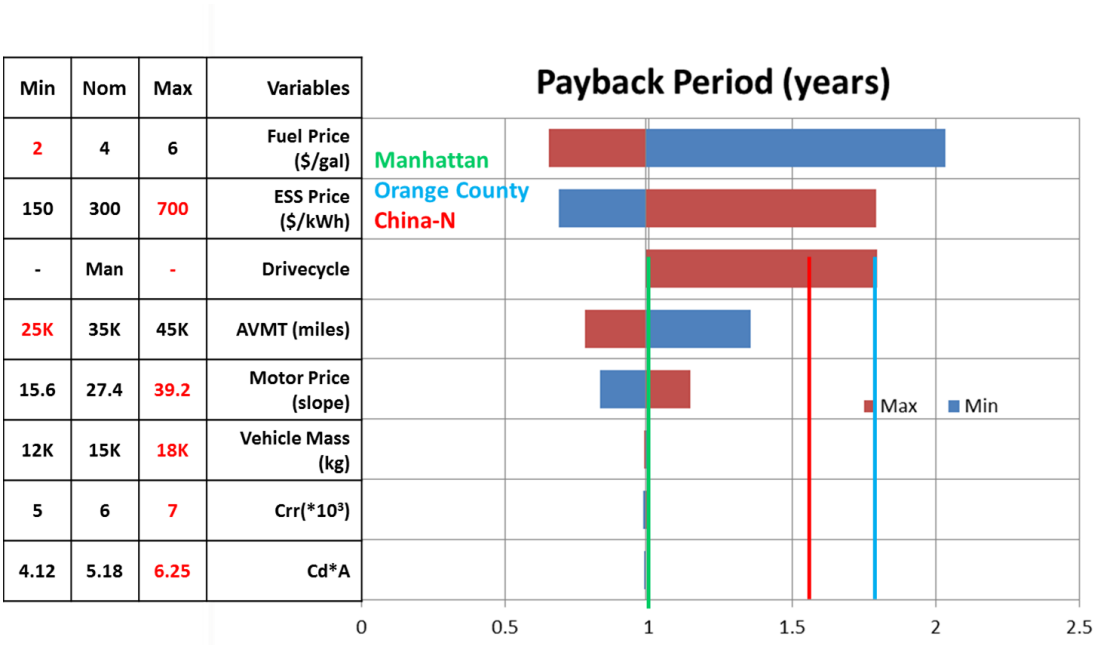

Figure 4.4. Tornado plot for payback period.

are the fuel savings ($) of a PHEV with respect to a conventional vehicle. Similarly, for AVMT, higher the number of miles more are the fuel savings and hence higher is the NPV. The urban drivecycles use the battery more due to more start-stop conditions leading to higher NPV. ESS Price has a significant impact on the NPV as well, lesser the ESS price higher NPV will be obtained. Motor price, coefficient of drag and coefficient of rolling resistance and vehicle mass do not have a big impact on the NPV. NPV, in the worst case scenario, is negative. This implies that there are more losses than gains from hybridizing the transit bus to a PHEV, under this scenario on the Manhattan drivecycle.

The tornado plot for payback period is shown in Figure 4.4. Lower value of Payback Period is desirable. Fuel price and ESS price have the highest impact on payback period. Higher the fuel price, higher are the fuel savings ($) with respect to a conventional vehicle, and the incremental initial system cost can be recovered earlier. Higher the ESS price, more is the operational cost, leading to higher payback period. The NPV on the non-urban drivecycles is lower suggesting that time taken to

Min	Nom	Max	Variables
-	Man	-	Drivecycle
12K	15K	18K	Vehicle Mass (kg)
25K	35K	45K	AVMT (miles)
5	6	7	Crr(*10³)
4.12	5.18	6.25	Cd*A
2	4	6	Fuel Price ($/gal)
150	300	700	ESS Price ($/kWh)
15.6	27.4	39.2	Motor Price (slope)

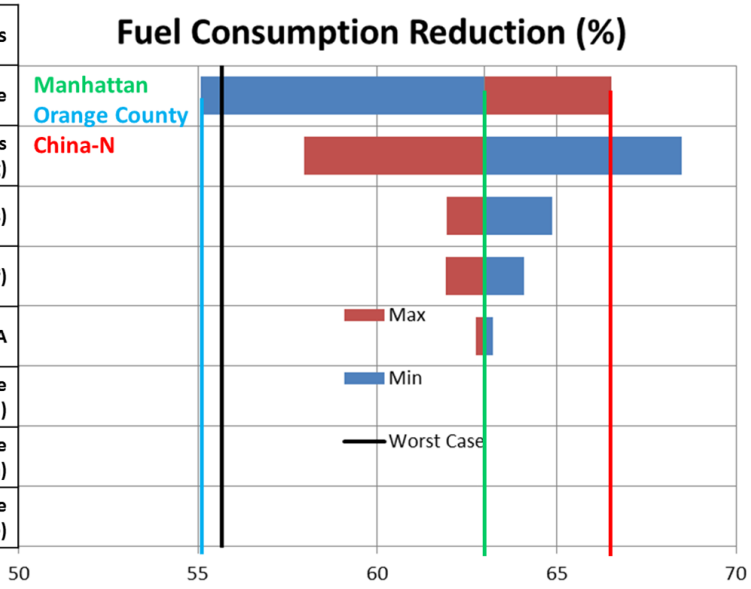

Figure 4.5. Tornado plot for fuel consumption reduction.

recover the incremental initial cost will be more. Higher AVMT and lower motor price are required to minimize the payback period. Since the worst case NPV is negative (Figure 4.3), the worst case payback period does not exist. It is interesting to note that to minimize number of ESS replacements AVMT needs to be minimized, whereas to minimize the payback period, the AVMT needs to be increased, hence there is a trade-off.

The tornado plot for fuel consumption reduction is shown in Figure 4.5. Here the fuel consumption (Wh/km) of the PHEV is compared with that of an equivalent conventional vehicle, and the percentage reduction is plotted. Higher fuel consumption reduction is desirable. Higher fuel consumption reduction is obtained over the China normal drivecycle than the Manhattan drivecycle. Vehicle mass has a significant impact on fuel consumption reduction. Lesser the vehicle mass, higher is the reduction in fuel consumption. The coefficient of rolling resistance (hence the condition of tires) has some impact on the fuel consumption reduction as well, though the coefficient of drag does not. The worst case fuel consumption reduction is way above 50%.

4.5 Conclusions

A method to select one solution out of the multiple solutions that were found to be viable in Chapter 3 was presented in this chapter. The Net Benefits to Investment Ratio was used for this purpose, and the powertrain configuration with the highest NBIR was selected. A sensitivity analysis was performed to understand the impact of variation in the drivecycle, vehicle usage parameters and economic parameters that were a part of the DOE in Chapter 3, on the fuel consumption reduction, Net Present Value, payback period, and ESS replacements. It was found that the fuel price, ESS price, AVMT and vehicle mass affect these metrics the most.

For the worst-case operating parameters considered, the fuel consumption reduction drops from 64% to about 55%, showing that even for the worst vehicle mass, AVMT, coefficient of drag and rolling resistance, the PHEV saves significant fuel as compared to the conventional vehicle, and also results in less than three ESS replacements. However, when combined with the worst case component costs and fuel price, the PHEV configuration considered here is no longer viable due to the resulting negative Net Present Value, showing that even though the performance of the vehicle is better than the conventional vehicle, high initial costs combined with high fuel price makes the vehicle economically impractical. This lays further stress on the requirement for performing a total cost-of-ownership analysis, and not just performance optimization, for powertrain design.

5. DETERMINING VARIABILITY IN BATTERY LIFE

5.1 Introduction

The efforts explained in the previous chapters are aimed at determining the feasibility of hybridization, optimizing the powertrain design for a use case and understanding the robustness of the feasibility of the design to economic, vehicle and usage parameters. One point has been clear through these chapters that battery degradation and therefore the number of battery replacements contribute significantly to the total cost of ownership. In order to reduce the number of battery replacements over a vehicle's lifetime it is inevitable to understand the factors that impact battery degradation significantly. This understanding will help us determine the "rules" for battery operation in a battery conscious manner.

Until now, the drivecycles and hence the battery duty cycles (battery current vs time) were deterministic, so were the operating conditions. These led us to deterministic values of battery life. In reality, the operating conditions, including battery duty cycles, battery charging, temperature of operation are not constant values, they vary even over operation on a single day. This implies that given a powertrain and control strategy, even a drivecycle, the battery life is no more a single value but set of values with a probability associated with each value. This chapter outlines a framework to understand the variability in battery life due to the variability in operating conditions.

5.2 Battery Degradation Model

In order to understand the key factors for battery degradation from a system level, it is necessary to have a sufficiently accurate and fast battery degradation model. The degradation model used in the previous chapters (for NMC+LMO/Graphite chem-

istry) was a regression based model. Such types of models can be fast and accurate only over the use cases over which it has been developed. A detailed comparison of accuracy and computational efficiency for the battery degradation models, available in literature, for Li-ion batteries, is performed in [77]. This reference also motivates the need for a physics-based computationally efficient battery degradation model for Li-ion batteries. In reference [78], the authors have developed one such model for Li-ion batteries with graphite anodes and further validated it for the LFP/Graphite battery. This model considers that there are two dominant anode-side degradation mechanisms viz., Solid-Electrolyte Interface (SEI) layer growth and Active Material (AM) loss, that contribute to capacity loss in a Li-ion battery with graphite anodes. The mathematical equations for the loss model are shown in Equations (5.1) to (5.3), where $Q_{\text{SEI}}, Q_{\text{AM}}$ are the capacity losses due to SEI layer growth and active material loss, Q_{loss} is the total capacity loss, $k_{\text{SEI}}, k_{\text{AM}}$ are the pre-exponential factor for SEI and AM loss, $E_{\text{SEI}}, E_{\text{AM}}$ are the activation energies for SEI formation and AM loss, R is the ideal gas constant, T is the temperature, λ, θ are fitting parameters, I is the current, SOC is the state of charge and t is time. This is a cell-level model and has been used in the effort outlined in this chapter, assuming a LFP/Graphite battery chemistry.

The empirical battery degradation model used previously (for NMC+LMO/Graphite chemistry) can also be used provided the operating conditions such as the charge and discharge C-rates and temperature are maintained within the ranges defined in the experimental data used to tune the model.

$$Q_{\text{SEI}} = \int_0^t -k_{\text{SEI}} \exp\left(\frac{-E_{\text{SEI}}}{RT_{\text{batt}}}\right) \frac{dt}{2(1+\lambda\theta)\sqrt{t}} \tag{5.1}$$

$$Q_{\text{AM}} = \int_0^t k_{\text{AM}}. \exp\left(\frac{-E_{\text{AM}}}{RT_{\text{batt}}}\right) |I|.\text{SOC}.dt \tag{5.2}$$

$$Q_{\text{loss}} = Q_{\text{SEI}} + Q_{\text{AM}} \tag{5.3}$$

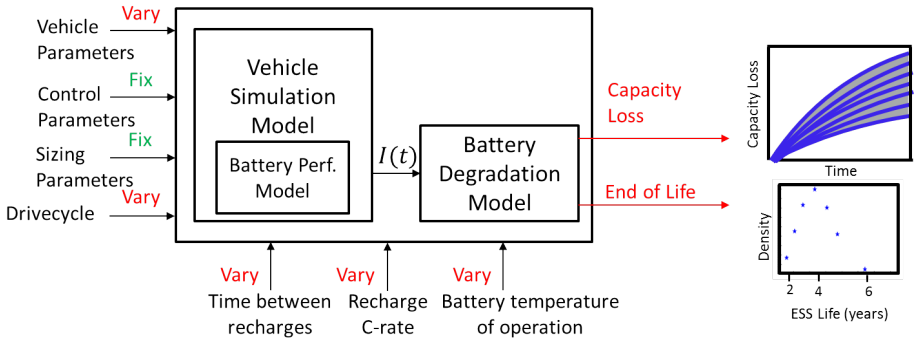

(a) Approach 1 - Parametric analysis.

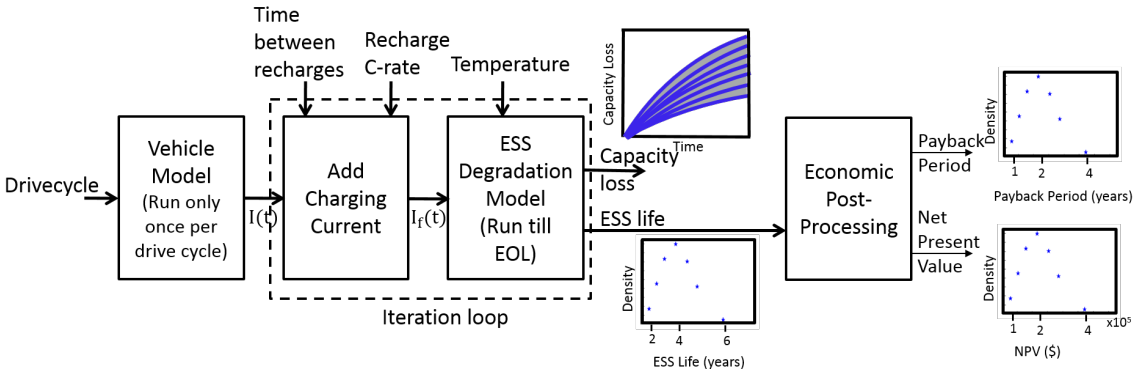

(b) Approach 2 - Simulation framework for estimating variability in battery life and economic viability

Figure 5.1. Approaches for determining variability in battery degradation.

5.3 Framework

One approach to understanding the variability in battery degradation due to variation in operating conditions is to start with the baseline framework discussed earlier, fix the powertrain and control, but vary the vehicle and usage parameters, as shown in Figure 5.1a. The battery degradation model is run until the battery reaches end-of-life, thus giving the variation in capacity loss and end-of-life. A probability density of end-of-life is also expected at the output. In this approach, three additional parameters that describe the battery usage, further, have been considered. These are number of charges a day (time between consecutive charges), C-rate at which the battery is charged and the temperature at which the battery is operated. Note that the temperature at which the battery is operated is different from the ambient temper-

ature, and relates more to the battery thermal management strategy. It is assumed here that the battery heating/cooling system operates in a way such that the desired battery temperature is maintained.

In Figure 5.1a, the time between recharges modifies the input drivecycle and the recharge C-rate would also plug into the simulation model. This approach requires the vehicle simulation model to be run every combination of vehicle parameters, drivecycle, time between recharges and recharge C-rate. The vehicle simulation model takes approximately 20 min to simulate a day long drivecycle, which includes both the charge depleting and charge sustaining modes discussed earlier. If high resolution in input sampling (more number of combinations for given ranges of input parameters) is desired, a significant amount of time would be required for all the simulations.

Hence, for the purpose of this study, a variant of Approach 1, as shown in Figure 5.1b has been used. This framework captures the effect of variation in drivecycle, time between recharges, recharge C-rate and battery temperature. It does not capture the effect of change in vehicle parameters here, but that is considered acceptable, since this effect was captured in the previous Chapter, without associating probability to the vehicle parameters.

Practically, battery degradation also leads to change in battery performance, including drop in open circuit voltage and increase in internal resistance ([85]). This would change the battery duty cycle with battery age. This effect of battery degradation on battery performance has not been considered in this study and can be a topic of future study.

5.4 Validation of the Framework

The focus of this section is to validate the framework defined in Figure 5.1b. Given a battery duty cycle, the idea is to be able to correctly modify it for in-route charging and understand the effect of variation in any of the inputs (excluding the battery duty cycle) on the capacity loss and end-of-life. Three more inputs come

into picture after the vehicle simulation model. They are number of charges in a day (miles between charges), charging C-rate and battery temperature of operation. The battery chemistry considered here is LFP/Graphite and the physics based reduced order model developed in [78] is used. An example battery duty cycle generated in the previous study has been used as the input. The daily vehicle miles traveled are considered to be constant at 100 miles, and the battery end-of-life is defined to be at 20% loss in energy capacity. The battery degradation model used here does not capture the loss in power capacity. One thing to remember here is that the change in battery performance due to degradation has not been considered.

The variation in SOC, capacity loss and end-of-life with temperature is shown in Figure 5.2. The miles between charges is assumed to be 50 miles, and the charging C-rate is assumed to be 1C. As expected, there is no variation in SOC, and the capacity loss increases with increase in temperature. The battery life drops exponentially with increase in battery temperature of operation. This is representative of the Arrhenius relationship between capacity loss and temperature.

The variation in SOC, capacity loss and end-of-life with the charging C-rate is shown in Figure 5.3. The battery temperature of operation is assumed to be 30 °C, while the miles between charges is assumed to be 50 miles. Higher the C-rate of charging, higher is the average SOC, which results in higher capacity loss, but the increase in capacity loss is not very significant. Battery life drops almost linearly with increase in charging C-rate.

The variation with change in miles between consecutive charges is shown in Figure 5.4. The battery temperature of operation is assumed to be 30 °C, while the charging C-rate is assumed to be 1C. If the miles between charges is lesser than the vehicle CD mode range, the capacity loss is significantly high. Whereas, if the miles between charges is greater than the vehicle CD mode range, the capacity loss and hence the battery life does not vary as much with a change in miles between charges.

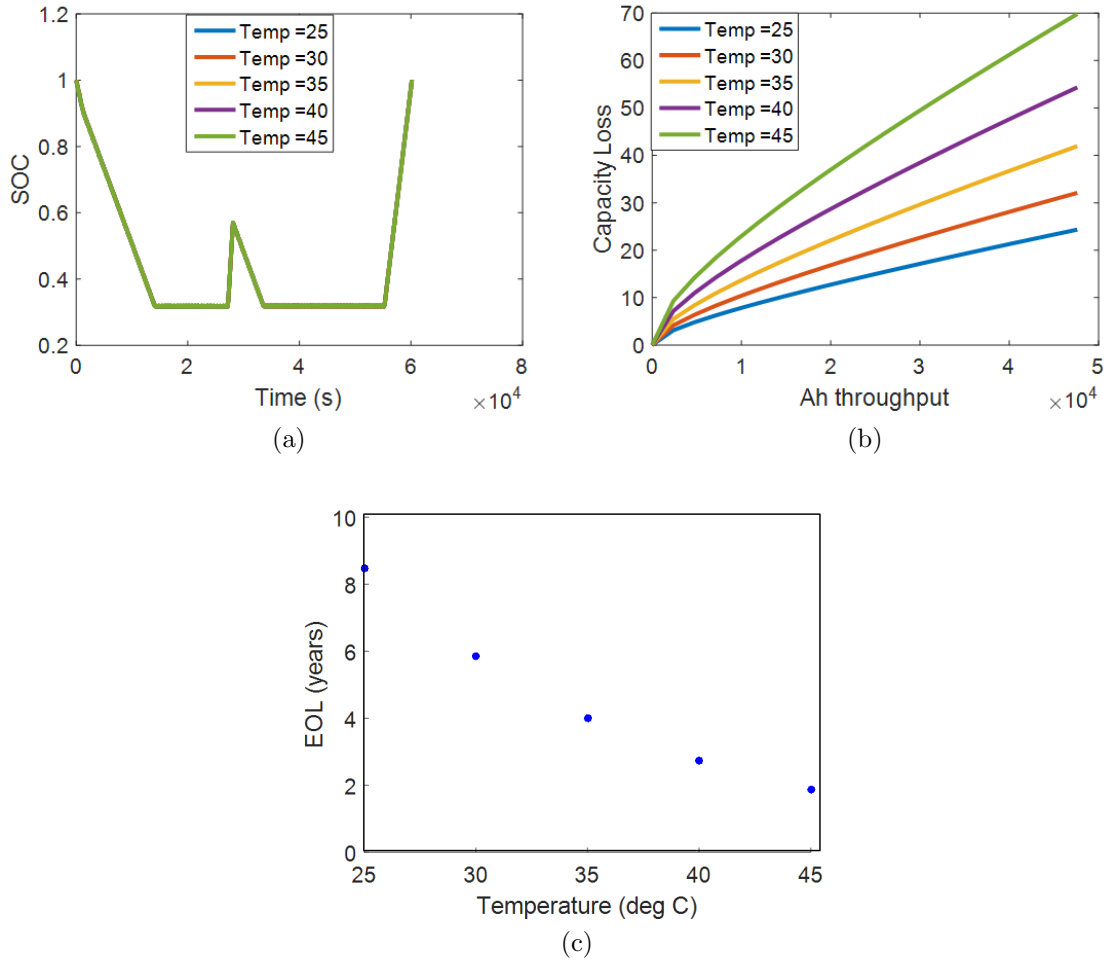

Figure 5.2. Validation for different temperatures (a) Variation in SOC (b) Variation in capacity loss (c) Variation in end-of-life.

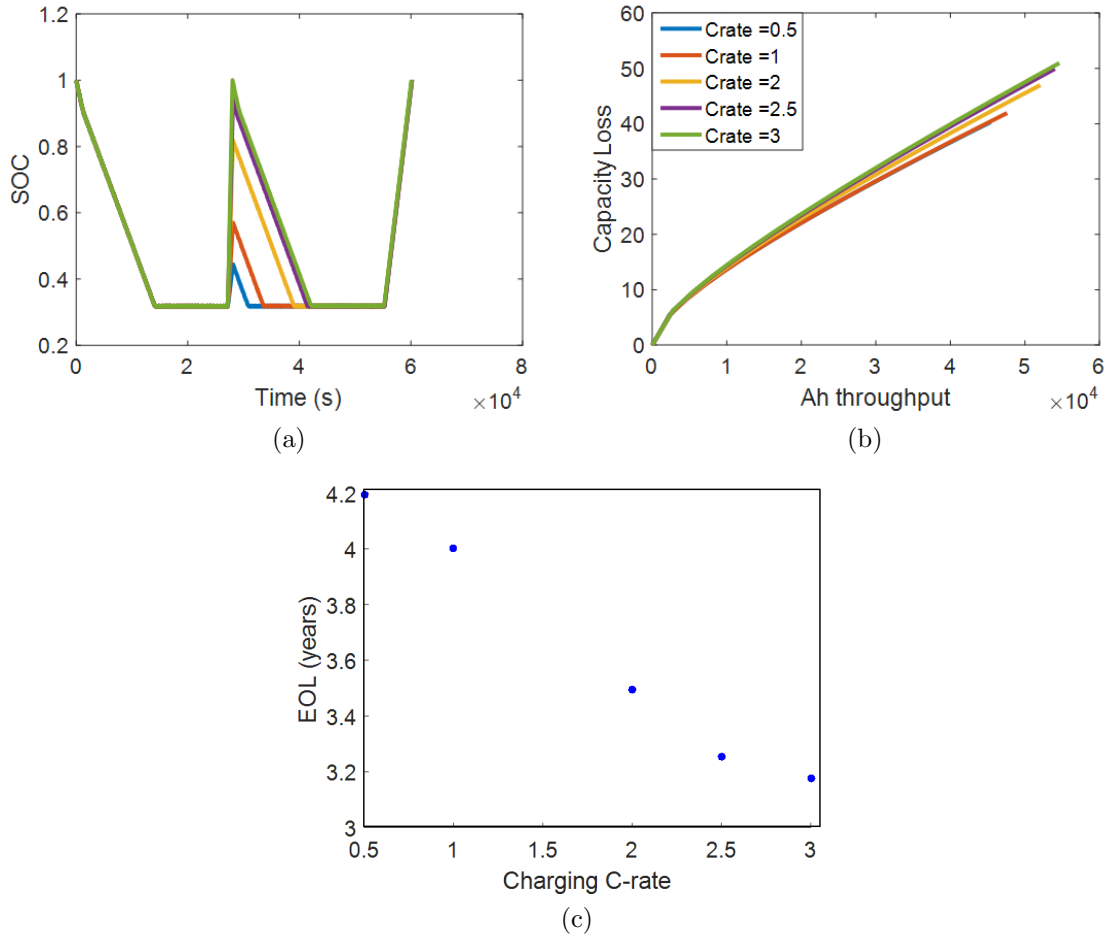

Figure 5.3. Validation for different charging C-rates (a) Variation in SOC (b) Variation in capacity loss (c) Variation in end-of-life.

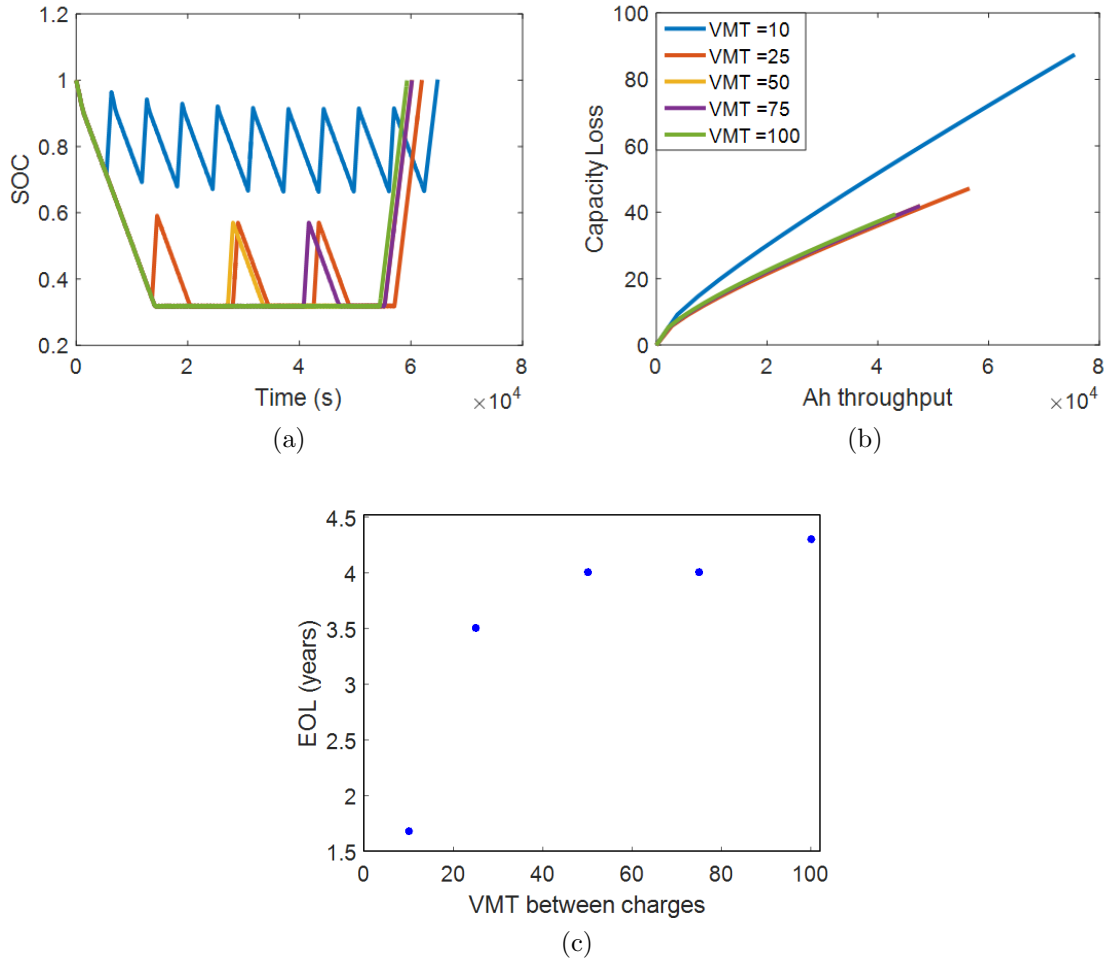

Figure 5.4. Validation for different miles between consecutive charges (a) Variation in SOC (b) Variation in capacity loss (c) Variation in end-of-life.

Table 5.1. PDF of C-rate of charging.

Charger type	kW	Charging Outlets		C-rate
		#	%	
Level1	1.9	2351	4.6	0.05
Level2	19.2	41815	81.93	0.5
DC Fast	50	6814	13.35	1

5.5 Defining Inputs

The time between charges has been assumed to be uniformly distributed between 2.5 to 5 hrs. It is assumed that the battery is used with a cooling system which maintains the battery at a desired battery temperature. Battery cooling systems are slow, in that they typically take an hour to cool the battery by 10°C and so the temperatures seen by the battery are normally distributed with the mean at 35°C, desired battery temperature [86], and with a deviation of 7°C considering that the battery operates at non-desired temperatures until the cooling system cools it to the desired temperature. A larger deviation can also be considered if battery exposure to higher temperature ranges is expected. The information about different types of chargers, their numbers and locations is available at [87], additionally, the kW rating of such chargers has been mentioned in [88]. This information is used to calculate the probability distribution of chargers and hence the PDF of C-rate for charging, as shown in Table 5.1.

5.6 Results

The powertrain configuration and control strategy is the Series Bus Winning Solution, the same one used for the previous sensitivity study. This configuration is simulated over the Manhattan drive cycle. It is assumed that the bus drives 100 miles in a day.

The effect of varying the inputs one at a time is shown in Figures 5.6 to 5.8. The other two inputs are kept fixed at their nominal values shown in Table 5.2. The PDFs were defined as discussed previously and each PDF was sampled 200 times. In Figure 5.6, it is shown that in the present scenario of charger availability and with one in-route recharge a day, there is little variation in the capacity loss and the battery end-of-life is always 4.5 years. This is because even with varying C-rate, a single charge a day results in less than 365 days variation in battery life. When the VMT between recharges is varied, there is little variation in capacity loss and battery end-of-life, as shown in Figure 5.7. This is because, varying the VMT between recharges from 20 to 35 results in two to five recharges on-route, resulting in the average SOC varying between 0.43 and 0.45. This small variation in average SOC results in the battery life varying between 3.7 and 4.1 years. Unless if the VMT between recharge is small enough to cause a significant change in the average SOC, the battery life would not be affected as much. Although C-rate of charging and VMT between recharges do not affect battery life, they do change the time spent in CD mode thereby affecting the utility factor. This effect is shown in Figure 5.5, where a step variation in the utility factor with VMT between charges is shown in Figure 5.5a. This is because, not all VMTs show increase in the number of charges per day, as is also illustrated in Figure 5.4. Figure 5.5b shows a linear increase of the utility factor with the recharge C-rate.

On the other hand, varying battery temperature affects capacity loss and end-of-life significantly. There are a couple "secluded" curves on the top, in the capacity loss plot in Figure 5.8. These are due to no samples of temperature between 49°C and 56°C. Higher temperature of operation of the battery leads to higher capacity loss and lesser battery life. It is shown that, for the given PDF of battery temperature, a battery life of 2.5-3.5 years is most probable, but can go as low as 1.5 years which is highly undesirable. Battery end-of-life is an exponential function of battery temperature, as shown in Figure 5.9. This is because capacity loss is an exponential function of temperature as is shown from the Arrhenius dependence shown in (5.4)

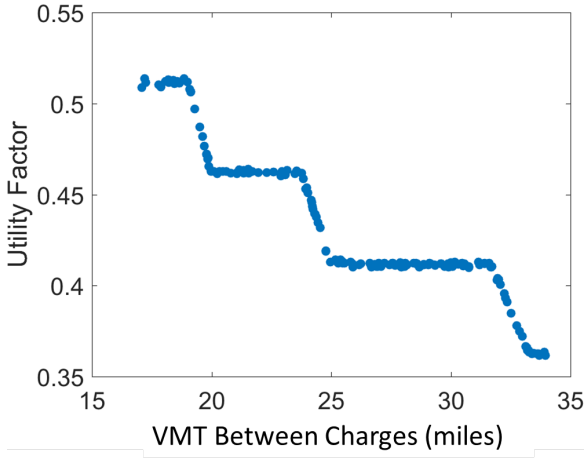

(a)

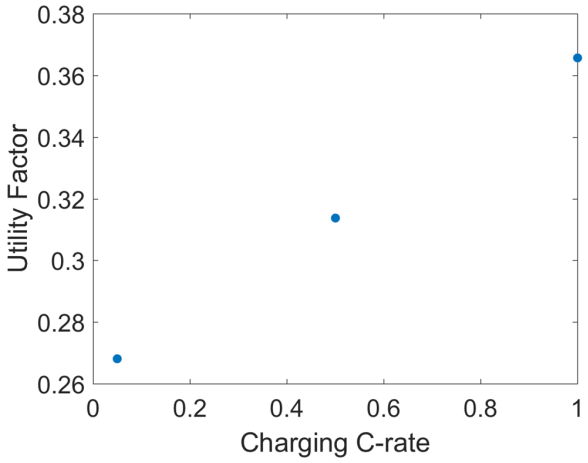

(b)

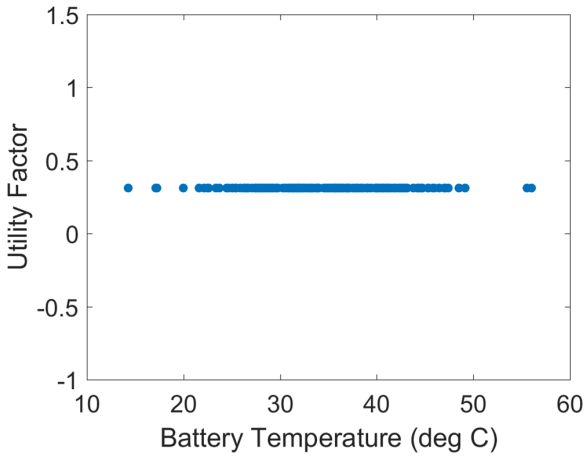

(c)

Figure 5.5. Variation of utility factor with VMT between charges, charging C-rate and battery temperature.

Table 5.2. Nominal value of all inputs.

C-rate	VMT Between Charges	Temperature
0.5	50 miles	35°C

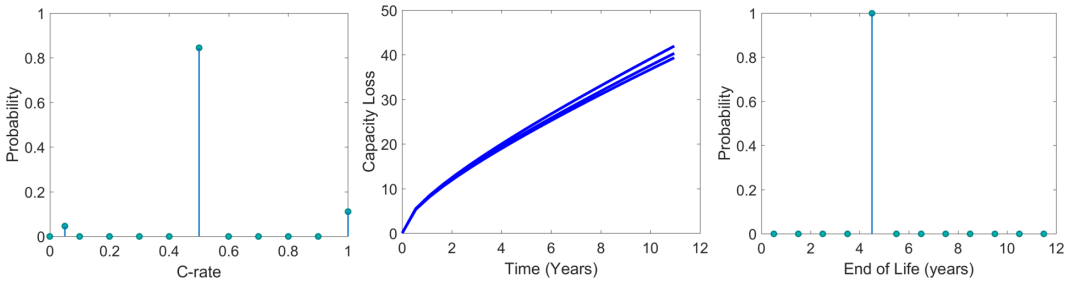

Figure 5.6. Effect of variation in C-rate on battery end-of-life.

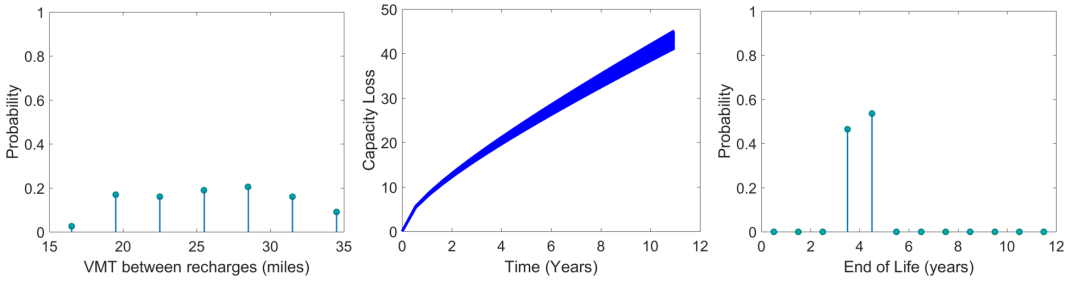

Figure 5.7. Effect of variation in VMT between recharges on battery end-of-life.

where a and b have been derived from the fit and have values 59.69 and -0.07592 respectively. The fit has $R^2 = 1$ and $RMSE = 0.0112$. The exponential variation of battery life with temperature results in the non-symmetric nature of the battery life PDF. Battery temperature itself is assumed to not affect the time spent in CD mode and hence not affect the utility factor, as shown in Figure 5.5c.

$$\text{EOL} = \text{a} * \exp(\text{b} * \text{Temperature(in}^\circ\text{C)}) \tag{5.4}$$

When all the inputs are varied, in Figure 5.10, a significant variation in capacity loss and battery life is observed. A total of 200 combinations of C-rate, VMT between charges and temperature are evaluated. The variation is similar to what is obtained

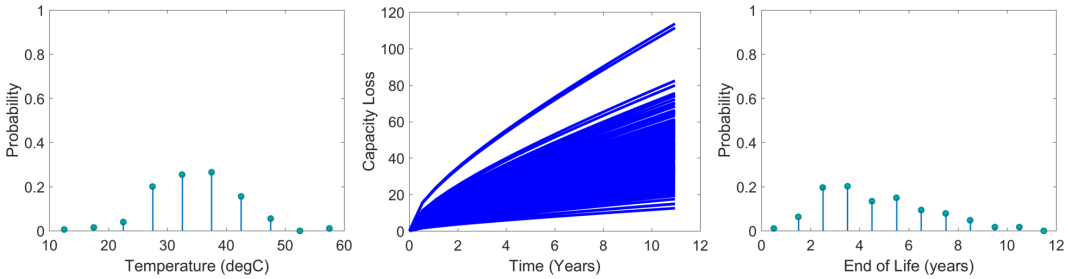

Figure 5.8. Effect of variation in battery temperature of operation on battery end-of-life.

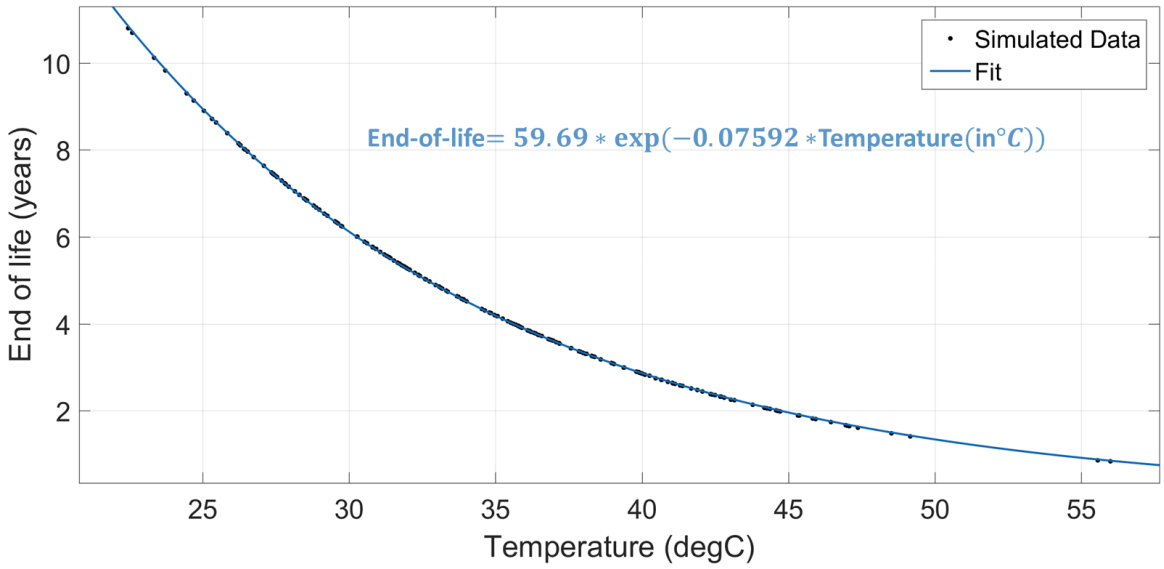

Figure 5.9. End-of-life as a function of temperature (in °C).

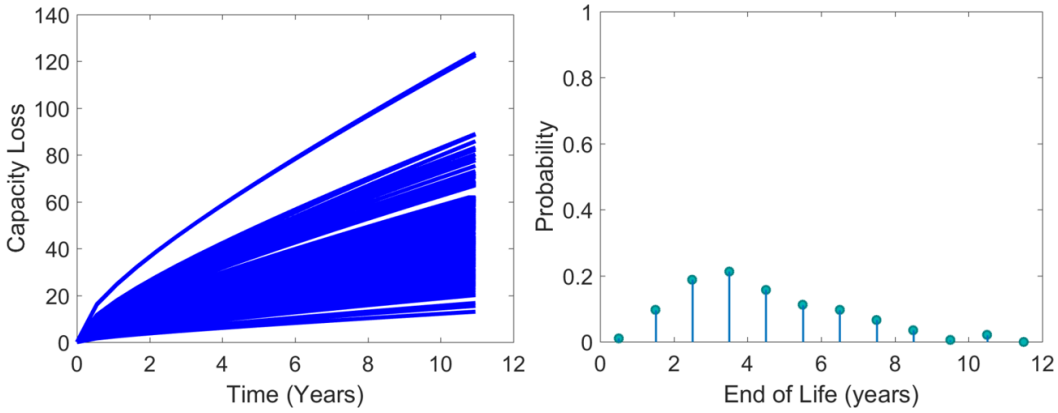

Figure 5.10. Total variation in battery capacity loss and end-of-life due to variation in C-rate, VMT between recharges and battery temperature of operation.

when only temperature is varied. It is observed that from among recharge C-rate, number of recharges in a day and battery temperature of operation, the temperature has the most impact on capacity loss and battery end-of-life. This also strongly motivates the need for a good battery cooling system.

The framework is then exercised over the Orange County drivecycle, with the same powertrain configuration for the Series Transit Bus, and results are compared with those over the Manhattan drivecycle in Figure 5.11. This happens because, Orange County is a faster drivecycle as compared to the Manhattan drivecycle, therefore a bus traveling on Orange County completes the 100 miles target faster and charges to 100% spending a greater amount of time at 100% SOC thereby leading to faster battery degradation and smaller life. Here again, battery temperature has a significant impact on battery life.

Baseline framework had predicted that this configuration would become viable in 2020 on the Manhattan drivecycle, and in 2025 on Orange County. The battery life was also deterministic in that case. Associating PDFs to usage scenarios has allowed us to bring in the uncertainty in battery life. The economic assumptions used here are same as those defined in Chapter 2. When the conditions for economic viability, as discussed in Chapter 2, are applied only some of the 200 simulations pass this criteria. Since the drivability, gradeability are only dependant on the powertrain

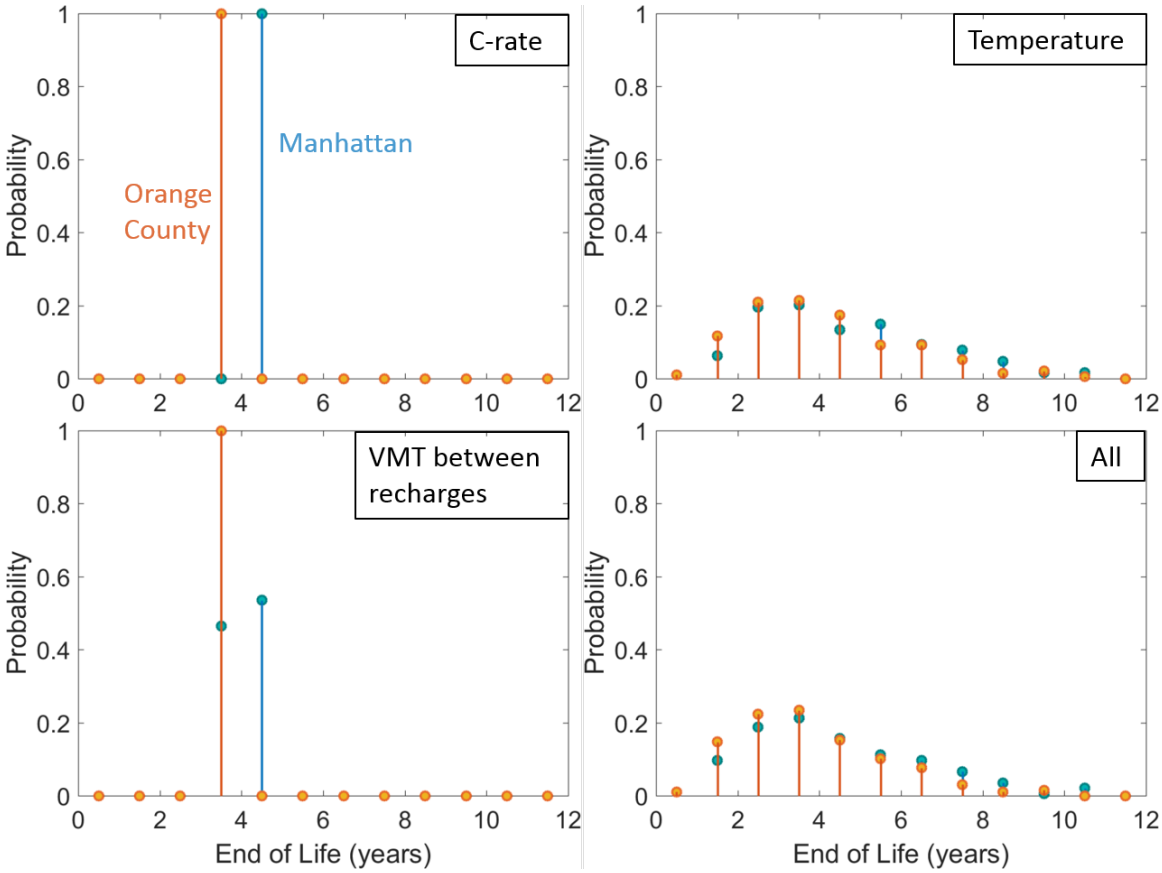

Figure 5.11. Effect of change in drivecycle on battery end-of-life.

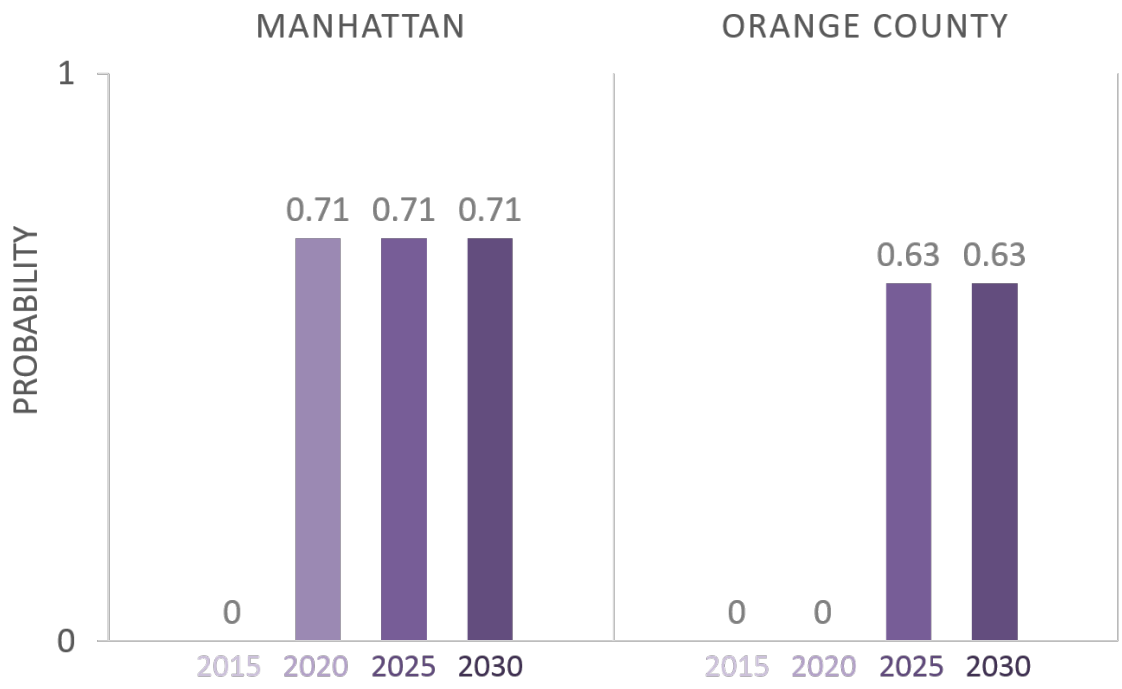

Figure 5.12. Effect of change in drivecycle on economic viability of the transit bus.

configuration, which is the same as the winning solution, these criteria do not affect the 200 solutions. The solutions need to have a payback period less than two years. To pass the battery replacement less than 3 criterion, a battery life of four or more years is required. As shown from Figure 5.11, not all solutions satisfy this criterion. The effect is shown in Figure 5.12, 71% of the solutions pass the viability criteria for Manhattan, and 62.5% of the solutions pass for Orange County.

Similar to the PDF obtained for battery life, a statistical distribution of the net present value, payback period, internal rate of return and the annualized cost savings can be obtained, as shown in Figure 5.13. The plot considers only those solutions that have a positive NPV for the 2025 economic scenario. The variation observed in annualized cost savings per mile is due to the variation in utility factor calculation. The calculation of this metric considers the fuel and electricity costs but does not consider the battery replacement cost. The simple payback period (PBPS) does not consider time discounted values for future battery replacement costs. But some

variation is observed in payback period due to a battery replacement occurring in the first 2 years for some solutions which delays the payback. NPV and IRR show some variation, due to the non-zero probability of having a small battery life that results in more battery replacements over the vehicle life. Longer battery life results in lower variation in NPV and IRR due to fewer battery replacements over the vehicle lifetime. Fewer samples of lower battery temperatures lead to fewer solutions with the highest NPV, leading to the one-sided nature if the NPV and IRR PDFs.

For temperature variation only, when an ellipse is fitted to the simulated data, as shown in (5.5) where a is 46, b is 127000, an RMSE of 1479$ and an R^2 value of 0.991 is obtained. Also interesting to see is the relation between NPV and battery life, as shown in Section 5.6, where the relationship looks like the time response of a first order system. The simulated data can be fitted using (5.6), where a is 147000, b is 1.6, c is 220000 yielding a root mean square error of $2847 and R^2 value of 0.967.

$$\frac{\text{Temperature}^2}{\text{a}^2} + \frac{\text{NPV}^2}{\text{b}^2} = 1 \tag{5.5}$$

$$\text{NPV} = -\text{a} * \exp(-\text{EOL}/\text{b}) + \text{c} \tag{5.6}$$

5.7 Conclusions

Impact of temperature and importance of cooling system: One key take-away from this analysis is that battery temperature of operation has significant impact on battery life. It is therefore key to design a battery cooling system that can maintain the temperature at a desired value at all times. At the same time, the cooling system needs to be fast enough to cool the battery to the desired temperature quickly and minimize the exposure of the battery to undesired temperatures. Also, the battery needs to be stored in cool places when the cooling system is not operational.

Stochastic aspect of battery life, and economic viability: The framework also helps us associate probability to expected battery life and scenario of economic

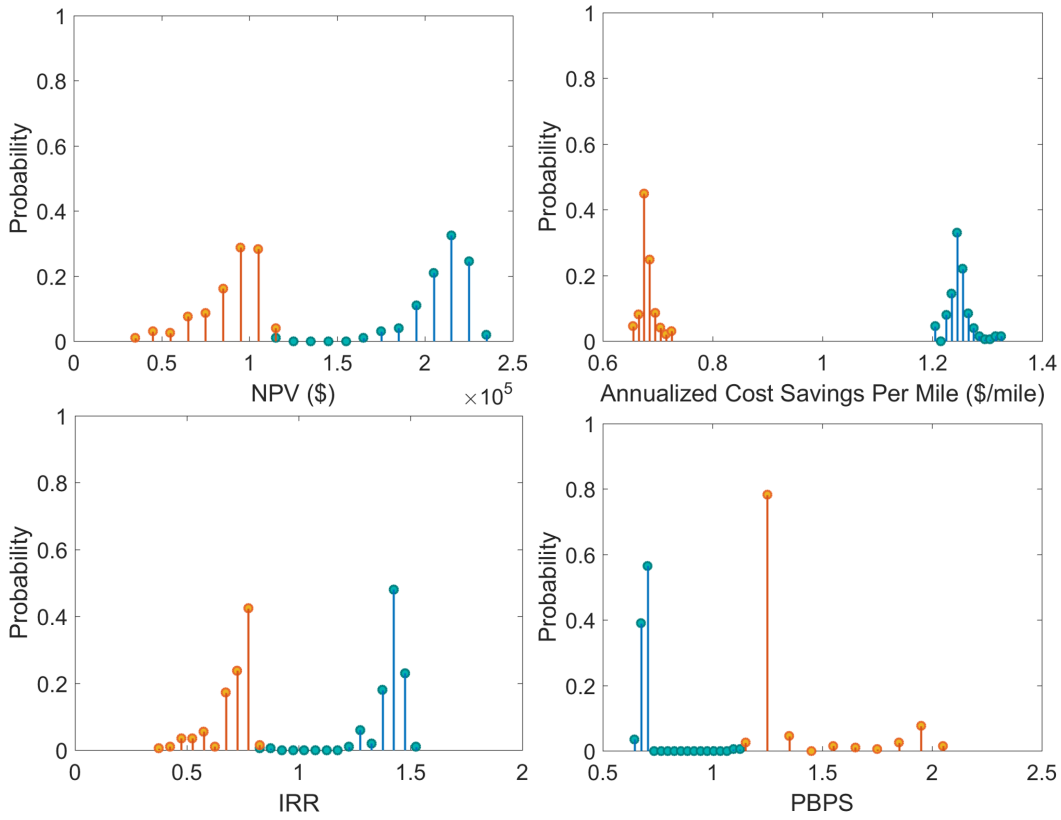

Figure 5.13. Total variation in battery capacity loss and end-of-life due to variation in C-rate, VMT between recharges and battery temperature of operation (solutions with positive NPV for the 2025 economic scenario have been considered).

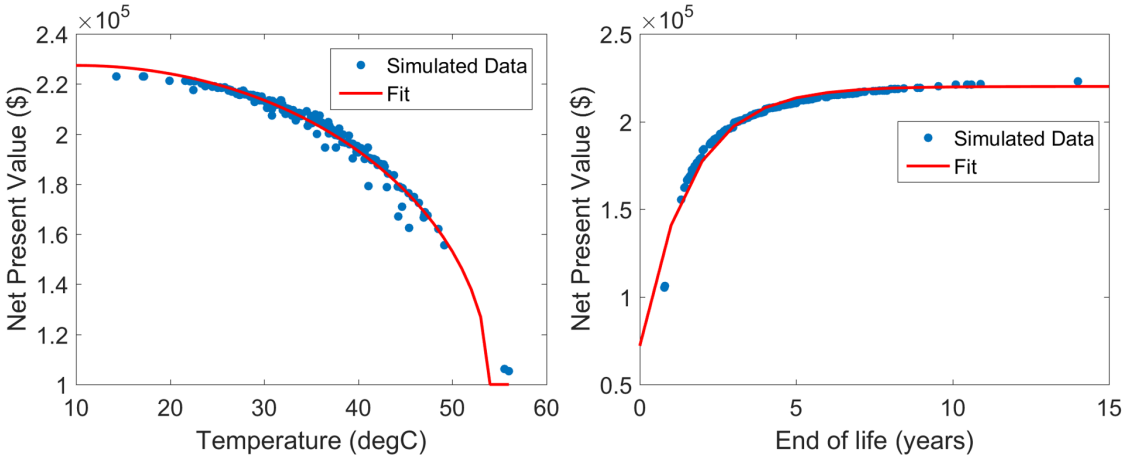

Figure 5.14. Variation of net present value with respect to temperature and battery life.

viability, thereby taking this simulation based analysis a step closer to realistic scenarios of usage. The stochastic estimations can be improved further by associating PDFs to economic predictions to get more confidence in the economic calculations. Further, empirical relations can also be obtained for dependence of NPV on temperature, C-rate and VMT between recharges.

6. IMPACT OF BATTERY HEATING/COOLING SYSTEM ON FUEL CONSUMPTION AND ECONOMIC VALIDITY

6.1 Introduction

The framework until now has assumed that the battery is maintained at the desired temperature at all times. But in practice, this is not the case. Batteries used in all hybrid electric vehicles, with all degrees of hybridization, are accompanied by either an passive or an active cooling system. There have been multiple studies ([41], [42], [43], [44]) that compare the kind of cooling systems that can be used by HEV/PHEV batteries.

In this section the heating/cooling system is approximated by a Coefficient of Performance (COP) map which links the ambient temperature to the work required to maintain the battery at a desired temperature. The required work is then used to calculate the excess fuel required to run the heating/cooling system at a given ambient temperature. This excess fuel can then be used to re-estimate the economic metrics and the effect of ambient temperature and the heating/cooling system on parameters such as fuel consumption reduction, NPV, payback period etc. can be estimated. It is assumed that the excess energy required by the heating/cooling system is provided by the engine. It is also assumed that the change in weight of the truck/bus due to the heating/cooling system is negligible.

6.2 Framework

The framework used in this section to estimate the effect of ambient temperature and a heating/cooling system on the economic metrics is shown in Figure 6.1. The vehicle simulation model considered here is the Autonomie model discussed previously. For the purpose of analysis in this chapter, no new simulation was run, rather the

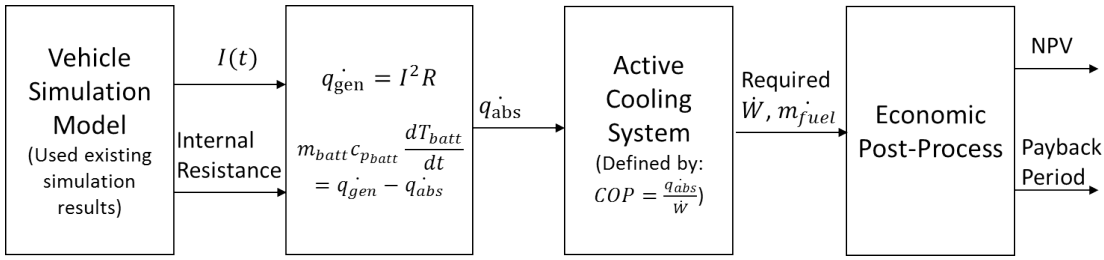

Figure 6.1. Framework for estimating effect of battery heating/cooling system on fuel consumption and economic viability.

Autonomie results from the pre-existing simulations were reused. The CD and CS mode battery current profiles ($I(t)$) and battery internal resistance profiles ($R_{\text{int}}(t)$) are used from the set of results. The framework described here can be used as "post-processing" to estimate the excess fuel required by the heating/cooling system. Although this approach allows us to estimate the excess fuel consumption due to the heating/cooling system and it's impact on the economic parameters and compare with the previous results in a fast manner, the effect of battery temperature variation on battery performance is not captured. It is assumed that during the time when the battery temperature is not equal to the desired temperature, the change in battery performance and hence it's impact on engine operation, battery degradation and hence fuel consumption and battery replacements is negligible.

To calculate the excess energy required to maintain battery temperature, the heat generated by the battery needs to be estimated first. The heat generated by the battery is given by, (6.1), where I is the current sourced/sunk by the battery and R is the effective internal resistance of the battery. The validation of this equation is discussed in the next section. Using First Law of Thermodynamics the temperature of the battery can be estimated. The first law energy balance for the battery is shown in (6.2), where m_{batt} is the mass of the battery, c_{batt} is the specific heat of the battery, T_{batt} is the instantaneous battery temperature, q_{gen} is the heat generated by the battery as given by (6.1) and q_{abs} is the heat absorbed by the heating/cooling system. When the heating/cooling system is in the heating mode, q_{abs} is negative, and q_{gen} and q_{abs} together help raise the temperature of the battery to the desired value. When in the cooling mode, q_{abs} is positive, when it's value is higher than q_{gen} the battery temperature falls, and when the value of q_{abs} is equal to q_{gen} the battery temperature is maintained. The rate of heat absorbed by the heating/cooling system, q_{abs}, is limited by the total capacity of the heating/cooling system. Typically, this value ranges between $1kW - 10kW$. For the purpose of this study, the heating/cooling system is assumed to be rated at $5kW$. Therefore, q_{abs} is limited to $5kW$. When the heating/cooling system is started, it operates at it's rated capacity, $q_{\text{abs}} = \pm 5kW$,

until the battery reaches the desired temperature, after which the system is assumed to operate so as to ensure $q_{\text{abs}} = q_{\text{gen}}$, i.e. all the generated heat is absorbed. This gives us the profile for rate of heat absorbed by the heating/cooling system over the CD and CS modes.

$$\dot{q}_{\text{gen}} = I^2 R_{\text{int}} \tag{6.1}$$

$$m_{\text{batt}} * c_{\text{batt}} * \frac{dT_{\text{batt}}}{dt} = \dot{q}_{\text{gen}} - \dot{q}_{\text{abs}} \tag{6.2}$$

The heating/cooling system is described by a map of variation of the coefficient of performance with respect to the ambient temperature as shown in Figure 6.2. Coefficient of performance of a refrigeration system is defined as the ratio of the refrigeration effect to the net work input to achieve that effect [89], as shown in (6.3), where $\dot{q}_{\text{abs}}$ is the rate of heat absorption by the heating/cooling system and $\dot{W}$ is the rate of work or power required to operate the heating/cooling system. COP of a vapor compression refrigeration system depends on ambient temperature, evaporator temperature, compressor speed, structure and design of the system etc. The system assumed here is shown in Figure 6.3. The primary loop consists of the compressor, evaporator, expansion valve and the condenser and uses a refrigerant such as R134a. The evaporator is connected to the primary loop where a coolant such as Ethylene Glycol + Water mixture is used as the heat transfer fluid, and consists of a pump that maintains the coolant mass flow rate. This coolant is circulated in small tubes around the battery so as to ensure effective heat absorption [90].

There is very limited literature on the experimental variation of cooling system COP with respect to ambient temperature. Fixing the heating/cooling system architecture further limits the availability of data. Studies [90] [91] [92] have either simulated or performed experimental studies relating to the use of heating and cooling systems for electric/hybrid electric vehicle applications using a heating/cooling set-up similar to the one defined in this section. Based on the coefficient of performance obtained by these studies, the variation of COP with ambient temperature for heating and cooling has been assumed as shown in Figure 6.2. Considering COP

variation with respect to the ambient temperature allows us to link climatic variations in temperature to efficiency of operation of the heating/cooling system and hence to fuel consumption. The closer the ambient temperature is to 15° C, more efficient the system is. In extreme hot/cold conditions, the system is less efficient. Using the map shown in Figure 6.2 and the relation shown in (6.3), the rate of change of work required to operate the heating/cooling system can be calculated. From the rate of change of work, the fuel rate can be calculated using (6.4), where $\dot{m}_{\text{fuel}}$ is the fuel rate in kg/s, $\text{LHV}_{\text{diesel}}$ is the lower heating value of diesel in J/kg, and $\eta_{\text{eng}} and \eta_{\text{gen}}$ are the engine and generator (when present) efficiencies respectively. The instantaneous efficiencies can be obtained from the vehicle simulation results, else average efficiencies can be assumed for each. The fuel rate ($\dot{m}_{\text{fuel}}$) can be integrated to get the total excess fuel (kg) required to operate the heating/cooling system over CD and CS modes, which can then be used to calculate the economic metrics.

$$\text{COP} = \frac{\dot{q}_{\text{abs}}}{\dot{W}} \tag{6.3}$$

$$\dot{W} = \dot{m}_{\text{fuel}} * \text{LHV}_{\text{diesel}} * \eta_{\text{eng}} * \eta_{\text{gen}} \tag{6.4}$$

$$\text{FC} = \frac{\int m_{\text{fuel}} dt}{\rho_{\text{diesel}} * distance} \tag{6.5}$$

6.3 Validation of $\dot{q}_{\text{gen}} = I^2 * R_{\text{int}}$

In reference [69], the authors performed electrochemical and thermal modeling of commercial 1.2 Ah 18650 cells with the nickel-manganese-cobalt oxide (NMC) cathode, graphite anode and 1.2M LiPF6 in EC/DMC electrolyte. They have also validated this model against experimental data. In their experiments, they cycled the NMC/Graphite cells at 1C, 2C, 3C, 5C, and 10C using constant current charge/discharge cycles with 100% DOD. The cell was kept in an environment chamber maintained at 25°C. The voltage and temperature profiles seen by the cell during cycling have been used in this section to validate our rate of heat generation model.

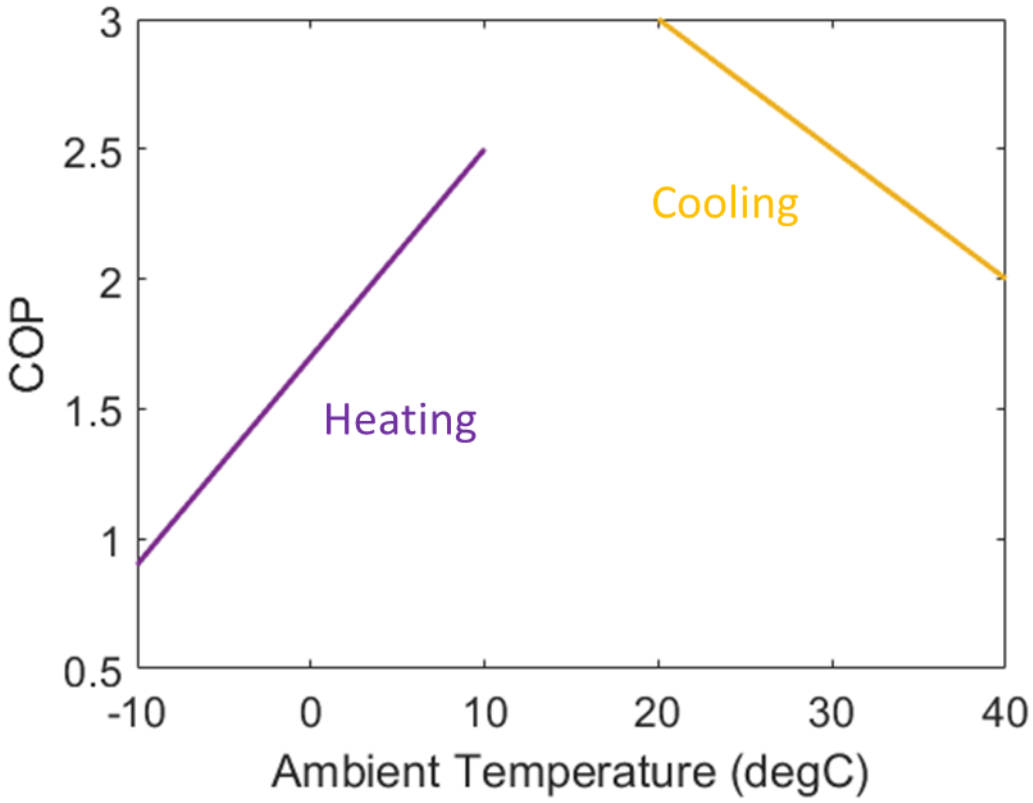

Figure 6.2. Assumed variation of COP with ambient temperature.

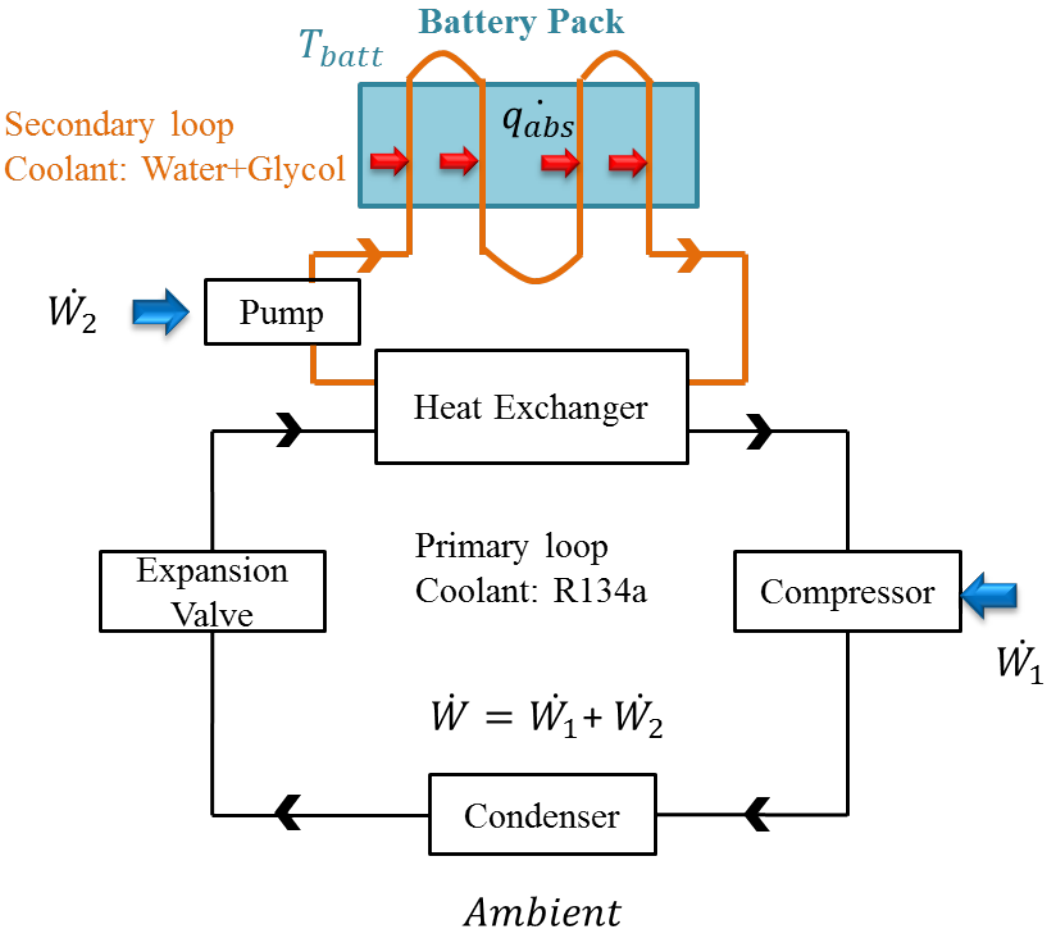

Figure 6.3. Assumed refrigeration system.

Table 6.1. $R_0(\Omega)$ variation with temperature, SOC and charge/discharge.

Charge	0°C	25°C	Discharge	0°C	25°C
40% SOC	0.078	0.031	40% SOC	0.083	0.037
60% SOC	0.073	0.029	60% SOC	0.075	0.034

The current and resistance of the battery are required to validate the heat generation model. While the current is known from the cycle specifications, the internal resistance of the specific cell used during experimentation needs to be estimated. The voltage response of the cell to pulse tests, as given in [69], along with Equations (2.5) to (2.7) are used, to fit values to R_0, R_1. The cell was subjected to 10s charge and discharge pulses at rates of 1C, 2C, 5C and 10C with 10s open circuit relaxation between each discharge and charge pulse of the same C-rate and 30s relaxation between discharge and charge pulses of other C-rates. This was performed for two initial SOCs, viz. 40% and 60%, and for two chamber temperatures, viz. 0°C and 25°C. Battery internal resistance is different during charge and discharge [73], hence R_0, R_1 were fitted separately for these events. The first sudden change in voltage after applying the current pulse is due to R_0, while the slower change in voltage seen after the sudden drop is due to the R_1C_1 time constant. This logic was used along with the equations to ensure a good fit. The fitted values of R_0, R_1 are shown in Tables 6.1 to 6.2. C_1 is kept fixed at 6000F, since good match to the curved portion of the pulse was obtained at this value. The result of the fit is shown in Figure 6.4, where less than 2% error is observed for the 25°C data-set across all C-rates, whereas less than 7% error is shown for the 0°C data-set because of voltage under-prediction at 10C. This suggests using higher order equivalent-circuit models at low temperatures.

Once the resistance values are known, the model for rate of heat generation can be validated. The resistance at all temperatures and SOCs has been linearly interpolated/extrapolated from the previously obtained values. The authors of [69] also measured the cell temperature during CC-CV charge and CC-CV discharge. For

Table 6.2. $R_1(\Omega)$ variation with temperature, SOC and charge/discharge. C_1 is assumed to be 6000F always.

Charge	0°C	25°C	Discharge	0°C	25°C
40% SOC	0.011	0.009	40% SOC	0.014	0.011
60% SOC	0.01	0.007	60% SOC	0.013	0.007

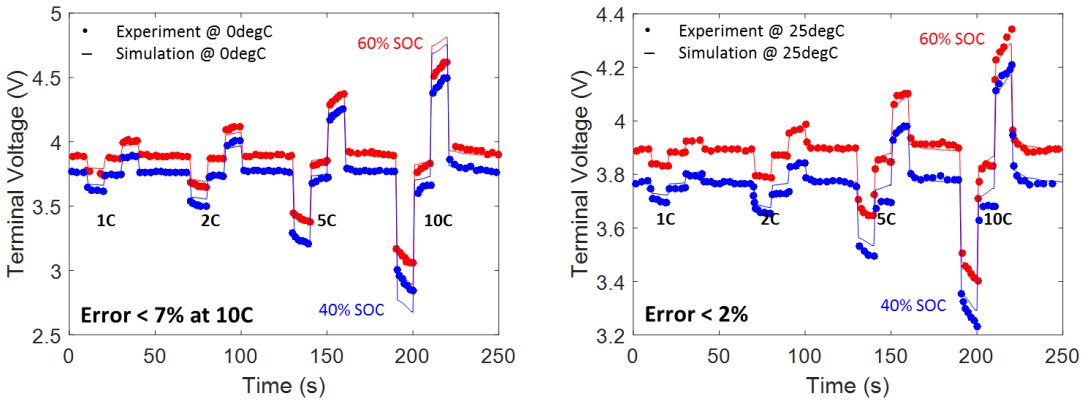

Figure 6.4. Validation of voltage response at 0°C *(left)* and 25°C *(right)*.

Table 6.3. Cell specific parameters.

Parameter	Value
h [69] (W/m^2K)	20
A (m^2)	0.0037
c_{batt} (J/kg-K)	1000
Cell Capacity (Ah)	1.2
m_{batt} (g)	50
T_{amb} (K)	298.15

simplicity, only the constant current (CC) part for charge and discharge has been simulated here, i.e. the battery is subjected to 1C/2C/5C/10C current until the SOC reaches 100% during charge and until the SOC reaches 0% during discharge. Since the cell was kept in an environment chamber during the experiment, the heat loss to the ambient can be assumed to occur only through convective heat transfer. Energy balance of the cell yields (6.6). The cell specific parameters used here are given in Table 6.3. The resulting comparison between the experiment and simulated cell temperature is shown in Figure 6.5. It is shown that there is very little temperature rise for 1C, and the rate of temperature rise is higher for higher C-rates, since the current is higher. For both the charge and discharge conditions, the error percentage between the simulated and experimental data at all C-rates is less than 10%, where the simulated results over-predict the temperature. The difference between simulated and experimental data could be a result of inaccurate resistance estimation and/or difference in actual cell specific parameters listed in Table 6.3.

$$m_{batt}c_{batt}\frac{dT}{dt} = -hA(T_{batt} - T_{amb}) + I_0^2R_0 + I_1^2R_1 \tag{6.6}$$

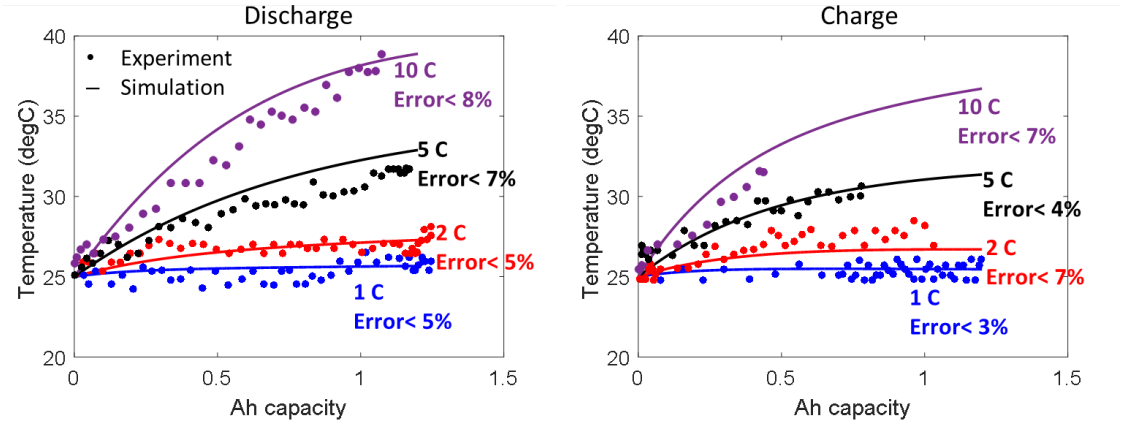

Figure 6.5. Validation of temperature during discharge *(left)* and charge *(right)*.

6.4 Results

This section describes the results obtained for battery temperature, heating/cooling system COP, resulting increase in fuel consumption and change in the economic metrics. For the purpose of this study, the vehicle simulation results for the Series Transit Bus winning solution (Table 4.1) over the Manhattan cycle have been re-used. The cell chemistry used in those simulations was NMC+LMO/Graphite with 33.1Ah capacity/cell. The battery performance model in the vehicle simulations was a 0^{th} order model, without the R_1C_1 branch, hence only R_0 is considered in the rate of heat generation model.

6.4.1 Temperature Estimation

The rate of heat generation seen when cooling the Series Transit Bus winning solution battery from a constant ambient temperature of 45°C to the desired temperature of 20°C, at the beginning of the day is shown in Figure 6.6a. The powertrain is operating in the CD mode and only the first 5000s (83 mins) of the day are shown. The cooling system operates at the maximum cooling capacity (5kW) until the battery reaches the desired temperature, which takes 2200s (36 mins), as shown in Figure 6.6d, hence the rate of heat absorption is 5kW during that time, after which the rate of heat absorption is equal to the rate of heat generation, as shown in Figure 6.6b. Practically, since the coolant temperature cannot change with the same rate as variation of heat generation, the rate of heat absorption after the first 2200s (36 mins) will settle to the average rate of heat generation and would not show such high transients. Also, some of the generated heat will be lost to other battery surroundings, it is assumed here that this heat is negligible. The COP of the cooling system, as shown in Figure 6.6c, stays constant because the ambient temperature is constant.

Figure 6.7 shows that when the battery is heated from a constant ambient temperature of −5°C to a desired temperature of 20°C, the rate of heat absorption (Fig-

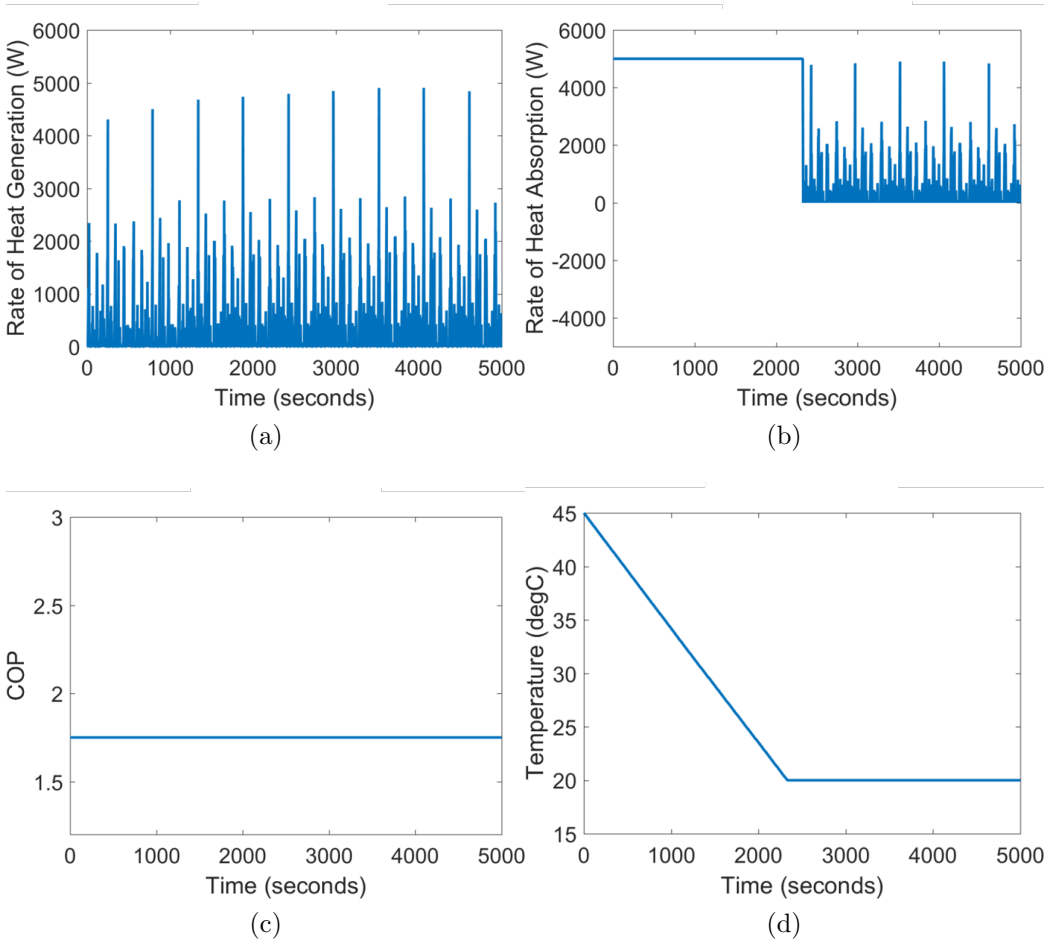

Figure 6.6. Temperature estimation results for cooling system.

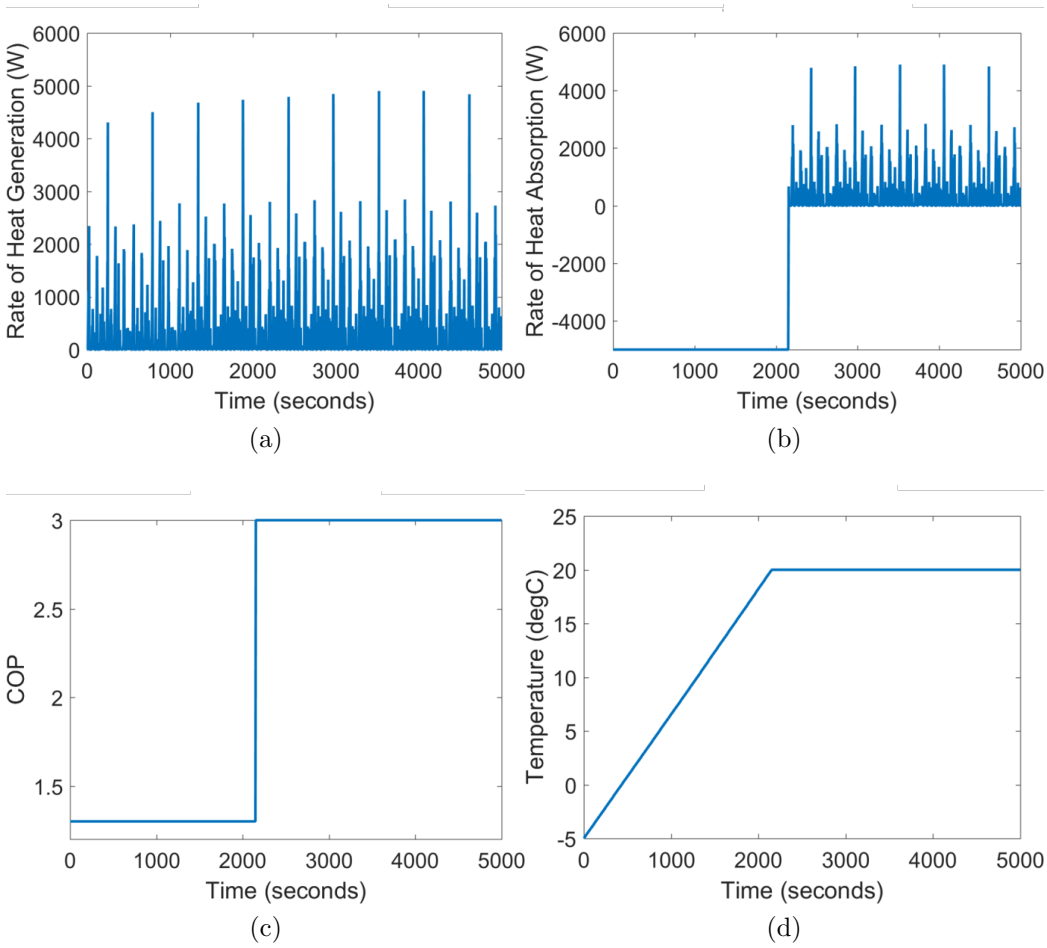

Figure 6.7. Temperature estimation results for heating system.

ure 6.7a) is negative initially because heat is provided to the system. The heat generated by the battery is helping the heating system in raising the battery temperature. Once the battery reaches the desired temperature, the cooling system is used to absorb the heat generated by the battery so as to maintain temperature. Since the COP for heating and cooling are different for the same ambient temperature, a step change in COP is observed when the battery reaches the desired temperature.

6.4.2 Change in Fuel Savings and Economic Parameters

The excess fuel consumption is calculated using (6.4) and (6.5) for the CD and CS modes, and combined using the utility factor. Since there is no change in the CD mode range, in this study, the winning solution utility factor remains unchanged. The percentage change in fuel consumption as compared to that of the winning solution is plotted for all the bus drivecycles for the heating and cooling cases in Figure 6.8. Across all drivecycles, for the considered ambient and desired temperatures, and COP assumptions, the fuel consumption increase is between 0.8% and 1.9% only. More increase in fuel consumption is observed for the cooling case because of the lower overall COP, as compared to the heating case. It is important to note that the current sourced/sunk by the battery is different for all drivecycles as is the baseline winning solution fuel consumption. Therefore, the percentage increase in fuel consumption in the heating and cooling cases is different for all drivecycles.

When the percentage fuel savings with respect to the conventional vehicle are compared for the winning solution with and without the heating/cooling system, as shown in Figure 6.9a, compared to the original fuel savings between 60%-70%, the 0.8%-1.9% change is very small. With the increased fuel consumption, the Net Present Value is expected to reduce, as it does in Figure 6.9b, but by a very small value (0.7% - 3%). Due to the reduction in fuel savings, it will take longer to recover the initial system cost, as shown in Figure 6.9c, but the change is small (0.4% - 1.5%).

6.5 Conclusions

The study performed in the previous chapters assumed that there exists a heating/cooling that always maintains the battery at a desired temperature of 20°C, and the battery performance and number of replacements were calculated accordingly. In practice, such a heating/cooling system would require excess energy for operation, which would be supplied by the engine or the battery.

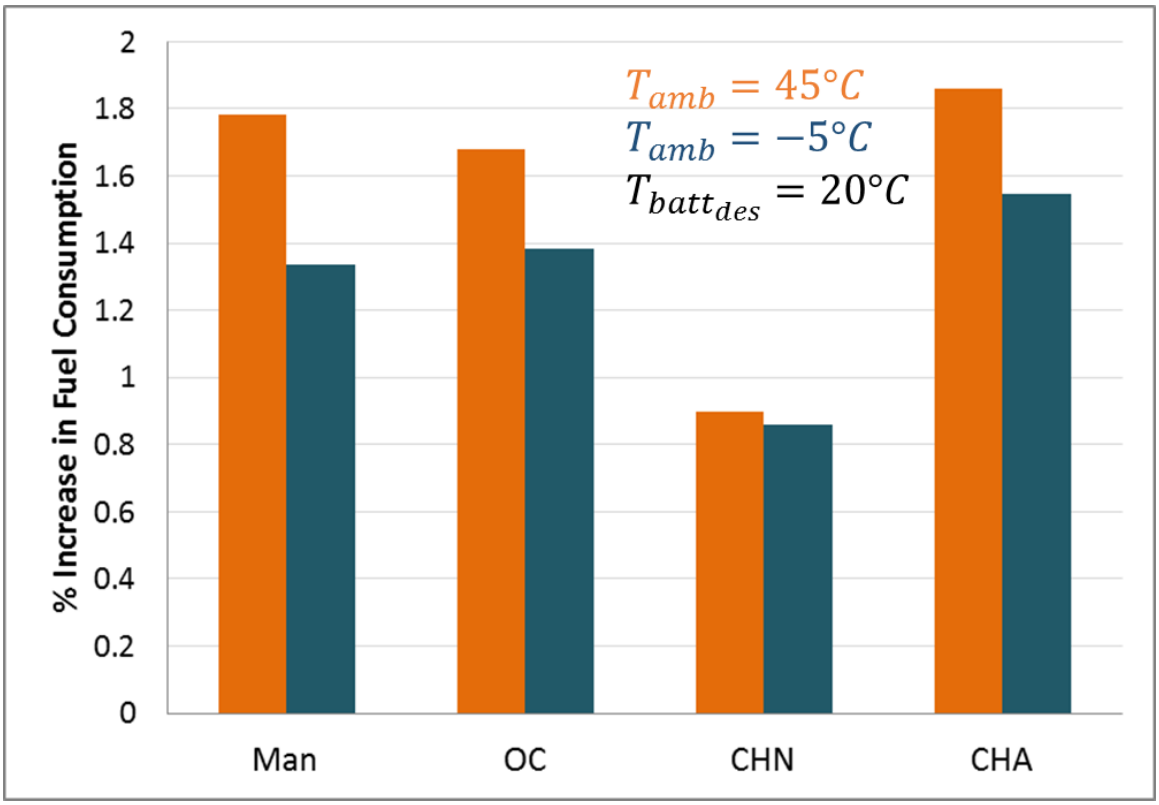

Figure 6.8. Percentage increase in fuel consumption due to power required by the heating/cooling system.

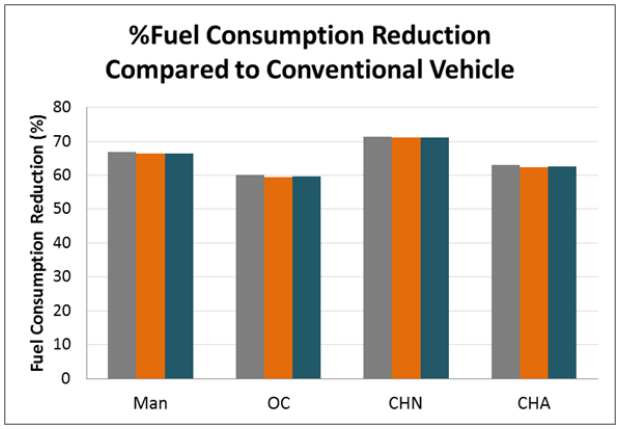

(a)

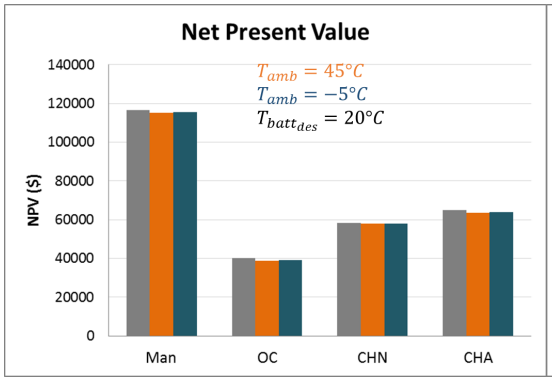

(b)

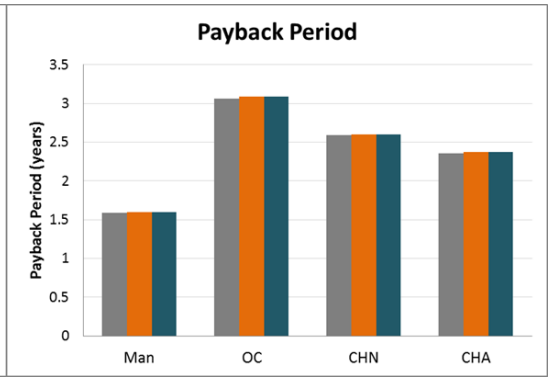

(c)

Figure 6.9. Comparing change in economic metrics due to heating and cooling with the winning solution results (a) Change in percentage fuel savings (b) Change in NPV (c) Change in payback period.

Assuming all the energy required for the operation of the heating/cooling system was supplied by the engine, a framework for estimating the excess fuel consumption required to operate the heating/cooling system was proposed which is run as a post-process step after the vehicle simulation. A COP based heating/cooling system was evaluated for excess fuel consumption resulting from operation in two ambient temperature conditions (45°C and −5°C) and with 20°C desired temperature. It is shown that for the Series Transit Bus winning solution, the percentage increase in fuel consumption lies between 0.8%-1.9% across all drivecycles.

The resulting reduction in fuel savings with respect to the conventional vehicle, reduction in Net Present Value and increase in Payback Period as compared to the base case is very small.

The battery takes about 35 mins to heat/cool to 20°C from $-5°C/45°$C. It is assumed that exposure to these temperatures for only 35 mins out of the 10 hr work day does not affect the number of battery replacement or battery performance.

Additionally, the model of rate of heat generation ($\dot{q} = I^2R$) was validated for a 18650 NMC/graphite 1.2 Ah cell. The error percentage between temperature predictions using this model with the experiment data was found to be less than 10% during charge and discharge for currents with C-rates upto 10C. This accuracy of temperature prediction depends on the accuracy of estimation of the cell internal resistance, as well as the estimation of the heat transfer coefficient and other cell specifications.

If the energy required for heating/cooling system is assumed to come from the battery, the effect of the system on the CD mode range can be evaluated in the future. Additionally, existing physics based models of heating/cooling system, can be used as a part of the vehicle simulation model, to evaluate the effect of time taken to reach the desired battery temperature on battery performance and number of battery replacements. Further, the impact of storage temperature of the battery, especially winter temperatures, on battery degradation and strategies to store the battery at the desired temperature need to be evaluated.

7. UNDERSTANDING WTW EMISSION IMPACTS OF PHEV TRANSIT BUSES

7.1 Introduction

Previous chapters have demonstrated, in simulation, the fuel saving potential of PHEV medium-duty trucks and PHEV heavy-duty transit buses using powertrain sizing, controls optimization and architecture selection and the resulting cost savings achieved with respect to conventional medium-duty trucks and heavy-duty transit buses, respectively. This analysis was done considering battery degradation and replacement and under variable usage conditions. The importance of maintaining the battery temperature was emphasized and the fuel penalty of using a heating/cooling system was calculated, using a series transit bus on Manhattan as an example case. Under all usage conditions, the benefits of plug-in hybridization for medium and heavy duty vehicles are clear, subject to the economic time frame. But cost implications, although of significant importance, are not the only aspects to be considered with hybridization. Since PHEVs require battery charging from the grid, there is significant concern about the resulting greenhouse gas emissions. This chapter aims at throwing some light on the greenhouse gas emission reductions possible via plug-in electric hybridization taking the series transit bus as the base case. The WTW greenhouse gas emissions have been calculated for two use cases of the series transit bus winning solution, when used in Indiana and California. These states differ significantly in their electricity sources, where Indiana derives most of its electricity from coal, Californias electricity comes majorly from natural gas along with significant contributions from renewable resources. Therefore, well to pump greenhouse gas emissions from these states are very different. As such they pose as good examples to evaluate and compare greenhouse emission reductions, if any, achievable through plug-in electric hybridization of medium/heavy-duty vehicles.

This chapter looks at the well to wheel emissions resulting from usage of PHEV series transit bus over a city drivecycle (Manhattan drivecycle) and compares that with the emissions resulting from operating a conventional vehicle on the same route. The emissions resulting from component manufacturing processes have not been considered here. The GREET well to wheel emissions analysis tool (GREET2017) have been used for this purpose.

About GREET: GREET [93] is a vehicle emission calculator developed by Argonne National Labs that calculates $CO_2, CH_4, N_{2O}, PM, NO_x$ and other criteria pollutants resulting from transportation life cycles. It also combines the CO_2, CH_4, N_{2O} emissions with their global warming potentials (1, 25 and 298 respectively) to give the greenhouse gas emissions for 100 years (IPCC 2008) [60]. Emission calculations are performed in 2 parts: well to pump (WTP) and pump to wheel (PTW). Multiple fuels are defined for transportation technologies, for each fuel different fuel paths are defined, which include fuel sources, production stage and distribution stage, and emissions are calculated for each fuel path. This constitutes the WTP emissions. Additionally, the software also defines different vehicle types and technologies and specifies the emissions per MJ of fuel combustion for these vehicle types and technologies. This constitutes the PTW emissions. For the purpose of this analysis a heavy-duty CIDI Transit Bus, and it's PTW emissions/MJ of Low-sulfur diesel as defined in the software, is used as the base scenario.

7.2 Framework

In order to understand the well to wheel (WTW) emissions resulting from PHEV heavy-duty Transit Bus, the amount of electricity and fuel used per day need to be known. Although GREET2017 already has pre-existing WTW emissions for a variety of vehicles and fuels, in this study, the vehicle has been modeled and simulated in Autonomie, since Autonomie allows greater flexibility in modifying the vehicle powertrain and control, as well as in defining vehicle use cases. Pre-existing vehicle

simulation results for the PHEV heavy-duty Transit Bus winning solution have been reused in the following sections.

As mentioned earlier, GREET provides emissions/MJ of fuel used for WTP as well as PTW for the chosen vehicle. A flexibility to choose the fuel pathway for the WTP emissions exists. A subset database of WTP and PTW emissions for electricity and diesel sources was created to interface well with the Autonomie results. The interface is used to user select the desired source of fuel, and combine the WTW emissons/MJ for that fuel with the estimated fuel energy from Autonomie to yield the daily WTW emissions from the vehicle. Since, the emissions are considered per MJ of fuel used by the end-user, the WTP and PTW values can be simply added to give the WTW emissions per MJ of fuel used, as shown in (7.1).

$$\text{WTW emissions [g/(MJ of fuel used)]} = \text{WTP} + \text{PTW} \tag{7.1}$$

Diesel is used in both the CD and CS modes, since this is the blended CD mode. The diesel energy used in both the modes is calculated on a per mile basis (MJ/mi), and then combined using the utility factor, as shown in (7.2) where $E_{\text{diesel}}, E_{\text{diesel\_CD}}$ and $E_{\text{diesel\_CS}}$ are the total, CD mode and CS mode diesel energy consumption per mile (MJ/mi). This is input to the interface to get emissions/mile (g/mi), which can then be scaled depending on the daily VMT to give the daily emissions, as given in (7.3) where $\text{WTW}_{\text{diesel}}$ is the WTW emissions per mile due to the diesel energy used per mile ad Daily_VMT is the vehicle miles traveled in a day. Electricity is assumed to be used once daily, to recharge the battery from 30% SOC to 100% SOC. Multiple grid charges during the day have not been considered in this study. The MJ of energy required to recharge the battery from the grid is input to the interface to get the daily emissions due to battery charging, where the energy is calculated as given in (7.4), AhCap being the battery capacity in Ampere-hrs and η_{charging} being the charging efficiency assumed to be 90% as in Chapter 3. The daily emissions from diesel and electricity can then be added to get the overall daily WTW emissions from the

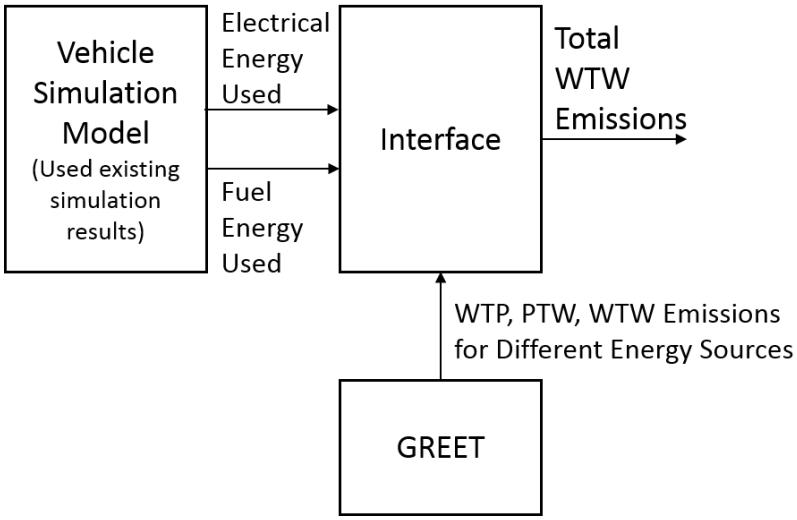

Figure 7.1. Framework for estimating WTW emissions from PHEV transit bus.

PHEV heavy-duty Transit Bus with the winning solution powertrain configuration, as given in (7.5) where $\mathrm{WTW}_{\mathrm{daily\_total}}, \mathrm{WTW}_{\mathrm{daily\_diesel}}$ and $\mathrm{WTW}_{\mathrm{daily\_electricity}}$ are the daily total, diesel, and electricity WTW emissions respectively .

$$E_{\mathrm{diesel}}[\mathrm{MJ/mi}] = E_{\mathrm{diesel\_CD}} * \mathrm{UF} + E_{\mathrm{diesel\_CS}} * (1 - \mathrm{UF}) \tag{7.2}$$

$$\mathrm{WTW}_{\mathrm{daily\_diesel}}[\mathrm{g}] = \mathrm{WTW}_{\mathrm{diesel}}[\mathrm{g/mi}] * \mathrm{Daily\_VMT}\ [\mathrm{mi}] \tag{7.3}$$

$$E_{\mathrm{daily\_electricity}} = \frac{0.7 * \mathrm{AhCap}}{\eta_{\mathrm{charging}}} \tag{7.4}$$

$$\mathrm{WTW}_{\mathrm{daily\_total}} = \mathrm{WTW}_{\mathrm{daily\_diesel}} + \mathrm{WTW}_{\mathrm{daily\_electricity}} \tag{7.5}$$

7.3 Results

The major sources of electricity in the US are

1. Coal
2. Natural Gas
3. Nuclear

4. Biomass

5. Hydroelectric, Solar, Wind, Geothermal, and other renewables

The WTP emissions arising during the generation of electricity from these sources are shown in Figure 7.2 [93]. There are no PTW emissions when a battery and electric machine are used to provide tractive power to a vehicle. For the purpose of comparison, these PTW emission values are obtained at the generation stage and do not include the emissions or losses during the transmission and distribution stages. It is observed that most CO_2 is produced because of electricity generation from coal, natural gas fired plants emit 55% less CO_2 than coal-fired plants, followed by geothermal (90% less), biomass (97% less) and nuclear (99% less). Although electricity generation through biomass produces 97% less CO_2 than coal-fired power plants, CO, NO_x, and PM emissions from biomass-based power plants are significantly higher. Hence, it is known that more percentage of coal-fired power plants in a state would result in significant CO_2 emissions per MJ of electricity produced.

Indiana gets 81% of it's electricity form coal-fired power plants, followed by 13% from natural gas fired power plants, and the rest is obtained mostly from renewable resources [94]. So, the individual emissions/MJ from coal-fired power plants, natural gas fired power plants, etc. can be weighted by these percentage contribution of each of these power plants to obtain average emissions/MJ of electricity generated in Indiana. California, on the other hand, gets majority (55%) of it's electricity from natural gas fired power plants and only 6% form coal-fired power plants. The mix of resources for electricity generation in California also includes a significant contribution by renewable resources such as geothermal, hydro-electric, wind power etc as well as from cleaner nuclear power plants [95]. This mix of less CO_2 producing power plants inherently makes electricity usage in California cleaner. thus it is expected to see lesser greenhouse gas emissions resulting from a PHEV heavy-duty transit bus operating in California than the one operating in Indiana, assuming the same powertrain, same

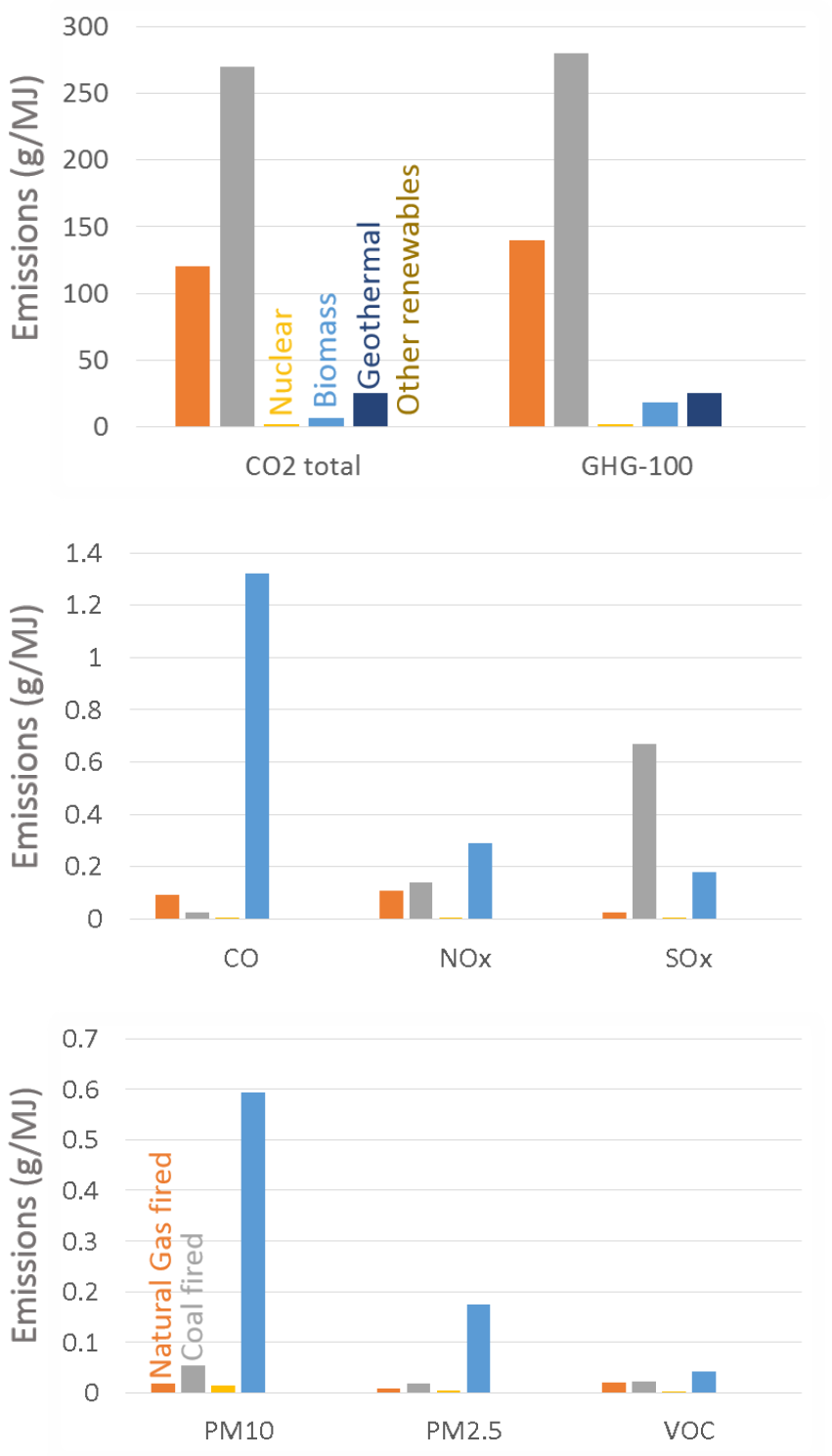

Figure 7.2. Emissions according to source of electricity (in g/MJ of electricity used).

diesel fuel, it's production and distribution. The sources of electricity in both the states have been compared in Figure 7.3.

For a battery powered transit bus, the PTW emissions are zero, hence the WTP emissions can be treated as WTW emissions. For a diesel powered transit bus, the WTW calculations need to consider the emissions resulting from diesel production, transmission and usage. The emissions/MJ of electricity or diesel used by a only battery operated or only diesel operated transit bus respectively can be compared, as shown in Figure 7.4. The WTW emissions/MJ of diesel used have been taken from GREET for a heavy duty transit bus operating on low-sulfur diesel obtained from crude oil. For every MJ of electricity used by the vehicle more greenhouse gases, CO, NO_x, SO_x, VOC and PM are produced as compared to those produced due to 1MJ of low-sulfur diesel fuel usage. Additionally, if that electricity was generated in Indiana, significantly more greenhouse gases(2.5 times), NO_x (1.75 times) and PM (2.3-3 times) would be produced than if it was generated in California.

But the total emissions also depend on the MJ of energy used in both the cases, where the MJ of energy not only depends on the drivecycle requirements but also on the efficiency of the fuel converter (engine or electric machine) itself. This is taken into account when the total diesel fuel used or the total grid electricity required for charging is considered. Therefore, when a PHEV transit bus is considered, the battery capacity as well as the fuel consumption reduction plays a significant role in reducing the overall emissions. As shown in Figure 7.5, for a PHEV transit bus the electrical energy required from the grid (70% of battery capacity, with 90% charging efficiency) is only 125 MJ, and the diesel energy required in CD and CS modes is 1811 MJ, as compared to the 5370 MJ of diesel energy required by a conventional transit bus on Manhattan drivecycle. This energy use is calculated for 1 day, where 100 miles are driven by the bus in a day, considering a single overnight battery re-charge from 30% - 100% SOC. If multiple recharges are considered during the day, the electrical energy component would increase, and the diesel energy component would reduce. This figure also shows the significant reduction in energy consumption by the vehicle,

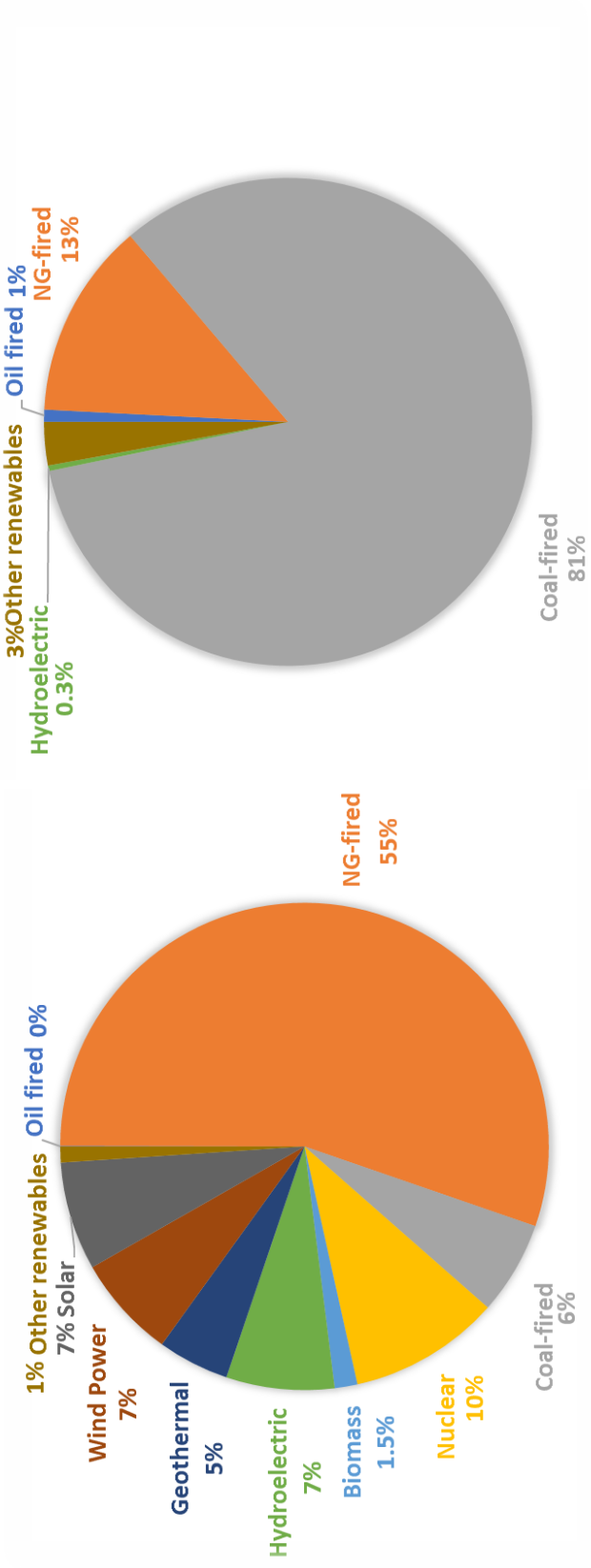

Figure 7.3. Sources of electricity in California and Indiana.

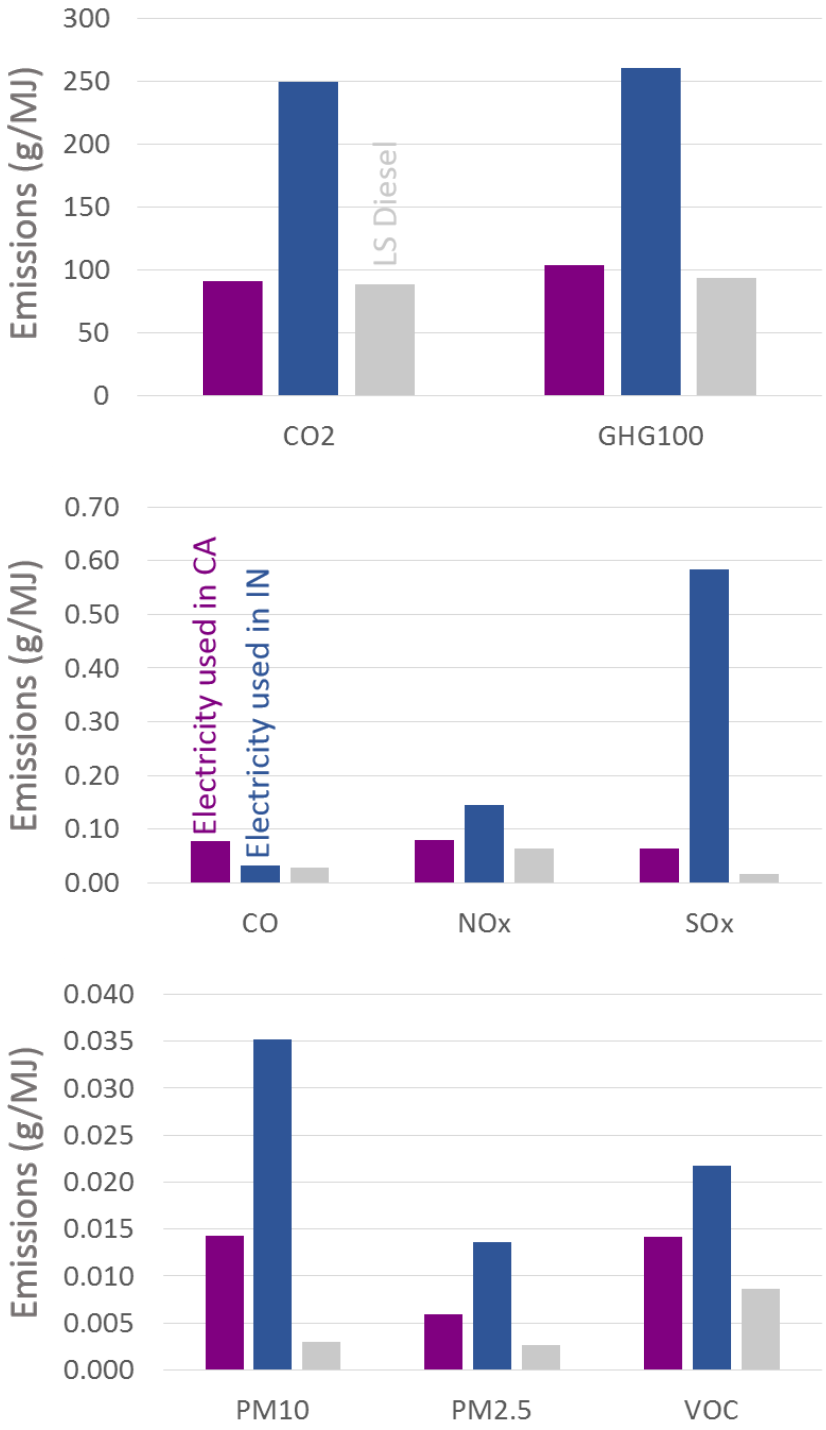

Figure 7.4. Comparison of WTW emissions from buses operated on electricity in California and Indiana with those from buses operated on low-sulfur diesel.

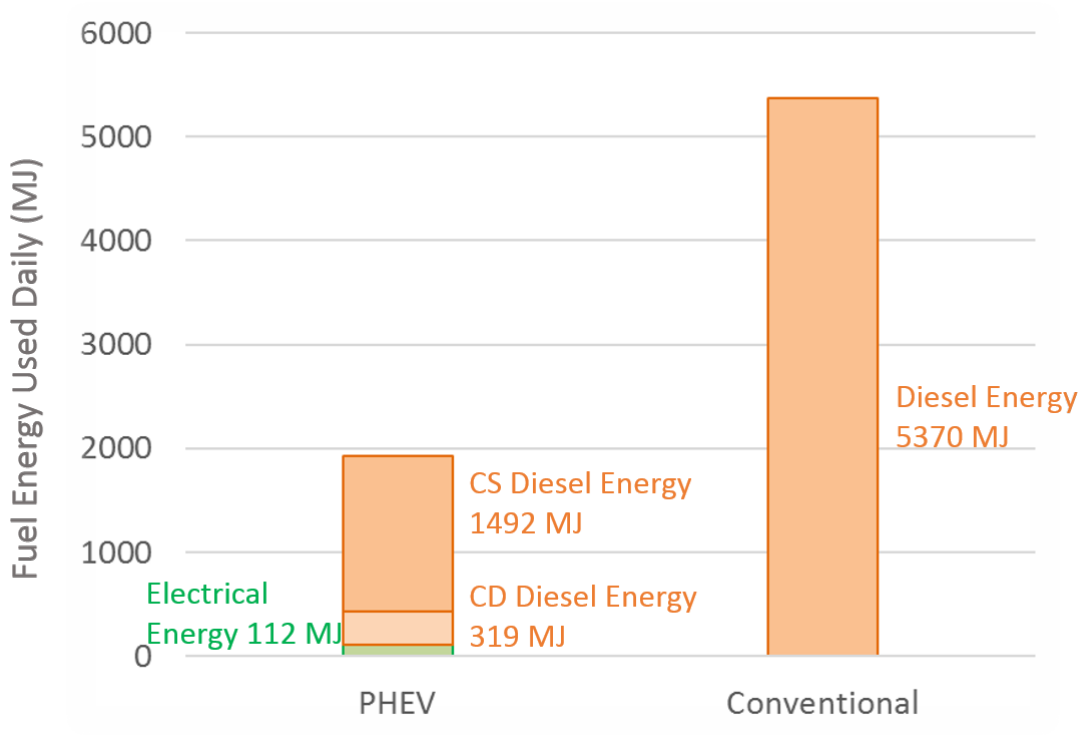

Figure 7.5. Fuel energy used per day (100 miles) by conventional and PHEV transit bus (winning solution).

due to regenerative braking, engine downsizing as well as efficient engine operation. Specifically, for this powertrain configuration, component size and control, the fuel consumption reduction was 63% on the Manhattan drivecycle.

These values of electrical and diesel energy usage can then be multiplied by the corresponding emissions/MJ of fuel to obtain the daily emissions as shown in Figure 7.6. There is 59% to 63% reduction in the greenhouse gas emissions for the PHEV transit bus as compared to the conventional vehicle. The emission reductions are more for California than Indiana. There is a 54% to 61% reduction in both CO and NOx. PM2.5 reduces by35% in Indiana and 52% in California, while, VOC emisisons reduce by 16% in Indiana and 33% in California. There are more PM_{10} emissions for a PHEV transit bus used in Indiana as compared to the conventional vehicle due to the significant PM emissions from electricity generated in Indiana, as shown in Figure 7.4, which is because majority of the electricity produced in Indiana

comes from coal-fired power plants. Also, the SO_x emissions are significantly higher for both Indiana and California due to a significant difference in the SO_x emissions resulting from electricity and diesel usage as shown in Figure 7.4

7.4 Emissions due to Battery Manufacturing

Apart from the difference in daily energy consumption and the corresponding energy sources that set the PHEVs apart from the conventional vehicles, the PHEVs also undergo battery replacements over their lifetime. The emissions caused during battery manufacturing and recycling is also a point of comparison between these two types of vehicles. GREET 2017 does include the emissions caused during battery production and assembling for a few battery chemistries like LMO/Graphite, NMC/Graphite and LFP/Graphite. The emissions, specifically CO_2 emissions, resulting from the production and assembling of these batteries differ, due to the different materials and their preparation processes involved [96]. But some back of the envelope calculations, about emissions from battery production and assembling, can be made for reference by assuming a chemistry close to the type of application being considered here.

The NMC/Graphite battery weight can be assumed to be 20 kg/kWh [96], alongwith a battery capacity of 44kWh and with 2 battery replacements (3 total batteries used) over the vehicle lifetime, as calculated for the Series PHEV Transit Bus winning solution. These assumptions can be used to calculate the emissions resulting from battery production and assembling. These when divided by the total number of days give the "non-discounted" daily emissions due to battery production and assembling for this transit bus. On comparison of the resulting no-discounted daily emissions with the WTW emissions due to electricity and fuel consumption, the CO_2 and GHG-100 emissions are shown to increase by only 3% (4-4.5 kg), the CO, NO_x and SO_x emissions increase by 3 g, 8g, and 126 g, respectively while the PM10, PM2.5 and VOC emissions increase by 2.7g, 1.4g and 1g respectively. Therefore, the CO_2, GHG-100, CO, NO_x, $PM_{2.5}$ and VOC emissions are still lower than those of the con-

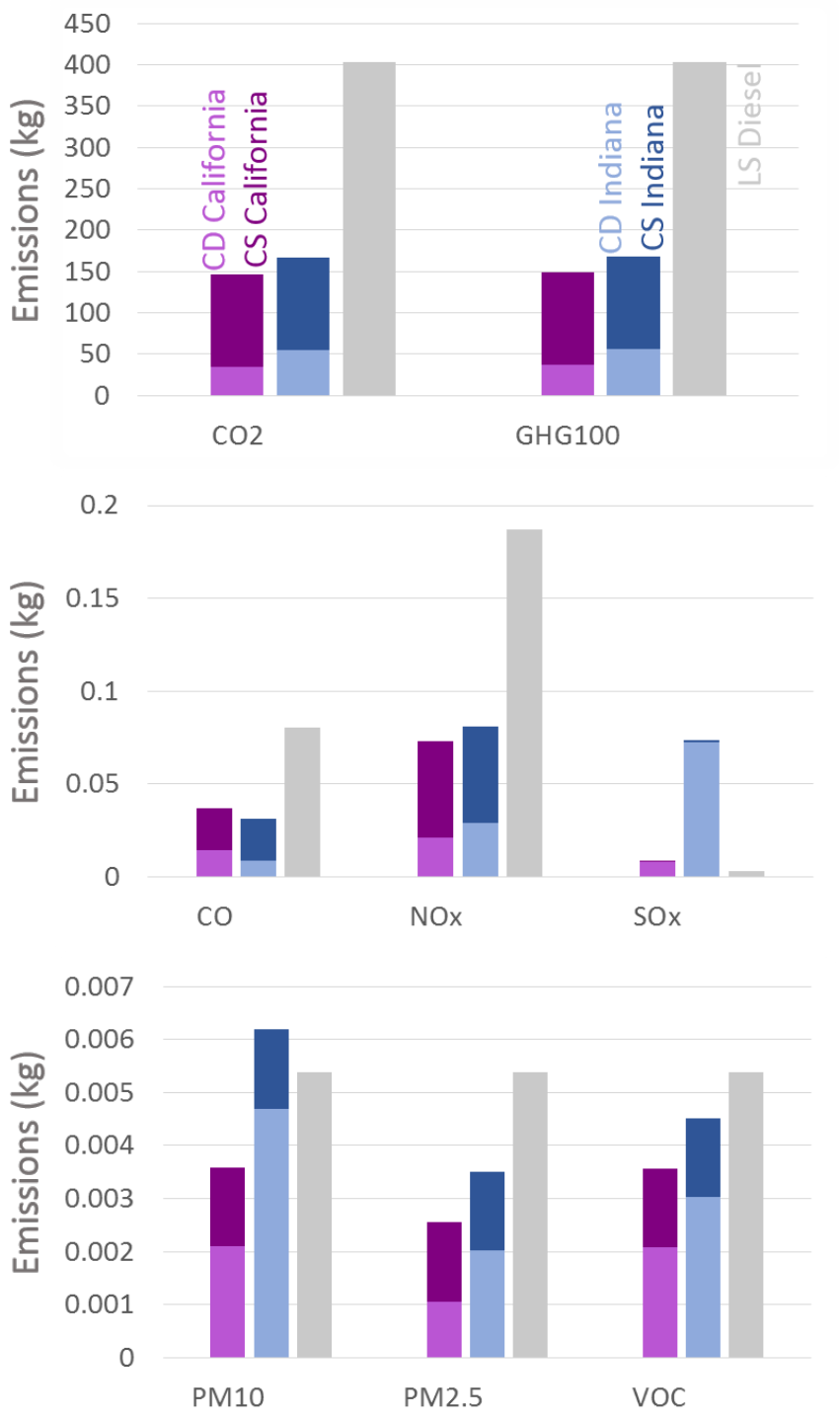

Figure 7.6. Daily emissions from a PHEV transit bus used in California or Indiana compared to those from a conventional transit bus.

ventional bus for both Indiana and California. SO_x and PM_{10} emissions are more than the conventional bus for both the states. The emissions due to battery recycling have not been considered here due to lack of those numbers for the NMC/Graphite chemistry, although studies regarding battery recycling have been conducted for other chemistries [97]. To perform a more holistic comparison of the emissions from these two types of vehicles, the entire vehicle cycle emissions including those from manufacturing and recycling of other vehicle components as well as recycling of batteries needs to be performed.

7.5 Conclusions

A simple framework using Autonomie and GREET, is proposed in this chapter, to calculate and compare the WTW emissions for the PHEV and conventional vehicles. The emissions of a pre-designed PHEV transit bus, operating in Indiana and California, are compared to the conventional transit bus using low-sulfur diesel as the fuel. It is shown that although more greenhouse gases are produced when 1 MJ of electrical energy is used as compared to using 1 MJ of low-sulfur diesel energy, because there is significant energy consumption reduction for PHEVs, the overall emissions are also low. Specifically, with 63% fuel consumption reduction and 44 kWh battery, with a single battery recharge a day, 57% reduction is obtained in the greenhouse gas emissions in Indiana and 63% reduction in greenhouse gases is obtained in California. There is a slight increase in the PM emissions in Indiana, due to the significant portion of electricity being generated in the coal-fired plants. In the future, as more electricity is expected to be generated from cleaner energy sources like, hydroelectric, geothermal sources, the PM emissions per PHEV transit bus would reduce. PHEV transit buses recharging with the California electricity generation mix produce lower greenhouse gas, CO, NO_x as well as PM emissions, but higher SO_x emissions.

This analysis did not include the emissions resulting from battery manufacturing or other component manufacturing. These factors affect the life-long emissions of the

vehicle, more than just the daily emissions. Life-long emission calculations, including vehicle-cycle and recycling emissions, can be performed and then can be used to understand the per mile emission reduction/increase of PHEV transit buses over conventional transit buses.

These emission values can further be assigned a carbon cost/emission cost which, along with the initial component costs and fuel costs, can be used to perform a more holistic powertrain design. Additionally, the impact of change in electricity sources with time, like the economic scenarios, can be used to understand when a application becomes viable to be implemented in a state and with what powertrain configuration.

Further, the impact of multiple recharges during a day on the emissions can be used to optimize vehicle operation to minimize cost and emissions.

8. SUMMARY AND CONCLUSIONS

This dissertation presents frameworks and methodologies to enable battery conscious powertrain design of medium-duty (MD) and heavy-duty (HD) plug-in hybrid electric vehicles (PHEVs) and understand the operating conditions necessary for them to be advantageous over the conventional vehicles. In Chapter 3, the framework used for performing a total-cost-of-ownership based powertrain design is discussed. A comparison of economic viability for the series and parallel architectures over two PHEV applications - a MD Truck and a HD Transit Bus, is presented. The parallel architecture requires significantly lower initial system cost as compared to the series architecture, and therefore shows earlier payback, becoming economically viable earlier for both the applications. The transit bus, due to the higher fuel cost savings, is seen to become economically viable earlier for hybridization. Also, urban driveycles are seen to be more favorable for plug-in hybridization of both the MD Truck and HD Transit Bus.

Of the multiple viable powertrain configurations proposed by the framework in Chapter 3, one solution needs to be selected. In Chapter 4, a method to select the one component sizing and control strategy solution, based on maximizing the net benefits using the Net Benefit to Investment Ratio (NBIR), is proposed. Further, the effect of deterministic variation in economic and vehicle parameters on the Net Present Value (NPV), payback period, fuel consumption reduction, and energy storage system (ESS) replacements, is assessed. It is seen the that the Fuel Price, ESS Price, annual vehicle miles traveled (AVMT), vehicle mass and the nature of the drivecycle are the key parameters that impact ESS replacements, payback period and fuel consumption reduction. This analysis also helps understand the usage cases that would lead to the solution becoming impractical, i.e. have payback period greater than two years and/or more than three ESS replacements.

Battery usage can further vary depending on other operating factors such as time between recharges, recharge C-rate and battery temperature. In Chapter 5, a framework to understand the impact of probabilistic variation of these parameters on battery life is proposed and demonstrated. The results show that, among the variables considered, the temperature of battery operation has the most impact on battery life. Further, for the variation of inputs considered, it is shown that the winning solution selected in Chapter 4 has a 70% chance of becoming viable for hybridization at all, owing to high battery temperatures. This motivates the necessity of an efficient battery thermal management system to maximize battery life.

Heating/cooling required to maintain the battery at the desired temperature requires excess energy consumption. The powertrain analysis in the previous chapters had assumed that the battery was maintained at 20°C by the battery thermal management system. In Chapter 6, the fuel consumption required to maintain the battery at this temperature for two ambient temperatures, 45°C and −5°C, is calculated using a coefficient of performance (COP) based definition of the battery heating/cooling system. For the assumed heating/cooling system architecture and variation of Coefficient of Performance (COP) with ambient temperature, the fuel consumption is seen to increase by 0.8%-1.9% depending upon the drivecycle and ambient temperature. This method can be extended to compare the relative increase in energy consumption for different heating/cooling system architectures and materials. In this Chapter, the validation of the rate of heat generation model for batteries is also presented for an 18650 NMC/Graphite cell. It is shown that the model is able to predict the temperature within 10% error for C-rates 10C.

The emissions associated with the operation of the PHEV are calculated in Chapter 7 using the Greenhouse Gases, Regulated Emissions, and Energy Use in Transportation (GREET) model. The well-to-wheel emissions resulting from operation of a PHEV Transit Bus in Indiana and California are compared to the emissions resulting from operation of the conventional diesel bus. The greenhouse gas (GHG) emissions are shown to reduce by 59% and 63% when a PHEV is operated in Indiana and

California, along with reductions in carbon monoxide (CO), nitrogen oxides (NO_x), particulate matter with diameter less than 2.5 microns ($PM_{2.5}$) and volatile organic compounds (VOC). But an increase in the sulfur oxides (SO_x) emissions for both the states and emissions of particulate matter with diameter less than 10 microns (PM_{10}) for Indiana, are observed.

9. RECOMMENDATIONS

While only the fuel-cycle related emissions have been considered in this study, the vehicle-cycle related emissions can further be considered. These can then be combined with the life-cycle cost-based powertrain design framework to perform a more holistic life-cycle cost- and emissions-based powertrain design-space exploration and best solution selection.

Further, a physics based battery heating/cooling system model can be combined with the vehicle simulation model and employed to understand the effect of the ambient temperature on battery performance and hence battery degradation.

Additionally, it has been shown for the light-duty vehicles that vehicle usage would increase with increase in cost benefits through the usage of alternative vehicle technologies. Whether such an effect will also be seen in the heavy-duty market is a point of study for many. The global emission impacts of the heavy-duty vehicle usage can also be studied.

Another possible direction of study would be to understand the impact of battery degradation on fuel consumption and CD mode range of the PHEV. This will further affect battery power management, number of battery replacements and life-cycle cost.

Further, a sensitivity analysis considering variation of the control parameters considered in Chapter 3 can be performed to understand which of these parameters finally have a significant impact on battery degradation and the economic metrics. Those parameters that do not have a significant impact can then be fixed to a constant value.

It is shown in Chapter 4 that variation in drivecycle has a significant impact on the economic metrics and battery degradation. The impact of drivecycle variation on the desired metrics can be used to improve the methodology for selecting one candidate powertrain configuration for implementation.

REFERENCES

[1] United States Environmental Protection Agency. Climate change indicators in the united states, 2016.

[2] United States Environmental Protection Agency. Inventory of u.s. greenhouse gas emissions and sinks, 2017.

[3] U.S. Energy Information Administration. Annual energy outlook, 2017.

[4] United States Environmental Protection Agency. Greenhouse gas emissions and fuel efficiency standards for medium- and heavy-duty engines and vehicles - phase 2, 2016.

[5] A. P. Vora, X. Jin, V. Hoshing, X. Guo, G. Shaver, W. Tyner, E. Holloway, S. Varigonda, and J. Kupe. Simulation framework for the optimization of hev design parameters: Incorporating battery degradation in a lifecycle economic analysis. *IFAC-PapersOnLine*, 48(15):195 – 202, 2015. 4th IFAC Workshop on Engine and Powertrain Control, Simulation and Modeling E-COSM 2015.

[6] R. Fellini, N. Michelena, P. Papalambros, and M. Sasena. Optimal design of automotive hybrid powertrain systems. In *Proceedings First International Symposium on Environmentally Conscious Design and Inverse Manufacturing*, pages 400–405, Feb 1999.

[7] W. Gao and S. K. Porandla. Design optimization of a parallel hybrid electric powertrain. In *2005 IEEE Vehicle Power and Propulsion Conference*, pages 6 pp.–, Sept 2005.

[8] L. C. Fang and S. Y. Qin. Concurrent optimization for parameters of powertrain and control system of hybrid electric vehicle based on multi-objective genetic algorithms. In *2006 SICE-ICASE International Joint Conference*, pages 2424–2429, Oct 2006.

[9] B. Zhang, Z. Chen, C. Mi, and Y. L. Murphey. Multi-objective parameter optimization of a series hybrid electric vehicle using evolutionary algorithms. In *2009 IEEE Vehicle Power and Propulsion Conference*, pages 921–925, Sept 2009.

[10] X. Hu, Z. Wang, and L. Liao. Multi-objective optimization of hev fuel economy and emissions using evolutionary computation. In *SAE 2004 World Congress & Exhibition*. SAE International, mar 2004.

[11] B. Huang, Z. Wang, and Y. Xu. Multi-objective genetic algorithm for hybrid electric vehicle parameter optimization. In *2006 IEEE/RSJ International Conference on Intelligent Robots and Systems*, pages 5177–5182, Oct 2006.

[12] V. Galdi, L. Ippolito, A. Piccolo, and A. Vaccaro. A genetic-based methodology for hybrid electric vehicles sizing. *Soft Computing*, 5(6):451–457, Dec 2001.

[13] X. Hu, S. J. Moura, N. Murgovski, B. Egardt, and D. Cao. Integrated optimization of battery sizing, charging, and power management in plug-in hybrid electric vehicles. *IEEE Transactions on Control Systems Technology*, 24(3):1036–1043, May 2016.

[14] B. M. Baumann, G. Washington, B. C. Glenn, and G. Rizzoni. Mechatronic design and control of hybrid electric vehicles. *IEEE/ASME Transactions on Mechatronics*, 5(1):58–72, Mar 2000.

[15] V. H. Johnson, K. B. Wipke, and D. J. Rausen. Hev control strategy for real-time optimization of fuel economy and emissions. In *Future Car Congress*. SAE International, apr 2000.

[16] A. Piccolo, L. Ippolito, V. zo Galdi, and A. Vaccaro. Optimisation of energy flow management in hybrid electric vehicles via genetic algorithms. In *2001 IEEE/ASME International Conference on Advanced Intelligent Mechatronics. Proceedings (Cat. No.01TH8556)*, volume 1, pages 434–439 vol.1, 2001.

[17] G. Paganelli, G. Ercole, A. Brahma, Y. Guezennec, and G. Rizzoni. General supervisory control policy for the energy optimization of charge-sustaining hybrid electric vehicles. *JSAE Review*, 22(4):511 – 518, 2001.

[18] R. M. Patil, J. C. Kelly, Z. Filipi, and H. K. Fathy. A framework for the integrated optimization of charging and power management in plug-in hybrid electric vehicles. *IEEE Transactions on Vehicular Technology*, 62(6):2402–2412, July 2013.

[19] C. Yang, S. Du, L. Li, S. You, Y. Yang, and Y. Zhao. Adaptive real-time optimal energy management strategy based on equivalent factors optimization for plug-in hybrid electric vehicle. *Applied Energy*, 203(Supplement C):883 – 896, 2017.

[20] Z. Chen, R. Xiong, and J. Cao. Particle swarm optimization-based optimal power management of plug-in hybrid electric vehicles considering uncertain driving conditions. *Energy*, 96(Supplement C):197 – 208, 2016.

[21] Z. Chen, R. Xiong, C. Wang, and J. Cao. An on-line predictive energy management strategy for plug-in hybrid electric vehicles to counter the uncertain prediction of the driving cycle. *Applied Energy*, 185(Part 2):1663 – 1672, 2017. Clean, Efficient and Affordable Energy for a Sustainable Future.

[22] Y. Zhang, L. Chu, Z. Fu, N. Xu, C. Guo, X. Zhang, Z. Chen, and P. Wang. Optimal energy management strategy for parallel plug-in hybrid electric vehicle based on driving behavior analysis and real time traffic information prediction. *Mechatronics*, 46(Supplement C):177 – 192, 2017.

[23] C. S. Ernst, A. Hackbarth, R. Madlener, B. Lunz, D. U. Sauer, and L. Eckstein. Battery sizing for serial plug-in hybrid electric vehicles: A model-based economic analysis for germany. *Energy Policy*, 39(10):5871 – 5882, 2011. Sustainability of biofuels.

[24] X. Wu, B. Cao, X. Li, J. Xu, and X. Ren. Component sizing optimization of plug-in hybrid electric vehicles. *Applied Energy*, 88(3):799 – 804, 2011.

[25] X. Hu, C. M. Martinez, and Y. Yang. Charging, power management, and battery degradation mitigation in plug-in hybrid electric vehicles: A unified cost-optimal approach. *Mechanical Systems and Signal Processing*, 87(Part B):4 – 16, 2017. Signal Processing and Control challenges for Smart Vehicles.

[26] S. J. Moura, J. L. Stein, and H. K. Fathy. Battery-health conscious power management in plug-in hybrid electric vehicles via electrochemical modeling and stochastic control. *IEEE Transactions on Control Systems Technology*, 21(3):679–694, May 2013.

[27] L. Serrao, S. Onori, A. Sciarretta, Y. Guezennec, and G. Rizzoni. Optimal energy management of hybrid electric vehicles including battery aging. In *Proceedings of the 2011 American Control Conference*, pages 2125–2130, June 2011.

[28] S. Bashash, S. J. Moura, J. C. Forman, and H. K. Fathy. Plug-in hybrid electric vehicle charge pattern optimization for energy cost and battery longevity. *Journal of Power Sources*, 196(1):541 – 549, 2011.

[29] B. Lunz, Z. Yan, J. B. Gerschler, and D. U. Sauer. Influence of plug-in hybrid electric vehicle charging strategies on charging and battery degradation costs. *Energy Policy*, 46(Supplement C):511 – 519, 2012.

[30] R. Finesso, E. Spessa, and M. Venditti. Cost-optimized design of a dual-mode diesel parallel hybrid electric vehicle for several driving missions and market scenarios. *Applied Energy*, 177(Supplement C):366 – 383, 2016.

[31] K. Bayindir, M. A. Gözüküçük, and A. Teke. A comprehensive overview of hybrid electric vehicle: Powertrain configurations, powertrain control techniques and electronic control units. *Energy Conversion and Management*, 52(2):1305–1313, 2011.

[32] C. C. Chan, A. Bouscayrol, and K. Chen. Electric, hybrid, and fuel-cell vehicles: Architectures and modeling. *IEEE transactions on vehicular technology*, 59(2):589–598, 2010.

[33] M.F.M. Sabri, K.A. Danapalasingam, and M.F. Rahmat. A review on hybrid electric vehicles architecture and energy management strategies. *Renewable and Sustainable Energy Reviews*, 53:1433–1442, 2016.

[34] V. Freyermuth, E. Fallas, and A. Rousseau. Comparison of powertrain configuration for plug-in hevs from a fuel economy perspective. *SAE International Journal of Engines*, 1(1):392–398, 2009.

[35] X. Li and S. S. Williamson. Comparative investigation of series and parallel hybrid electric vehicle (hev) efficiencies based on comprehensive parametric analysis. In *Vehicle Power and Propulsion Conference, 2007. VPPC 2007. IEEE*, pages 499–505. IEEE, 2007.

[36] E. Vinot, R. Trigui, B. Jeanneret, J. Scordia, and F. Badin. Hevs comparison and components sizing using dynamic programming. In *Vehicle Power and Propulsion Conference, 2007. VPPC 2007. IEEE*, pages 314–321. IEEE, 2007.

[37] X. Li and S. S. Williamson. Efficiency and suitability analyses of varied drive train architectures for plug-in hybrid electric vehicle (phev) applications. In *Vehicle Power and Propulsion Conference, 2008. VPPC'08. IEEE*, pages 1–6. IEEE, 2008.

[38] X. Zhou, D. Qin, and J. Hu. Multi-objective optimization design and performance evaluation for plug-in hybrid electric vehicle powertrains. *Applied Energy*, 208:1608–1625, 2017.

[39] P. Tulpule, V. Marano, and G. Rizzoni. Effects of different phev control strategies on vehicle performance. In *American Control Conference, 2009. ACC'09.*, pages 3950–3955. IEEE, 2009.

[40] S. S. Williamson, S. G. Wirasingha, and A. Emadi. Comparative investigation of series and parallel hybrid electric drive trains for heavy-duty transit bus applications. In *Vehicle Power and Propulsion Conference, 2006. VPPC'06. IEEE*, pages 1–10. IEEE, 2006.

[41] A. A. Pesaran. Battery thermal management in ev and hevs: issues and solutions. *Battery Man*, 43(5):34–49, 2001.

[42] H. S. Hamut, I. Dincer, and G. F. Naterer. Performance assessment of thermal management systems for electric and hybrid electric vehicles. *International Journal of Energy Research*, 37(1):1–12, 2013.

[43] G. Karimi and X. Li. Thermal management of lithium-ion batteries for electric vehicles. *International Journal of Energy Research*, 37(1):13–24, 2013.

[44] D. Chen, J. Jiang, G. H. Kim, C. Yang, and A. Pesaran. Comparison of different cooling methods for lithium ion battery cells. *Applied Thermal Engineering*, 94:846–854, 2016.

[45] Z. Rao and S. Wang. A review of power battery thermal energy management. *Renewable and Sustainable Energy Reviews*, 15(9):4554–4571, 2011.

[46] S. Al Hallaj and J. R. Selman. A novel thermal management system for electric vehicle batteries using phase-change material. *Journal of the Electrochemical Society*, 147(9):3231–3236, 2000.

[47] R. Mahamud and C. Park. Reciprocating air flow for li-ion battery thermal management to improve temperature uniformity. *Journal of Power Sources*, 196(13):5685–5696, 2011.

[48] Z. Rao, S. Wang, M. Wu, Z. Lin, and F. Li. Experimental investigation on thermal management of electric vehicle battery with heat pipe. *Energy Conversion and Management*, 65:92–97, 2013.

[49] A. Greco, D. Cao, X. Jiang, and H. Yang. A theoretical and computational study of lithium-ion battery thermal management for electric vehicles using heat pipes. *Journal of Power Sources*, 257:344–355, 2014.

[50] S. Park and D. Jung. Numerical modeling and simulation of the vehicle cooling system for a heavy duty series hybrid electric vehicle. Technical report, SAE Technical Paper, 2008.

[51] Z. Tian, W. Gan, X. Zhang, B. Gu, and L. Yang. Investigation on an integrated thermal management system with battery cooling and motor waste heat recovery for electric vehicle. *Applied Thermal Engineering*, 136:16–27, 2018.

[52] H. Huo, Y. Wu, and M. Wang. Total versus urban: Well-to-wheels assessment of criteria pollutant emissions from various vehicle/fuel systems. *Atmospheric Environment*, 43(10):1796 – 1804, 2009.

[53] B. Sen, T. Ercan, and O. Tatari. Does a battery-electric truck make a difference? life cycle emissions, costs, and externality analysis of alternative fuel-powered class 8 heavy-duty trucks in the united states. *Journal of Cleaner Production*, 141:110 – 121, 2017.

[54] W. Ke, S. Zhang, X. He, Y. Wu, and J. Hao. Well-to-wheels energy consumption and emissions of electric vehicles: Mid-term implications from real-world features and air pollution control progress. *Applied Energy*, 188:367 – 377, 2017.

[55] X. Ou, X. Zhang, and S. Chang. Alternative fuel buses currently in use in china: Life-cycle fossil energy use, ghg emissions and policy recommendations. *Energy Policy*, 38(1):406 – 418, 2010.

[56] B. Zhou, Y. Wu, B. Zhou, R. Wang, W. Ke, S. Zhang, and J. Hao. Real-world performance of battery electric buses and their life-cycle benefits with respect to energy consumption and carbon dioxide emissions. *Energy*, 96:603 – 613, 2016.

[57] H. Ma, F. Balthasar, N. Tait, X. Riera-Palou, and A. Harrison. A new comparison between the life cycle greenhouse gas emissions of battery electric vehicles and internal combustion vehicles. *Energy Policy*, 44:160 – 173, 2012.

[58] M. Yazdanie, F. Noembrini, L. Dossetto, and K. Boulouchos. A comparative analysis of well-to-wheel primary energy demand and greenhouse gas emissions for the operation of alternative and conventional vehicles in switzerland, considering various energy carrier production pathways. *Journal of Power Sources*, 249:333 – 348, 2014.

[59] A. Elgowainy, A. Burnham, M. Wang, J. Molburg, and A. Rousseau. Well-to-wheels energy use and greenhouse gas emissions of plug-in hybrid electric vehicles. *SAE International Journal of Fuels and Lubricants*, 2(1):627–644, 2009.

[60] A. Elgowainy, J. Han, L. Poch, M. Wang, A. Vyas, M. Mahalik, and A. Rousseau. Well-to-wheels analysis of energy use and greenhouse gas emissions of plug-in hybrid electric vehicles. Technical report, Argonne National Lab.(ANL), Argonne, IL (United States), 2010.

[61] A. Elgowainy, A. Rousseau, M. Wang, M. Ruth, D. Andress, J. Ward, F. Joseck, T. Nguyen, and S. Das. Cost of ownership and well-to-wheels carbon emissions/oil use of alternative fuels and advanced light-duty vehicle technologies. *Energy for Sustainable Development*, 17(6):626 – 641, 2013.

[62] T. Katranik. Impact of vehicle propulsion electrification on well-to-wheel co2 emissions of a medium duty truck. *Applied Energy*, 108:236 – 247, 2013.

[63] C. N. Shiau, N. Kaushal, C. T. Hendrickson, S. B. Peterson, J. F. Whitacre, and J. J. Michalek. Optimal plug-in hybrid electric vehicle design and allocation for minimum life cycle cost, petroleum consumption, and greenhouse gas emissions. *Journal of Mechanical Design*, 132(9):091013, 2010.

[64] O. Karabasoglu and J. Michalek. Influence of driving patterns on life cycle cost and emissions of hybrid and plug-in electric vehicle powertrains. *Energy Policy*, 60:445 – 461, 2013.

[65] E. Mulholland, J. Teter, P. Cazzola, Z. McDonald, and B. P. Gallachir. The long haul towards decarbonising road freight a global assessment to 2050. *Applied Energy*, 216:678 – 693, 2018.

[66] J. J. Michalek, M. Chester, P. Jaramillo, C. Samaras, C. N. Shiau, and L. B. Lave. Valuation of plug-in vehicle life-cycle air emissions and oil displacement benefits. *Proceedings of the National Academy of Sciences*, 108(40):16554–16558, 2011.

[67] X. Jin, O. Wasynczuk, and G. Shaver. Computationally efficient and flexible magnetic-field-analysis-based scaling strategy for permanent magnet machines. *IEEE Transactions on Energy Conversion*, 2018.

[68] EC Power. *Autolion ST User's Manual*.

[69] W. Fang, O. J. Kwon, and C. Y. Wang. Electrochemical–thermal modeling of automotive li-ion batteries and experimental validation using a three-electrode cell. *International journal of energy research*, 34(2):107–115, 2010.

[70] J. Newman and W. Tiedemann. Porous-electrode theory with battery applications. *AIChE Journal*, 21(1):25–41, 1975.

[71] T. R. Tanim, C. D. Rahn, and C. Y. Wang. State of charge estimation of a lithium ion cell based on a temperature dependent and electrolyte enhanced single particle model. *Energy*, 80:731–739, 2015.

[72] M. Einhorn, F. V. Conte, C. Kral, and J. Fleig. Comparison, selection, and parameterization of electrical battery models for automotive applications. *IEEE Transactions on Power Electronics*, 28(3):1429–1437, 2013.

[73] E. Samadani, S. Farhad, W. Scott, M. Mastali, L. E. Gimenez, M. Fowler, and R. A. Fraser. Empirical modeling of lithium-ion batteries based on electrochemical impedance spectroscopy tests. *Electrochimica Acta*, 160:169–177, 2015.

[74] X. Hu, S. Li, and H. Peng. A comparative study of equivalent circuit models for li-ion batteries. *Journal of Power Sources*, 198:359–367, 2012.

[75] J. Wang, J. Purewal, P. Liu, J. Hicks-Garner, S. Soukazian, E. Sherman, A. Sorenson, L. Vu, H. Tataria, and M. W. Verbrugge. Degradation of lithium ion batteries employing graphite negatives and nickelcobaltmanganese oxide+spinel manganese oxide positives: Part 1, aging mechanisms and life estimation. *Journal of Power Sources*, 269(Supplement C):937 – 948, 2014.

[76] J. Wang, P. Liu, J. Hicks-Garner, E. Sherman, S. Soukiazian, M. Verbrugge, H. Tataria, J. Musser, and P. Finamore. Cycle-life model for graphite-lifepo4 cells. *Journal of Power Sources*, 196(8):3942 – 3948, 2011.

[77] X. Jin, A. P. Vora, V. Hoshing, T. Saha, G. M. Shaver, O. Wasynczuk, and S. Varigonda. Comparison of li-ion battery degradation models for system design and control algorithm development. In *2017 American Control Conference (ACC)*, pages 74–79, May 2017.

[78] X. Jin, A. Vora, V. Hoshing, T. Saha, G. Shaver, R. E. Garca, O. Wasynczuk, and S. Varigonda. Physically-based reduced-order capacity loss model for graphite anodes in li-ion battery cells. *Journal of Power Sources*, 342(Supplement C):750 – 761, 2017.

[79] U.S. Energy Information Administration. Annual energy outlook, 2015.

[80] S. Rogers and S. Boyd. Overview of the doe advanced power electronics and electric motor r and d program, 2014.

[81] B. Nykvist and M. Nilsson. Rapidly falling costs of battery packs for electricvehicles. *Nature Climate Change*, 5.

[82] F. Musavi, M. Edington, W. Eberle, and W. G. Dunford. Evaluation and efficiency comparison of front end ac-dc plug-in hybrid charger topologies. *IEEE Transactions on Smart grid*, 3(1):413–421, 2012.

[83] J. S. Kim, G. Y. Choe, H. M. Jung, B. K. Lee, Y. J. Cho, and K. B. Han. Design and implementation of a high-efficiency on-board battery charger for electric vehicles with frequency control strategy. In *Vehicle Power and Propulsion Conference (VPPC), 2010 IEEE*, pages 1–6. IEEE, 2010.

[84] M. M. Morcos, N. G. Dillman, and C. R. Mersman. Battery chargers for electric vehicles. *IEEE Power Engineering Review*, 20(11):8–11, 2000.

[85] E. Wood, M. Alexander, and T. H. Bradley. Investigation of battery end-of-life conditions for plug-in hybrid electric vehicles. *Journal of Power Sources*, 196(11):5147 – 5154, 2011.

[86] S. F. Schuster, T. Bach, E. Fleder, J. Mller, M. Brand, G. Sextl, and A. Jossen. Nonlinear aging characteristics of lithium-ion cells under different operational conditions. *Journal of Energy Storage*, 1:44 – 53, 2015.

[87] Alternative fuels data center: Electric vehicle charging station locations. `https://www.afdc.energy.gov/fuels/electricity_locations.html#/find/nearest?fuel=ELEC`.

[88] M. Yilmaz and P. T. Krein. Review of battery charger topologies, charging power levels, and infrastructure for plug-in electric and hybrid vehicles. *IEEE Transactions on Power Electronics*, 28(5):2151–2169, 2013.

[89] M. J. Moran and H. N. Shapiro. *Fundamentals of Engineering Thermodynamics, 2006*. John Wiley & Sons, Inc.: New York.

[90] F. Hasselby. Dynamic modelling of battery cooling systems for automotive applications, 2013.

[91] B. Brodie. Stand alone battery thermal management system. Technical report, Denso International America, Incorporated, Southfield, MI (United States); National Renewable Energy Lab.(NREL), Golden, CO (United States), 2015.

[92] J. H. Ahn, H. Kang, H. S. Lee, H. W. Jung, C. Baek, and Y. Kim. Heating performance characteristics of a dual source heat pump using air and waste heat in electric vehicles. *Applied Energy*, 119:1–9, 2014.

[93] Center for Transportations Research, Energy Systems Division, Argonne National Labs. *GREET Life-cycle Model*.

[94] Office of Electricity Delivery Department of Energy (DOE) and Energy Reliability (OE). State of indiana energy sector risk profile. Technical report.

[95] California energy commission: Total system electric generation. `http://www.energy.ca.gov/almanac/electricity_data/total_system_power.html`, 2016.

[96] J. B. Dunn, C. James, L. Gaines, K. Gallagher, Q. Dai, and J. C. Kelly. Material and energy flows in the production of cathode and anode materials for lithium ion batteries. Technical report, Argonne National Lab.(ANL), Argonne, IL (United States), 2015.

[97] J. Dunn, L. Gaines, M. Barnes, J. L. Sullivan, and M. Wang. Material and energy flows in the materials production, assembly, and end-of-life stages of the automotive lithium-ion battery life cycle. Technical report, Argonne National Lab.(ANL), Argonne, IL (United States), 2014.

VITA

EDUCATION

Purdue University, West Lafayette, IN

Ph.D., Mechanical Engineering, Aug 2014 - Dec 2018

Current GPA: 3.85

Hybrid Vehicle Systems Certificate, May 2017

Applied Management Principles Certificate, May 2017

Recipient of the Cummins Fellowship Program at Purdue, Aug 2014 - May 2015

Cummins College of Engineering for Women, University of Pune, India

Bachelor of Engineering, Electronics and Telecommunication Engineering, Aug 2010 - May 2014

Aggregate Percentage: 72.17% , Class: First Class with Distinction.

RESEARCH EXPERIENCE

Hybrid Electric Vehicle Powertrain Optimization, *funded by Cummins (Aug 2014 - present)*

Advised by Prof. Gregory M Shaver, Purdue University

- Leading the effort to understand the impact of active cooling on battery degradation and fuel consumption, for incorporation in a 'total cost of ownership' model for the medium-duty truck and transit bus PHEVs
- Led the effort to understand the sensitivity of the economic benefits and battery degradation to variation in vehicle parameters, charging C-rates and operating temperatures
- Co-developed a simulation framework for integrating the effect of battery degradation in the economic analysis of the vehicle

Wireless Communication*(Aug 2013 - May 2014)*

Advised by Ashok R Khedkar, Cummins College of Engineering for Women

- Developed methods for analysis and suppression of inter-carrier interference in faded orthogonal frequency division multiplexed systems.

MENTORSHIP AND LEADERSHIP EXPERIENCE

- Mentored two graduate and three undergraduate students in their respective research projects
- Introduced and led the community service initiative as a part of Herrick Labs social activities, as a **Herrick Student Representative Committee Member**

INTERNSHIPS

Cummins Inc, Columbus, IN *(May 2015 - Aug 2015)*

- Performed simulation testing of a PM sensor diagnostic.
- Tested and improved documentation of the 'Aftertreatment Maintenance Feature' in INSITE.

Eaton India, Pune, India *(May 2013)*

Developed a validation framework for Modbus TCP/ RTU protocol with focus on input and output configurability.